# Evaluation Tool for Demand-Side Management of Domestic Hot Water Load

by

Wong Koon Kong, BEng (Hons)

Submitted in fulfilment of the requirements for the Degree of

Master of Engineering Science


School of Engineering

University of Tasmania

September 2014

## Declaration of Originality

This thesis contains no material which has been accepted for a degree or diploma by the University or any other institution, except by way of background information and duly acknowledged in the thesis, and to the best of my knowledge and belief no material previously published or written by another person except where due acknowledgement is made in the text of the thesis, nor does the thesis contain any material that infringes copyright.

……..

Wong Koon Kong

Date: 02 September 2014

## Statement of Authority to Access

This thesis may be available for loan and limited copying and communication in accordance with the Copyright Act 1986.

……..

Wong Koon Kong

Date: 02 September 2014

# Preface

## Abstract

This thesis presents the development of an evaluation tool for demand-side management (DSM) of domestic hot water systems (DHWSs). The developed tool provides accurate modeling and predictions of potential peak demand reductions through direct control of DHWSs. It aims to assist distribution system operators (DSOs) in designing a DSM program to deliver desired peak load reductions while maintaining a satisfactory level of comfort for all consumers.

The developed tool estimates the available domestic hot water load in a controlled area, and determines optimal switching programs for direct load control (DLC). A switching program refers to a direct control schedule that strategically switches DHWSs on and off in order to achieve a desired load reduction during peak periods.

To calculate the power consumption and temperature profile of a DHWS, we developed a multi-layer thermally stratified hot water system model and validated it with experimental data. The tool employs Monte Carlo probabilistic simulations to generate hot water consumption profiles for domestic consumers, and uses the hot water system model to obtain the loads associated with these hot water consumption profiles. Switching programs for DLC found via iterative optimizations, are applied to these hot water loads to meet the peak reduction targets set by the tool user. Key performance indicators (KPIs) to evaluate the performance of these switching programs and the impact on consumers' comfort as a result of implementing DLC, were also developed.

# Outline of the research

This research focuses on DLC of DHWSs, as a DSM approach to reduce the peak domestic load in a power distribution network. DHWS is chosen as the control target of this research for two main reasons:

- The domestic hot water load represents a significant share of the total domestic energy load. Water heating accounts for up to 40% of domestic energy consumption in Australia and approximately one third in Tasmania [1], [2]. Hence, a DLC program that can effectively reduce the peak domestic hot water load will have a significant impact in reducing the peak load of the substations. For example, Integra Energy (New South Wales, Australia) has successfully reduced its system peak demand by 389 MW through implementing DLC on DHWSs [3].
- A DHWS represents an interruptible load because it is an insulated thermal energy storage that continually supplies hot water to consumers even during the period of power interruptions. The deferred energy is recovered when the power is restored. Hence, a well-designed DLC program has a minimal impact on consumers' existing comfort levels.

This research has two main objectives:

1. To develop a domestic hot water evaluation tool that can accurately model the available hot water load and predict the potential peak reduction achievable through direct control of domestic electric hot water systems.
2. To use the developed tool to assist distribution system operators in designing their load management (LM) programs, with the aim of delivering optimal peak reduction in domestic loads while ensuring minimal impact on consumers' existing comfort levels.

Achieving these objectives requires research in the areas summarized below:

1. Develop an accurate model to predict the power consumption and temperature profile of a domestic electric hot water system.
2. Develop a generic approach to estimate hot water consumption profiles in individual households.

3. Derive a set of key performance indicators to measure, evaluate and compare the performance for various controlled scenarios.
4. Develop a control management system that produces DLC switching programs and employs effective algorithms to optimize them. These switching programs are applied to the DHWSs to reduce the aggregate peak load and improve the load factor.
5. Develop a user-friendly program that integrates the above functions into a tool that assists the DSOs in the evaluation and selection of DLC switching programs for their respective load management purposes.

Figure (I) shows the block diagram that summarizes the research objectives and the research areas to achieve these objectives.

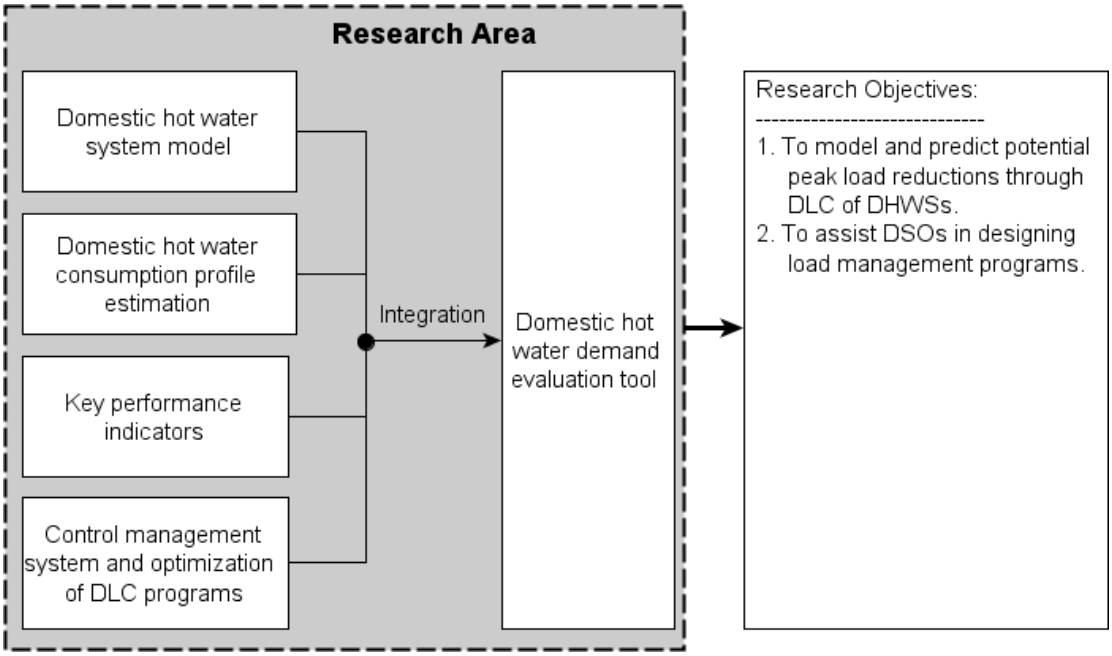


Figure (I) Block diagram illustrating research objectives and research areas.

With reference to the research areas discussed above, this thesis is organized as follows:

Chapter 1 provides an introduction to DSM. This chapter contains a general overview of the history of DSM, the implementation of DSM in some major countries, a review of methods and strategies to implement DSM, and values of DSM in an electric power system.

Chapter 2 presents the structure of the developed hot water evaluation tool. It introduces the high level structure of the tool and describes the functionality of individual modules in the tool. In addition, the high level operation of these modules and the flow of information between them are also discussed. Detailed descriptions of the main functional modules are provided in the following chapters.

Chapter 3 outlines the generic approach in the estimation of domestic hot water consumption profiles in Tasmania, Australia. It presents the Monte Carlo approach employed to generate hot water consumption profiles for individual households. Survey results, actual energy metering data, and demographic data are used in the estimation process. As a result, the estimated hot water consumption profiles are correlated to the demography and the consumer behavior in the controlled area. The operation of the hot water consumption generator module is described in this chapter.

Chapter 4 presents the development of the domestic hot water system model. This chapter provides the mathematical modeling with heat energy equations of the most common DHWS in Tasmania. Furthermore, the validation with experimental data is also presented.

Chapter 5 describes the operation of the performance calculator and the details of the control management system. This chapter defines the KPIs used by the tool to evaluate the performance of DLC switching programs, as well as describing in detail the optimizer module and algorithms developed to optimize DLC switching programs.

Chapter 6 evaluates the developed tools with a number of case studies. The studies assess the scalability of the results, impacts of assuming certain parameters as constant in simulations, as well as the performance of different DLC switching programs applied to DHWSs under different operating scenarios. In addition, this chapter also includes discussions of the simulation results.

Chapter 7 summarizes the research and gives some recommendations for future studies aiming to extend the research work reported in this thesis.

# Publications

Journal and conference papers given in the following list have been produced as the outcome of this research.

Journal papers

1. M. Negnevitsky and K. Wong, "Demand side management evaluation tool," *IEEE Trans. Power Syst.*, vol. 99, pp. 1-11, 2014.
2. M. Negnevitsky and K. Wong, "A practical approach to modelling of domestic electric hot water systems for load management programs," *Applied Thermal Engineering*, under review.

Refereed conference papers

1. K. Wong and M. Negnevitsky, "Development of an evaluation tool for demand side management of domestic hot water load," in *Proc. IEEE PES General Meeting*, 2013, pp. 1-5.
2. K. Wong and M. Negnevitsky, "Optimisation of switching programs for demand side management of domestic hot water load," in *Australasian Universities Power Engineering Conf.*, 2013, pp. 1-6.

# Acknowledgements

First of all, I would like to express my deep gratitude to my supervisor, Professor Michael Negnevitsky. I thank you for being a great mentor to me. I appreciate very much your patience, and the advice and motivation you have given me throughout my research. I would also like to thank Dr. Osman Haruni for all the significantly useful and constructive discussions we had during the early stage of my research. Furthermore, I wish to say thank you to all the technical staff in the School of Engineering, especially Calverly Gerard, James Lamont, Peter Seward and Andrew Bylett, who helped me in setting up the test system in the laboratory.

In addition, I wish to thank Aurora Energy, Australia for providing the financial support and the survey data required in my research. I also gratefully acknowledge Peter Milbourne, James O'Flaherty, Daniel Capece, Cherry Wynn and Dr. Thanh Nguyen of Aurora Energy for productive discussions of the results presented in this thesis.

A special thanks to my fellow postgraduate researchers at the School of Engineering, especially Dinh Hieu Nguyen, Zane Smith, Sarah Lyden and Ahmad Tavakoli. We had a great number of positive discussions which were helpful to my work.

Lastly, I would like to thank my family and loved ones. My research work has only been possible with your support and love.

# Contents

# List of tables

# List of figures

# List of abbreviations

| | |
|---|---|
| AC | Air conditioner |
| AMI | Advanced metering infrastructure |
| CLM | Conservation and load management |
| CO2-e | Carbon dioxide equivalent |
| CPP | Critical peak pricing |
| DCCEE | Department of climate change and energy efficiency |
| DG | distributed generation |
| DHWS | Domestic hot water system |
| DLC | Direct load control |
| DRED | Demand response enabling device |
| DSM | Demand-side management |
| DSO | Distribution system operator |
| ERF | Error function |
| EU | European Union |
| GUI | Graphical user interface |
| I/Os | inputs and outputs |
| KPI | Key performance indicator |
| LM | Load management |
| MAE | Mean absolute error |
| MAPE | Mean absolute percentage error |
| NEM | National Electricity Market |
| OCP | Optimized control period |
| PI | Proportional and integral |
| RMSE | Root mean square error |
| RTP | Real Time pricing |
| SWIS | South West Interconnected System |
| ToU | Time of use |
| TSO | Transmission system operator |
| UDCP | User defined control period |

# List of symbols

The following is a list of key symbols used in the thesis. Other symbols are introduced and described within the texts where they first appear.

| | |
|---|---|
| $H_L$ | Height of the entire layer zone measured from the top of the mixing zone. |
| $K_p$ | Proportional gain of the PI functions. |
| $L_C$ | Aggregate controlled hot water load curve. |
| $L_T$ | Target peak value for aggregate controlled hot water load. |
| $L_U$ | Aggregate uncontrolled hot water load curve. |
| $N$ | Number of stratified layers inside a hot water tank. |
| $N_H$ | Total number of households. |
| $N_S$ | Total number of Monte Carlo iterations. |
| $P$ | Rated power of the hot water system. |
| $P_{cold}$ | Probability of cold showers. |
| $R(\tau)$ | Peak load reduction in control period specified by $\tau$. |
| $T_a$ | Ambient temperature. |
| $T_c$ | Cold water temperature. |
| $t_f$ | Finishing time of a control period. |
| $t_s$ | Starting time of a control period. |
| $T_i$ | Integral time of the PI functions. |
| $T^j$ | Temperature of layer $j$ inside a hot water tank. |
| $T_{mz}$ | Mean temperature of the mixing zone in a hot water tank. |
| $T_{off}$ | Thermostat turn-off temperature. |
| $T_{on}$ | Thermostat turn-on temperature. |
| $T_{shwr}$ | Shower temperature. |
| $\bar{W}$ | Aggregate hot water consumption profile of a controlled area. |
| $w(i, j)$ | Hot water consumption profile of household $i$ in iteration $j$. |
| $Z^j$ | Height of layer $j$ inside a hot water tank. |
| $\alpha$ | The ratio of hot water flow to mixed water flow of a tempering valve |
| $\tau$ | Control period in a switching program. |
| $\tau_{off}$ | Turn-off period in a switching cycle. |
| $\tau_{on}$ | Turn-on period in a switching cycle. |
| $\tau_{sc}$ | Switching cycle in a switching program. |
| $\tau_{step}$ | Control step in a switching program. |

# Chapter 1

## Introduction

Electricity is a form of energy that is very costly to store in bulk with existing technologies. For example, the global energy storage capacity represented just 3% of the global generating capacity in 2010 [4], [5]. Hence, most of the time, electric energy is consumed as it is generated. Moreover, the demand for electricity is not consistent but exhibits daily and seasonal variations. These unique characteristics present major challenges in designing and planning for an electric power system[1].

In order to ensure a high level of supply availability, the capacity of an electric power distribution system is traditionally designed to support the peak load forecast in the network [6], [7]. Although this design approach is essential in minimizing supply interruptions, it creates excessive latent capacity in distribution networks with low load factors (ratio of average to peak load). This scenario represents inefficient utilization of network infrastructures. As an example, the cost of catering to peak loads has caused electricity prices to double in Australia over the last five years [7]. Capital expenditures of close to half of the total network investment and more than half of the transmission budget are spent to accommodate the peak load growth in the National Electricity Market (NEM) in Australia. This amount accounts for about A$10 billion in system capacity that is used for slightly more than one percent of a year [8]. Similar costly underutilization is reported in the South West Interconnected System (SWIS) of Western Australia. To meet peak demands in 2009, about 600 MW (or 12 %) of capacity in the SWIS was used for less than one percent of the year [9].

The characteristic of low load factor is commonly evident in domestic load profiles. The peaks are usually seasonal and persist only for a few hours of a day. For the rest of the time, the load is considerably lower than the peaks. For example, Figure 1.1 shows the average daily load profile (for winter months) of a substation

[1] "Power", unless explicitly stated otherwise, means "electric power" in this thesis.

serving residential areas in the Tasmanian (Australia) distribution network. The majority of this substation's loads were domestic demands. Its load factor (ratio of average to peak load) was about 0.7, and the load was below its average value for more than half of the time. The summer load in Tasmania is relatively lower than its winter load.

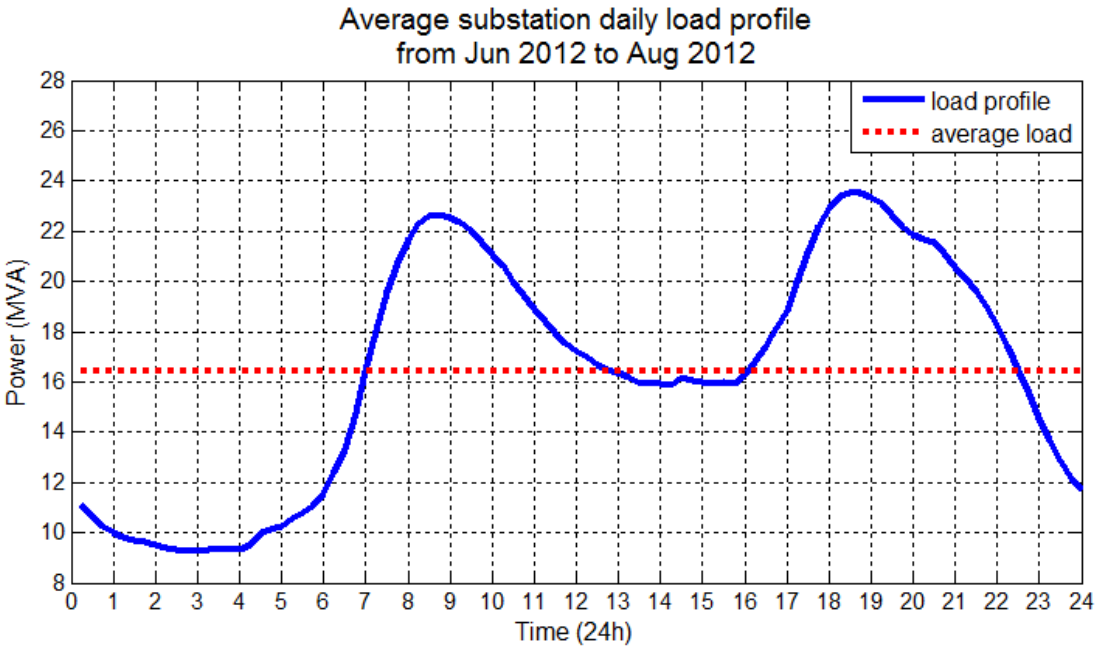


Figure 1.1 Average daily total load profile in winter months of a substation in Tasmania dominated by domestic load.

To overcome the problem of low efficiency in a power system, such as those in the aforementioned examples, active initiatives are needed to reduce peak loads, improve the load factor and enhance the overall network utilization. One of the widely implemented initiatives is DSM — the effort to reduce energy consumption and improve the overall power system efficiency through the implementation of policies and methods that modify consumer demand for electricity [10]. The following sections provide a review of DSM. Section 1.1 gives a brief overview on the history of DSM and its implementations in three major countries. Sections 1.2–1.4 describe different types of DSM initiatives and how they are implemented around the world. Section 1.5 discusses the values of DSM implementations in modern power systems.

## 1.1 Overview of Demand-side Management

The initial concept of DSM was coined during the Arab oil embargo in the early 1970s where the price of crude oil had quadrupled overnight from about US$2.50 to US$10.00 per barrel [11]. This incident had prompted an urgent requirement in the USA and other western countries for energy conservation programs to counter the adverse impact of the sharp rising cost in power generations. The early DSM programs in the USA were known as "conservation and load management" (CLM) [12]. At the same time, consumers responded positively to the DSM initiatives of the utilities under such circumstances.

Analysis made in [11] divides implementations of DSM in the USA, from its inception in the early 1970s to 1994 and onwards, into three phases. The first phase (from 1973 to the late 1980s) occurred in the period of high oil prices and DSM initiatives were implemented mainly to conserve energy and to reduce generation costs. When oil prices tumbled in the late 1980s, the DSM implementation entered its second phase where regulatory bodies had to provide incentives for the energy and utilities sector to continue pursuing DSM opportunities. The third phase began after the deregulation of the energy market in the USA in the 1990s where competition and market forces became the dominant drivers in DSM programs. Among other states in the USA, California (CA) and Vermont (VT) have very cost-effective DSM implementations [13]. Through its energy efficiency agency, VT has successfully reduced about 50% of the growth on its electricity load. Meanwhile, energy efficiency and DSM programs implemented in CA enabled that state to maintain almost constant electricity consumption per capita for the period between the early 1980s and 2004, while the rest of the USA had an average rise of about 50% in the same period [13].

To curb rising carbon emissions and the growth in energy intensity, the Chinese government has set an aggressive goal to reduce 20% of energy consumption per GDP for the period between 2005 and 2010 [13]. DSM initiatives are among the major initiatives to achieve this goal. Currently, DSM initiatives in China's power systems are primarily under central control. Studies in [14] reveal that the Chinese government has allocated an equivalent of US$3.08 billion to improve energy efficiency and to reduce pollution. As a result, reforms institutionalized at all levels

of government are expected to have long term positive effects in improving the energy efficiency for China.

Studies in [15] and [16] reveal that back in 2009, India faced major issues in its energy supplies. Its energy deficit was about 10%, while the shortage in peak capacity was about 13%. The Indian government enacted the Energy Conservation Act in 2001 to promote energy efficiency and conservation [16]. Plans to use more energy efficient devices and equipment represent the major DSM initiative for significant energy conservation in India [15]. DSM is estimated to potentially reduce peak demand in the range of 837 – 4,904 MW, and save energy in the range of 3,311 – 17,852 GWh. However, ineffective tariff systems hamper the effort to implement effective DSM programs in India, specifically its agricultural sector dominated by energy inefficient irrigation pumps.

## 1.2 Main Types of Demand-side Management Initiatives

Since its inception in the early 1970s, DSM is currently getting considerable attention in modern power systems around the world. The study conducted in [17] attributes the resurgence of DSM efforts in recent years to growing concerns over climate change, volatile fuel prices and shrinking utility reserve margins. Figure 1.2 shows the three major types of DSM that require different efforts to implement in a power system [17]. They are summarized below:

- Improve energy efficiency through technical advancements such as usages of energy efficient devices and equipment, upgrades of insulation, applications of enhanced building materials etc. Active consumer participation is expected to have a positive impact on the success of this DSM effort.
- Change demand profiles through LM programs that apply various methods of control mechanisms such as direct load control, autonomous demand response etc.
- Promote energy conservation through educational programs and financial incentives that alter consumer behavior to reduce wastage and conserve electricity [18]. The behavioral changes may be short term or become long term if they are incorporated into the lifestyle of a population [19].

The first two methods of DSM are further discussed in the following sub sections.

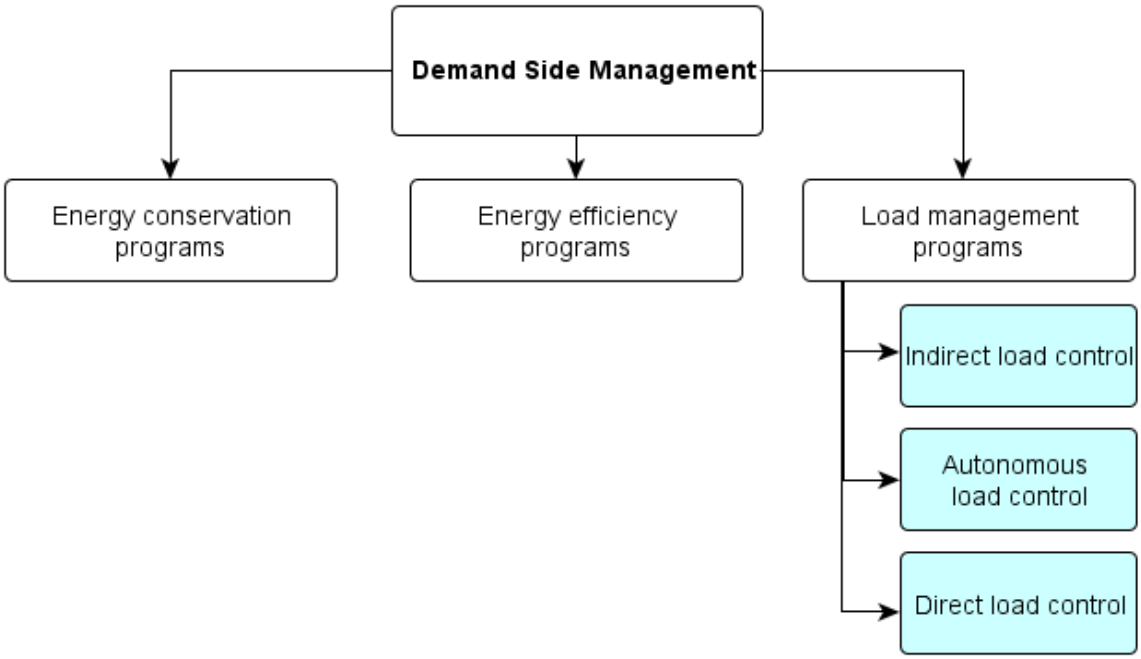


Figure 1.2 Block diagram of main components in DSM.

## 1.3 Energy Efficiency Programs

Energy efficient programs refer to initiatives that promote the permanent installation of energy efficient technologies and the elimination of energy losses in the existing system [19]. This section looks at the DSM policies and methods employed in some countries to improve energy efficiency in power systems.

Comprehensive analyses in [20] present the policy options in improving energy efficiency in Australia. Among other recommendations, this report proposes a multi-stage market reform that encompasses energy sectors and other related sectors such as building industry, commercial and industrial equipment sectors etc. To have long term effective results, the report also proposes to incorporate the energy efficiency criteria into future policies.

A number of DSM initiatives in stimulating technical changes to improve energy efficiency are discussed in [21]. These methods include encouraging the dissemination of energy efficient appliances through subsidy programs and comparison labeling, eliminating least efficient devices through standardization, and

advancing new technologies and innovations in energy efficiency through incentive. This paper provides the success story of comparison labeling in Australia where the sales of more energy efficient appliances have successfully reduced the average household energy consumption by 11% in 1992. Through standardization of efficiency for household appliances, Lawrence Berkeley Laboratory in the USA projected an energy saving of 7,000 TWh from 1990 to 2015 and an avoided power generation of about 21,000 MW in 2015 for the USA [21].

Meanwhile, research in [22] reports that national standards on minimum efficiency of appliances adopted in the USA have successfully cut electricity consumption by 88 TWh (equivalent to 2.5% of national electricity usage) in the year 2000. This paper also reports a projected energy saving of 0.35 EJ (equivalent to 97.2 TWh) by 2010 in Japan, from the revision of the Energy Conservation Law in 1998. This law introduces minimum energy performance standards for household appliances and promotes innovations in energy efficient technologies. Under the same law, the authors of [19] reports that energy-intensive industrial facilities in Japan are required to reduce their respective energy intensities by 1% annually. From reported statistics, about 52% of these facilities met the target in 2004.

Multinational energy efficiency policies adopted by the European Union (EU) countries in the 1990s have reduced the energy consumption of washing machines and dishwashers by 20%, and refrigerators and freezers by 27% [22]. In the case of China, the investments in end user devices with high efficiency have saved about 579 MW of generation in the Jiangsu province power system [10].

On the other hand, DSM initiatives to promote energy efficiency are sometimes perceived negatively as reduced revenue for the energy and utilities sector. Hence, regulatory or governmental incentives are occasionally required to support such initiatives. The study in [23] analyses the world's first trading scheme for energy efficiency certificates ("white certificates"), which commenced in New South Wales, Australia in January 2003. The findings discover that this trading scheme represents an effective mechanism for incentivizing the abatement of greenhouse gas emissions. An equivalent of about 10 million tonnes of carbon dioxide equivalent ($CO_2$-e) abatement was achieved by the end of 2006.

## 1.4 Load Management

Conventionally, LM represents various control methods that are applied to change the consumer demand profiles. As shown in Figure 1.2, there are three methods to implement LM in a power system:

- Indirect load control
- Autonomous load control
- Direct load control

### 1.4.1 Indirect load control

Indirect load control refers to demand response schemes that require active participation of consumers to make manual adjustments to change their respective consumption profiles. This LM method is usually associated with various time-sensitive pricing schemes such as time of use (ToU) pricing, real time pricing (RTP) and critical peak pricing (CPP) [24]. A common application of this LM method is the off-peak tariff for heating hot water storage tanks [25]. In a deregulated power sector, indirect load control relies strongly on market forces for effective demand responses during peak demand periods where the costs of electricity are the highest [26]. The research in [27] estimates the potential peak load reduction in the California (CA) power system via indirect load control of domestic air conditioner (AC) loads responsive to the RTP of electricity. In the case study presented, adjustment of the indoor temperature range between 68$^{o}$F (20$^{o}$C) and 72$^{o}$F (22.2$^{o}$C) is reported to shift more than 80% of energy consumption on AC during a peak period to non-peak periods, as compared to maintaining a constant indoor temperature at 70$^{o}$F (21.1$^{o}$C) throughout the entire period of measurement. Consumers responsive to such real time electricity pricing can potentially save about 30% of their respective costs on AC energy. In addition, this paper uses the actual “day ahead market clearing price” data of CA in its simulations and estimates a potential market cost saving of up to about US$600/MWh by shifting domestic AC loads from peak to non-peak hours. In [28], the Georgia Power Company in CA offers RTP to its large customers in an effort to reduce peak load of the network. As of 2002, 1,600 customers, representing about

5,000 MW of peak load, have enrolled in the program. As a result, about 18% of peak reduction is reported during periods of highest real time prices. Implementation of a time-sensitive tariff in each of two major load centers in China is discussed in [10]. The power system in Beijing city applies a differential tariff to its large customers and manages to shift about 200 MW of loads away from peak periods. Guangdong province counters its generation deficit effectively with an aggressive differential tariff that makes the peak hour rate 3.16 times more expensive than the off peak rate.

Voluntary load shedding is another form of indirect load control that provides significant peak load reductions by interrupting non time-sensitive but energy intensive loads in large commercial or industrial facilities [3]. For example, a potential 277 MW of peak load reduction is available from the commercial and irrigation customers in Texas and New Mexico (the USA) who voluntarily defer their respective electricity consumptions during network constraint periods. In return, the customers receive financial incentives in the form of discounted tariff or dispatch payments for the interruption events [3].

### 1.4.2 Autonomous load control

In autonomous load control, appliances or devices autonomously adjust their power consumption in response to detected changes in the power system, or to commands or pricing information sent from the network control center. This LM method relies on smart grid enabling technologies that provide bidirectional communications between the network control center and consumer premises. The study in [29] reports a recent trial in the distribution network of Western Australia (WA) to reduce its peak demand due to domestic AC systems. The trial utilizes smart grid enabling technologies to implement autonomous load control on 188 households. Advanced metering infrastructure (AMI) of individual participating households receives LM commands from the control center, and forwards them to the AC system fitted with a demand response enabling device (DRED) via a wireless channel. Initial results after one year of the trial indicate average demand reductions from 0.5 kW to 1.0 kW per AC system were achieved. Meanwhile, only one complaint related to consumer comfort was received for the entire duration of the trial. Currently, the Department of Climate Change and Energy Efficiency (DCCEE) in Australia is finalising the Australian

Standard AS4755 that defines the requirements for DREDs and ensures the interoperability between demand response enabling systems (including AMI), in-home devices and end use electrical appliances [30].

Experiments in [26] evaluated the price adaptive control mechanism of a meter gateway architecture on domestic AC units in response to real time, dynamic electricity pricing. Research conducted by the Pacific Northwest National Laboratory for the Department of Energy of USA examined the use of autonomous load control in providing primary frequency responses on a large interconnected grid [31]. This paper reports that in the event of supply imbalance, autonomous responsive loads can bring substantial benefits by responding to under-frequency events. Its frequency response characteristics were found to be analogous to the governor action of a generator.

### 1.4.3 Direct load control

Being a LM method where the loads are directly under central control, DLC has been traditionally utilized to reduce peak loads in distribution networks. Domestic hot water and AC loads are two common interruptible loads targeted for DLC. Consumers participating in DLC programs usually receive financial benefits from the utility companies in the form of rebates or upfront payments. In most of the implementations of DLC programs, bidirectional communications between the control center and controlled premises are not required.

For example, the DLC program implemented by Integral Energy of New South Wales (Australia) controls about 355,000 DHWSs and provides about 389 MW of potential peak load control [3]. In the USA, XcelEnergy® has successfully reduced 330 MW of peak summer load through direct control of central AC systems in the upper Midwest territory [3].

DLC of DHWSs is commonly implemented by applying a switching program that strategically switches the power supply of the controlled DHWSs on and off to achieve the required peak load reduction.

The first step in designing a DLC program for DHWS is to obtain the available domestic hot water load. There are different methods reported in the literature to

estimate this controllable load. The approaches used in [32]–[34] require actual measured load data in the estimation; whereas [35]–[39] use a modeling approach to approximate domestic hot water loads.

To estimate the total available domestic hot water load in a controlled area, a practical method reported in [32] uses a ripple injection system to cycle all the DHWSs at a regular interval (15 min) over 24 hours. During the periods when the DHWSs are switched off, dips are detected in the measured total load of a substation. These periodic reductions in the measured load represent the available domestic hot water load on that substation. Meanwhile, smart grid infrastructure enables energy consumptions of individual households to be measured in almost real-time. Although not directly measurable, domestic hot water load can be extracted and estimated from the measured load of a household. Such a load extractor based on an artificial neural network is proposed in [33]. Actual hot water and total load data of selected households are used as training data to train the neural network. This method achieves over 87% accuracy in matching the actual hot water consumption profiles over the test interval. A different approach is used in [34] to extract hot water load from measured total load data of individual households. The authors of this paper propose a method to scan the measured load data of a household and look for jumps and dips that are equal or close to the rated power of the installed DHWS. The hot water load profile of a single household can be estimated by using these jumps and dips to identify the starting and finishing times of hot water tank recharges throughout the measurement period.

On the other hand, the authors in [35] propose a generic model to estimate the aggregate hot water load profile for an area. They consider three significant hot water usages per day (in the morning, midday and evening) and assume the starting times of these usages are normally distributed. Then, the error function (ERF) is used to calculate hot water load profiles representing morning, midday and evening loads for the area. Additional loads, which are assumed constant throughout the day, are added to the sum of these load profiles to form the aggregate hot water load profile for the area. Another paper [36] makes further improvements to the above method of estimating hot water load profiles. This paper uses five significant hot water usages

(morning, mid-morning, midday, early evening and evening) instead of three as in [35]. It also proposes a model for calculating the load due to standing losses as opposed to using a constant value throughout the day. As a result, about 10% of improvement in representing the aggregate hot water load for an area is reported in [36], as compared to [35].

Meanwhile, [37]–[39] develop physical models of DHWS to estimate hot water load profiles without using actual measured load data. First, the hot water usage profiles of individual households are determined. Then, the physical model is used to calculate the loads associated with these hot water usage profiles. An aggregate hot water load profile is obtained by aggregating the average load profile of all the households in the area. However, these papers employ different approaches to determine their respective hot water usage profiles. The authors in [37] obtain hot water usage profiles based on data available from the NAHB Research Center Inc. and assign these profiles to individual households by employing the Monte Carlo approach. Data from load survey campaigns are used in [39] to determine the average hot water usage profiles. The authors in [38] derive hot water usage profiles for individual households in an area using the average load data obtained through load surveys for the area.

Many schemes for direct controlling of DHWSs have been proposed in the literature. Practical approaches in [3] and [32] use ripple injection systems to issue switching signals to households grouped under different modulation codes. Studies in [40] focus on voltage control to reduce domestic hot water loads. They demonstrate that the peak of hot water load can be reduced significantly by switching the operating voltage from 220 V to 110 V during peak hours. The water temperature inside each DHWS can be maintained between the thermostat set-points if the hot water flow rate is below a calculated value. In [39], hot water load profiles are simulated using physical models of domestic loads. Households are grouped by the family size to study the effect of DLC switching programs on peak load reduction and consumer comfort level. In [41], peak load reduction is studied by considering the number of switching groups, target value, control for ToU, and a single time-triggered control. In [42], evolutionary algorithms form the basis for optimizing DLC

switching programs to meet multiple objectives, such as maximizing peak reduction while maintaining network operator's profit and customer satisfaction. A smart grid based control algorithm performing DLC on modified DHWSs is proposed in [38] to regulate the aggregated power consumption. Linear programming is used in [43] to find optimal DLC strategies in achieving peak reduction on domestic hot water load.

## 1.5 Values of DSM in Modern Power Systems

This section presents the value of DSM implementation in modern power systems. The deregulation and restructuring of the electric power sector in many countries have created more competitive energy markets. A simplified structure of a power system in a deregulated market is shown in Figure 1.3 [44]. The flows of energy, money and information between the entities are indicated by different types of line. In a restructured power system, power generation is separated from transmission and distribution operations to encourage fair competition among the generation companies. An independent system operator oversees the operations of the whole power system to maintain the balance in supply and demand. It also ensures that an open and equal access of transmission and distribution facilities is provided to relevant network entities. Generation companies bid to supply electricity to a wholesale market which retailers buy from at spot prices. Consumers are free to choose the retailer who provides the best combination of price and services.

Staying cost efficient while ensuring supply security is a major challenge all the stake-holders in a power system face. DSM programs offer the opportunity to improve operational efficiencies and provide financial gains for the stake holders in a power system [45]. Besides, the reduction in energy consumption through various DSM efforts provides an overall prospect to reduce the net carbon emission produced in a power system.

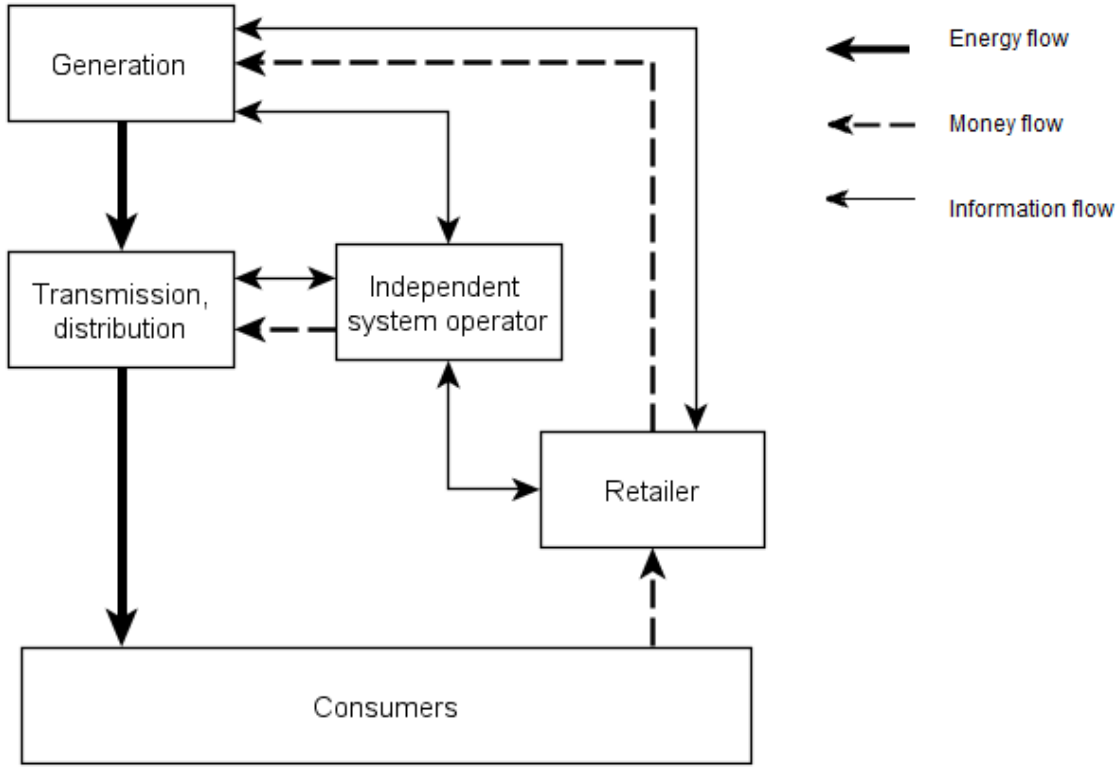


Figure 1.3 The simplified structure of a deregulated power system.

### 1.5.1 Value of DSM in power generation

Improved energy efficiency and reduced peak demand achieved through DSM efforts enable power generators to defer or avoid building new plants. This opportunity represents major cost reduction and potentially leads to lower energy prices.

Under normal operating conditions, significant generation reserves at a plant must be planned for and provided by standby resources to ensure security in supply. However, such generation resources planned for contingencies are rarely utilized and represent inefficient utilization of investments. With the growing integration of fundamentally intermittent renewable energy sources into modern power systems, conventional back-up generators are essential to ensure supply security by maintaining the balance of supply and demand at all times [46]. The *availability factor* of a generator is defined as the percentage of operational time over a period of one year [47]. As an example, Figure 1.4 shows the *availability factor* of four high-wind stations in Taiwan for a period of 12 months.

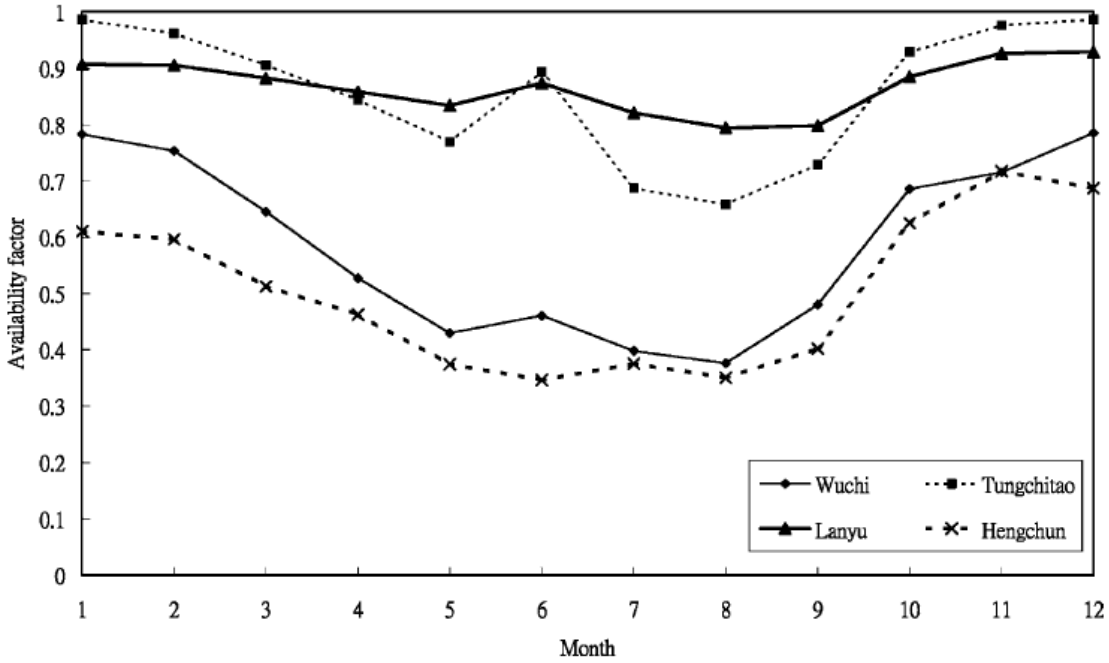


Figure 1.4 Monthly *availability factors* for four high-wind stations in Taiwan [47].

The intermittent nature of wind generation is obvious in Figure 1.4, where the *availability factor* varies from below 0.35 to close to unity. As a comparison, the *availability factor* of a combined cycle gas turbine power generator ranges from 0.87 to 0.97 [48].

DSM represents a significant capacity that can be utilized as an alternative reserve to reduce a portion of required back-up resources in generation. For example, the study in [49] estimates there was about 38 GW of demand response capacity in the USA in 2008. As reported in [31], autonomous responsive loads provide substantial benefits to a power system in frequency control during contingencies. Hence, DSM has the potential to replace part of the conventional back-up generation and allow substantial cost savings in a power system [45].

### 1.5.2 Value of DSM in power transmission systems

Preventive security is traditionally designed into the capacity of a transmission network to enable it to remain operational in a secure condition under an N−1 contingency [50]. N−1 contingency refers to the worst single contingency scenario following the outage of the most important transmission or generation facility. With the advancements in smart grid enabling technologies, [45] argues that swift DSM

action in curtailing specific loads after outages can provide an effective corrective security measure, which enables the transmission network to operate at a higher loading with the existing capacity. Hence, effective DSM programs potentially allow a transmission system operator (TSO) to operate a transmission network at an augmented utilization while maintaining the existing level of security. Furthermore, the implementation of effective DSM programs reduces the peak load flow on a transmission network. As a result, network congestions are relieved and transmission losses are reduced.

### 1.5.3 Value of DSM in power distribution systems

DSM programs are effective means to reduce peak loads and relieve overloads in distribution networks. As a result, the effective implementation of DSM programs provides financial and operational benefits to DSOs. DSOs have the opportunity to defer costly infrastructure upgrades and capacity expansions, while retaining the existing level of security [45]. At the same time, the author in [45] proposes that with reduced load flow over the distribution network, a higher number of distributed generations (DGs) can be integrated into the network. Distributed generations are small scale generations of low carbon energy sources (e.g. photovoltaic, small wind turbine etc.) and they are located near the loads. The main benefits of DG are reductions in carbon emissions, power delivery costs and energy losses [51].

### 1.5.4 Value of DSM to consumers

Most of the time, consumers receive financial incentives for their participation in DSM programs organized by the supplying utility companies. The financial incentives are offered as discounts on energy bills or cash payments [30]. For example, [3] reports that a discount of up to A$0.39 per kWh is offered to households charging their hot water storage systems during off peak hours in New South Wales (Australia). Meanwhile, [3] also reveals large commercial and industrial customers receive bill discounts and dispatch payments for voluntarily shedding non time-sensitive loads on short notifications. Hence, it is expected that DSM programs offering incentives to consumers will encourage active participation and achieve better results.

## 1.6 Conclusion

This chapter has provided a review of DSM, which includes an introduction to DSM and its brief history, different types of DSM and the respective implementations around the world, and the values of DSM to the stake-holders in a modern electric power system.

DLC is one of the DSM methods preferred by DSOs because implementations of DLC programs have produced positive results in distribution networks. Hence, we have developed an evaluation tool to assist a DSO in estimating and evaluating the results of a DLC implementation. Details of this tool and its individual components are presented in succeeding chapters.

# Chapter 2

## Hot Water Evaluation Tool

This chapter describes the hot water evaluation tool developed to estimate and evaluate the results of implementing DLC to domestic water heating loads. This tool was developed to assist the design and planning of DLC programs in implementing DSM in a power distribution system. We chose MATLAB as the platform to develop this tool because of its flexibility, powerful charting abilities and rich graphical user interface (GUI) features.

Section 2.1 presents the structure of the developed tool and the main functional blocks in the tool. Section 2.2 describes the user input data required by the tool in performing simulations. Section 2.3 provides brief descriptions for the main modules in the simulation block and outputs from the tool are presented in Section 2.4. A conclusion is provided in Section 2.5.

### 2.1 Structure of the tool

Figure 2.1 shows the overall structure of the developed hot water evaluation tool which consists of three main functional blocks. More specific modules defined under each main functional block are depicted as white rectangles. Numbered circles represent the inputs and outputs (I/Os) of the modules.

The input block contains all the user input interfaces to display and acquire the required data for the tool to run. Four independent modules within the simulation block perform essential simulations. The results of the simulations are evaluated and passed to the output block. Tool users have an option to export the results as a formatted output file. The operation of the tool is described as follows:

The input block represents the user interface, which allows the tool user to enter parameters required for performing simulations (e.g. the number of households in the controlled area, the number of Monte Carlo simulations, the desired peak reduction, etc.), as well as to view default parameters and change them if necessary. The main

block of the tool is the simulation block, which contains four modules that perform the required simulations. The output block contains the exporter, which exports the data to an external (MS Excel format) file.

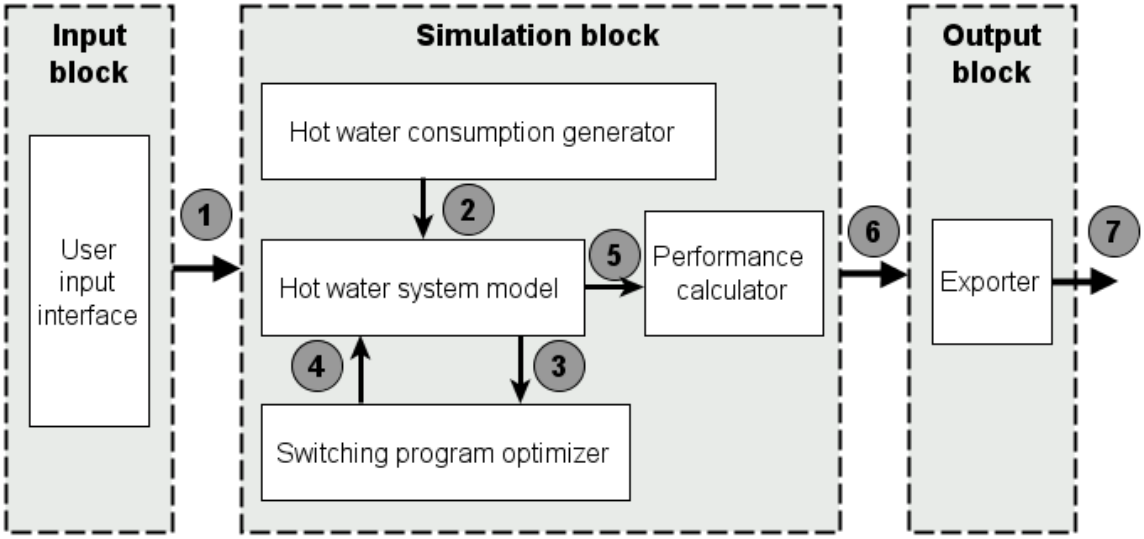


Figure 2.1 Overall structure of the hot water evaluation tool.

I/O 1 represents default parameters and parameters entered by the user via the user input interface. The hot water consumption generator receives I/O 1 and determines hot water consumption profiles for individual households; these profiles are represented by I/O 2. The hot water system model uses I/O 1 and I/O 2 to calculate uncontrolled hot water loads and shower temperatures for the households; the results are represented by I/O 3. The user can examine the aggregate uncontrolled hot water load curve of the households in the controlled area, and proceed with the optimization of switching programs. The switching program optimizer receives I/O 3 and produces switching programs based on the user-defined parameters (the desired peak reduction target, control periods etc.). The best switching programs are presented to the user, so that he/she can select the most suitable switching program. The hot water system model then calculates controlled hot water loads (I/O 5) by applying the user-selected switching program (I/O 4) and the hot water consumption profiles (I/O 2). The performance calculator receives I/O 5 and determines KPIs such as peak reductions and consumer comfort levels. Results in the form of 24-hour load curves and KPI tables are presented to the user (I/O 6), and exported to an external file (I/O 7) via the exporter.

The hot water evaluation tool is designed as a GUI-based tool. The main user interface of the tool that provides access to all functions developed for the tool is shown in Figure 2.2. In this figure, user interfaces belonging to the same functional block (Figure 2.1) are grouped and labeled as shown. Individual modules shown in Figure 2.1 are integrated into the tool.

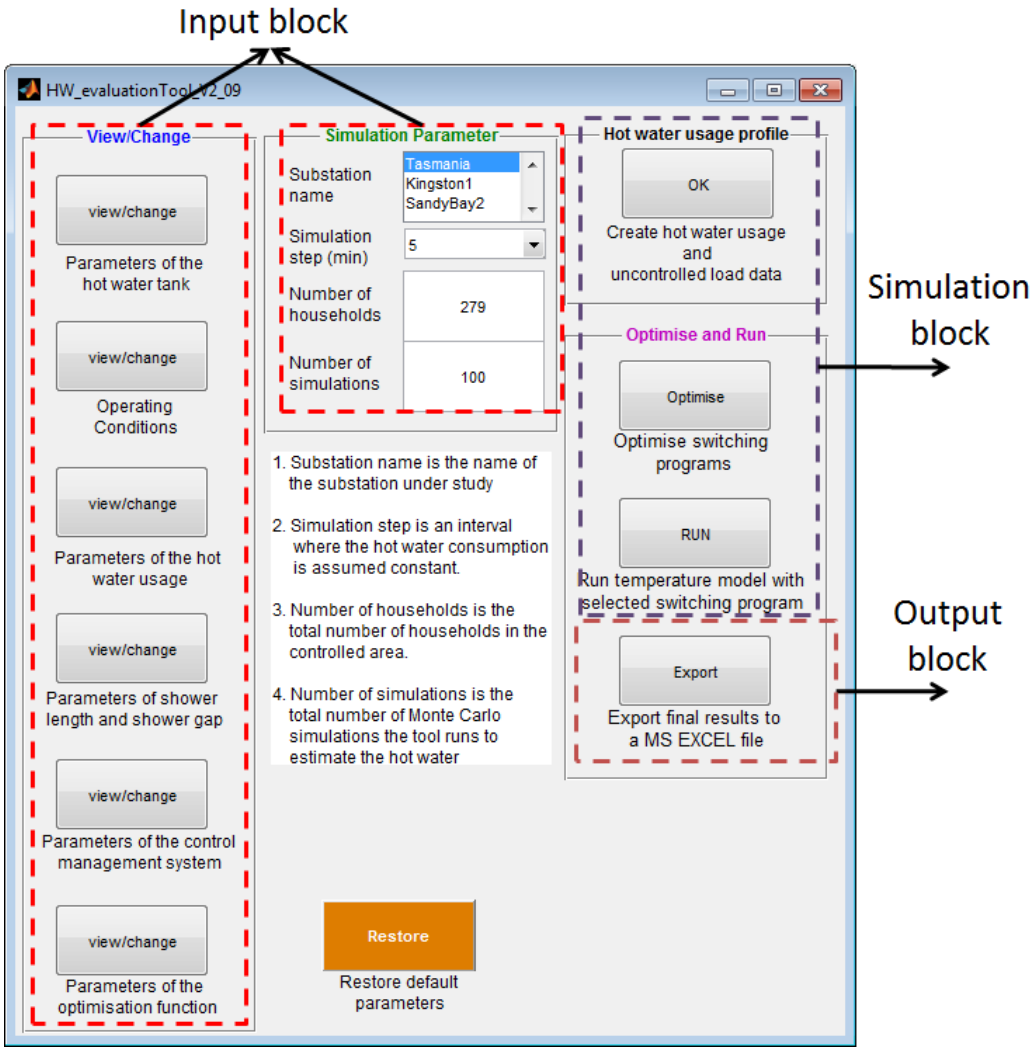


Figure 2.2 Main GUI of the hot water evaluation tool.

## 2.2 User inputs

The input block consists of several GUIs which the tool user utilizes to view or change the value of configuration parameters before starting a simulation. In the current version of the tool, there are seven categories of configuration parameters that a user can change freely. They are described in more detail in the following sections.

### 2.2.1 General operation of the user input GUIs

Every user input GUI has been built to perform inline data integrity checks on the entered values to reject any invalid entries such as text in place of numeric data, mixture of text and numeric data, complex numbers etc.

In addition, each configuration parameter has a predefined valid range and a predefined expected range. The tool displays an error message if the entered value for a parameter is not within its predefined valid range. A warning message is displayed if the entered value is outside of its predefined expected range. The examples of an error message and a warning message are shown in Figure 2.3 and Figure 2.4, respectively.

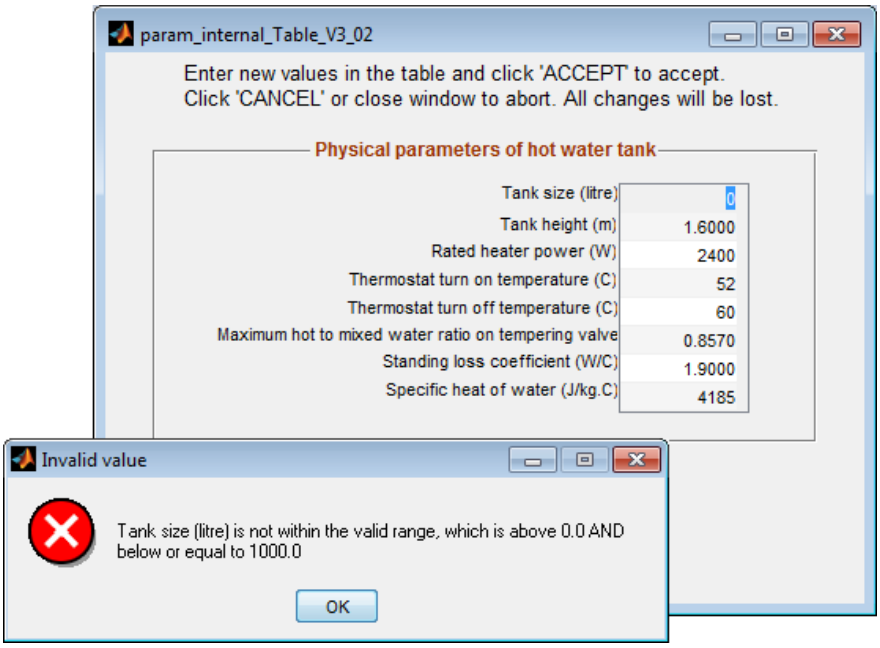


Figure 2.3 An error message due to the entered value being outside of the valid range.

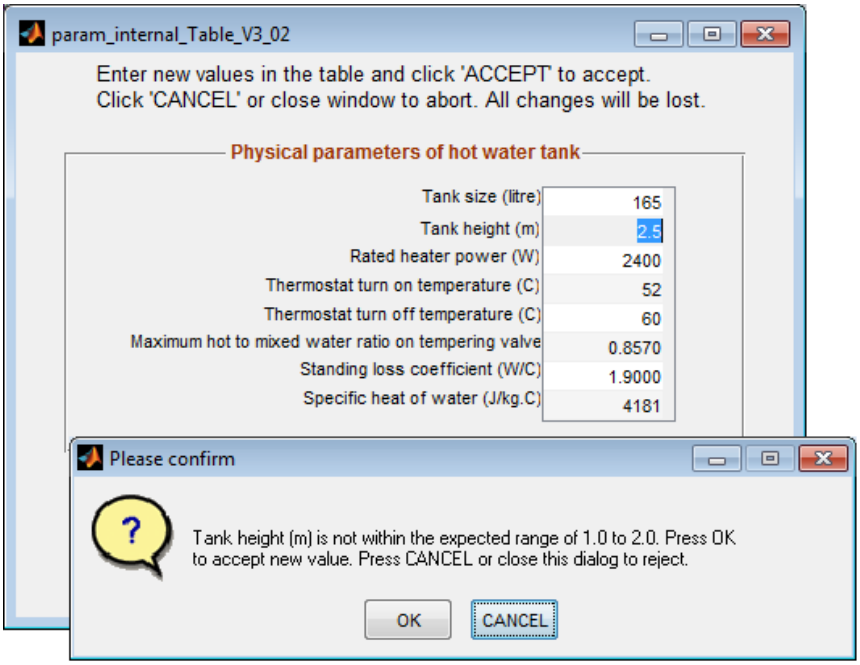


Figure 2.4 A warning message due to the entered value being outside of the expected range.

### 2.2.2 Simulation parameters

The parameters under this category determine the configuration of the simulations. These parameters are:

- Name of the substation under study
- Simulation time step in minutes
- Total number of participating households in a controlled area
- Total number of Monte Carlo iterations used in generating domestic hot water consumption profiles for the households

The tool maintains a database for each substation. This database consists of the average load profile and default values for the entire set of configuration parameters specific to the substation. When a substation is selected from a list, the tool retrieves all the data for this substation from the database and updates the configuration parameters on the input GUIs accordingly with the retrieved values. This feature ensures consistency in the configuration of simulations, as well as reducing potential errors in manual data entries. Nevertheless, the tool user still has the option to change these configuration parameters via the GUIs before starting a simulation.

### 2.2.3 Parameters of the hot water cylinder

The GUI to view or change the physical parameters of a DHWS is shown in Figure 2.5. This figure also shows the typical default values for physical parameters of a DHWS. The descriptions of these parameters are presented in Chapter 4 Section 4.2.

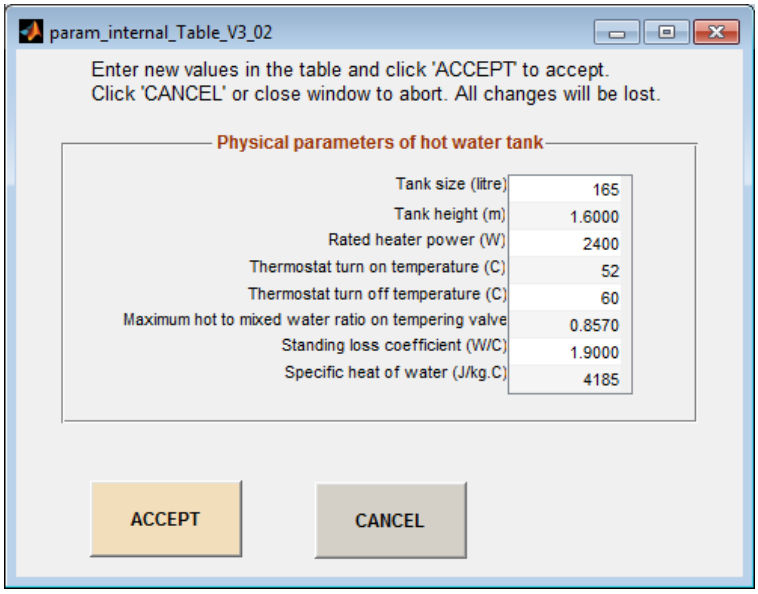


Figure 2.5 GUI for viewing or changing physical parameters of DHWS.

### 2.2.4 Operating conditions

Figure 2.6 shows the GUI for viewing or changing operating conditions of the DHWS. The typical default values of operating conditions are shown in the same figure.

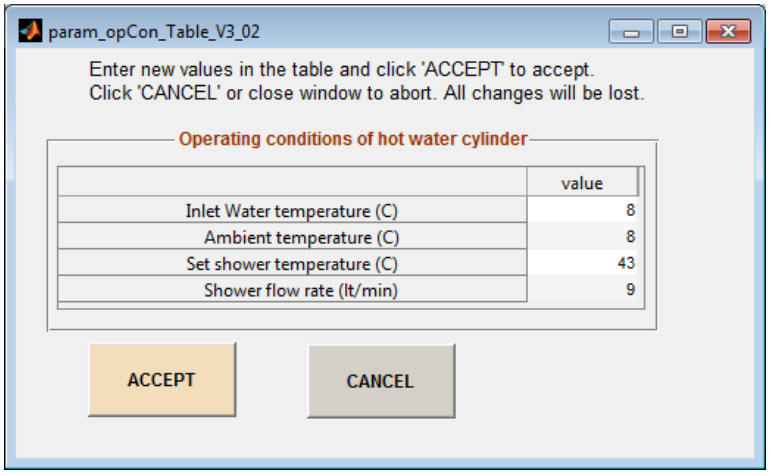


Figure 2.6 GUI for viewing or changing operating conditions of a DHWS.

### 2.2.5 Parameters of the hot water usage

This user input GUI lets the tool user view or change the configuration parameters used in determining the hot water consumption profile of individual households within a controlled area. The detailed descriptions for this set of configuration parameters are presented in Chapter 3.

### 2.2.6 Parameters of shower length and shower gap

This user input GUI lets the tool user view or change the configuration parameters used in configuring the shower schedules of individual households within a controlled area. The descriptions for this set of configuration parameters are presented in Chapter 3.

### 2.2.7 Parameters of the control management system

This user input GUI lets the tool user view or change the configuration parameters of the control management system, which the tool uses to produce DLC switching programs that are applied to the DHWSs in the controlled area. The descriptions for this set of configuration parameters are presented in Chapter 5.

### 2.2.8 Parameters of the optimization function

This user input GUI lets the user view or change the configuration parameters of the optimization function, which the tool uses in the optimization of DLC switching programs that are applied to the DHWSs in the controlled area. The descriptions for this set of configuration parameters are presented in Chapter 5.

## 2.3 Simulation block

As shown in Figure 2.1, the simulation block contains four main modules:

- Hot water consumption generator
- Hot water system model
- Performance calculator
- Switching program optimizer

They are integrated into the developed hot water evaluation tool to provide three different functions which are utilized in the design of a DLC program for controlling

DHWSs.

Details of the hot water consumption generator are discussed in Chapter 3 and the modeling of the most common DHWS model installed in Tasmania (Australia) is presented in Chapter 4. Chapter 5 describes performance calculations and presents details of the switching program optimizer.

## 2.4 Outputs from the tool

The developed hot water evaluation tool provides its users with an option to export the entire set of configuration parameters and simulation results to an external file. In the current version, the export file is a multiple-worksheet MS EXCEL workbook. This option allows tool users to maintain a record of configuration parameters and simulation results, as well as to perform further processing of the generated domestic hot water load profiles and the DLC switching programs.

## 2.5 Conclusion

This chapter has outlined the structure and the operation of the hot water evaluation tool developed to estimate and evaluate the results of implementing DLC on domestic water heating loads. The three main functional blocks and the respective modules under them have been described. The input block provides an interface for the tool user to view and enter values of configuration parameters, whereas the output block exports the simulation results to an external MS EXCEL format file. Interface windows of the input block are equipped with inline data integrity checking capability to reject invalid data. The simulation block contains four main modules, which are the hot water consumption generator, hot water system model, performance calculator and switching program optimizer. These modules perform core simulations in the tool and they will be presented in detail in the succeeding chapters.

# Chapter 3

## Estimation of Domestic Hot Water Consumption Profiles in Tasmania

This chapter presents the processes in estimating domestic hot water consumption in Tasmania, Australia. Section 3.1 discusses the data collected to estimate domestic hot water consumption patterns in Tasmania. It covers the results obtained from a telephone survey and the energy metering data downloaded from households across Tasmania. Section 3.2 outlines the development of a hot water consumption generator (shown in Figure 2.1) that estimates domestic hot water consumptions in Tasmania. The required input data as well as the estimation process are described. Section 3.3 presents some simulation examples, and a conclusion is provided in Section 3.4.

## 3.1 Domestic hot water consumption data

The first step in the development of the hot water consumption generator was to acquire knowledge of hot water consumption patterns of households in a controlled area. To achieve this objective, a telephone survey was firstly conducted on 1000 randomly selected households across Tasmania. Subsequently, actual energy metering data of 279 households across Tasmania was acquired. These data are utilized to obtain key characteristics in domestic hot water usage in Tasmania. Then, a hot water consumption generator uses these characteristics as inputs to estimate the hot water consumption profiles of individual households in a controlled area. The results obtained from these data are described in the following sections.

### 3.1.1 Survey results

The telephone survey recorded demographic data (e.g. number of usual residents, combined income etc.) and details of hot water usage (e.g. the average number of showers taken daily, average duration of each shower, etc.) of the surveyed households. This survey focused on two peak periods in the Tasmanian power distribution network, namely morning and evening peaks from 06:00 to 10:00 and

from 17:00 to 20:00, respectively. Figure 3.1 and Figure 3.2 show two major results of the survey. The questionnaire used in the survey is shown in APPENDIX 4.

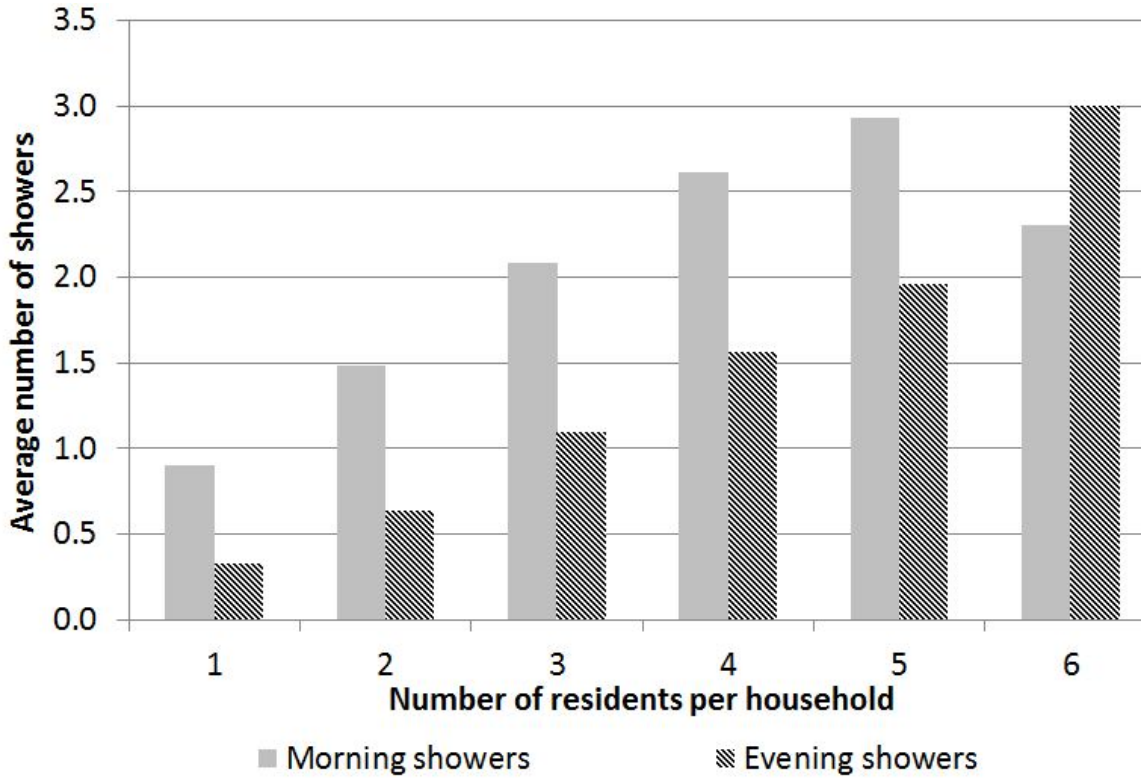


Figure 3.1 Average number of showers versus the number of residents per household.

Figure 3.1 suggests a positive correlation between the average number of showers and the family size, in the morning and evening peaks. This correlation agrees with the common expectation that bigger families take more showers than smaller families. The unexpected drop in the average number of morning showers in households with six or more residents is most likely due to the relatively small sample size of this category of households, which is just 2.3% of the total number of households surveyed.

We use statistical method to demonstrate the positive correlation between the average number of showers and the family size. First, we filter the survey results to discard the erroneous records. After that, we calculate from the filtered data the correlation coefficient *r* between the average number of showers and family size, and compare it with the critical *r* value in a 2-tailed test. If the calculated *r* is higher than the critical *r* value for the required significance level, we can conclude that a

correlation between these two parameters exists [52]. The results of the correlation test for morning and evening showers shown in Table 3.1 indicate a positive correlation exists between the average number of showers and the family size.

Table 3.1 Correlation between average number of showers and family size

| | **Calculated *r*** | **Degree of freedom** | **Significance level** | **Critical value of *r*** | **Correlation exists?** |
|---|---|---|---|---|---|
| Morning shower | 0.552 | 961 | 0.01 | 0.083 | Yes |
| Evening shower | 0.535 | 961 | 0.01 | 0.083 | Yes |

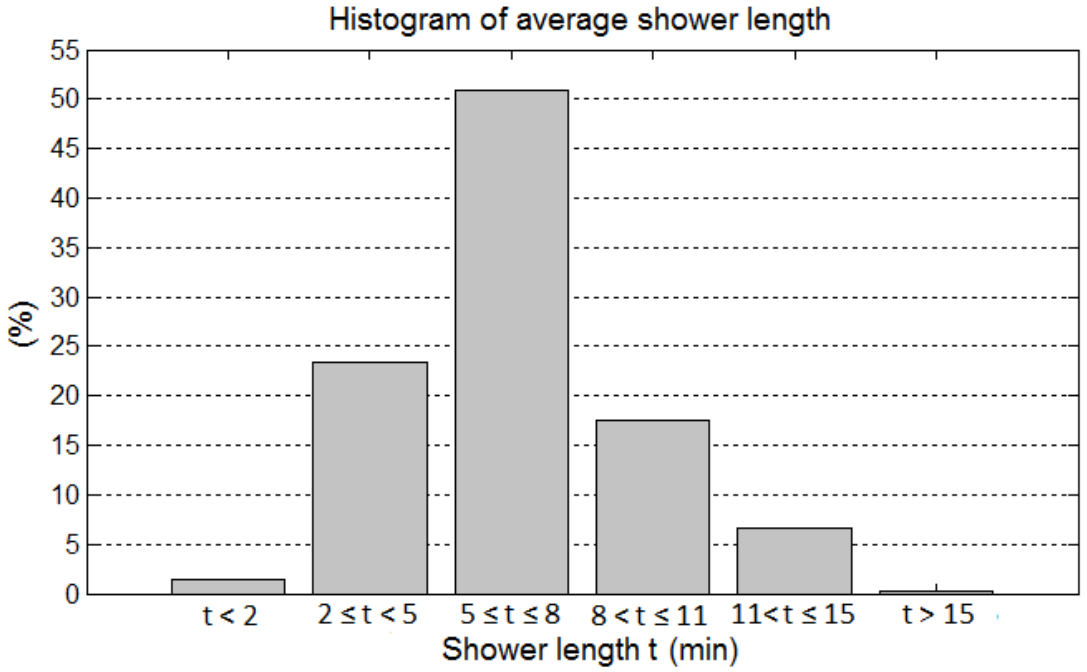


Figure 3.2 Histogram of the average duration of showers.

As seen from Figure 3.2, the average duration of a shower can vary from 2 min to 15 min, with a great majority of showers (about 51%) lasting from 5 min to 8 min. The mean and standard deviation of shower length were 6.5 min and 3.5 min, respectively, for the 963 filtered survey data.

Among other things, the survey also gathered data on the types of hot water system used in Tasmanian households. As shown in Figure 3.3, the majority (about 85%) of Tasmanian households use an electric hot water system. However, we cannot derive clear relationships between hot water usage and other demographic data such as

employment status and household income. For example, the vast variation of shower lengths within each demographic group prevents any conclusive inference.

Since the data obtained from the telephone survey were subjective answers given over the phone, the results are used as indicative guides in our development of the hot water consumption generator.

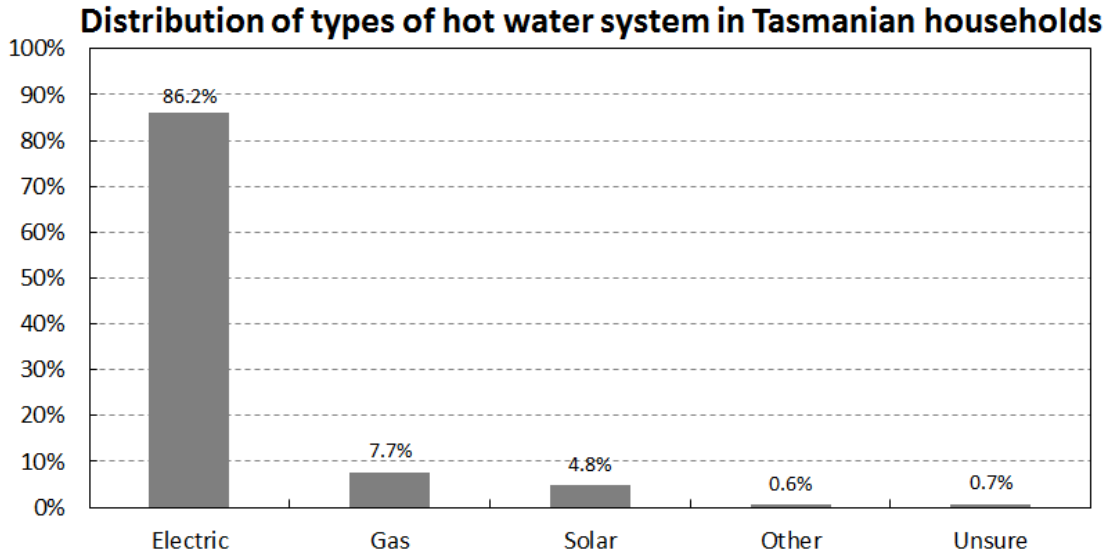


Figure 3.3 Distribution of types of DHWS among the surveyed households.

### 3.1.2 Actual energy metering data

To accurately estimate domestic hot water consumption profiles, we also acquired energy metering data from households across Tasmania. The collection period (from 20th June to 20th July 2012) included the coldest period in Tasmania. These data were obtained from meters dedicated for metering electricity in water heating alone, and represented water heating energy consumption of individual households recorded in 5-minute intervals. After the filtering process to discard erroneous data, we obtained the individual energy consumption profile of 279 households in water heating alone.

We considered two types of hot water usage:

- high volume usage that lasts for more than 5 min
- low volume usage that lasts for 5 min or less

Based on the results obtained from the modeling of DHWS (described in Chapter 4), 1 min of hot water usage requires approximately 10 min of heating to restore the

temperature set by the thermostat. Thus, a continuous energy consumption (a switched-on condition of the electric water heater) for a period of more than 50 min is regarded as a high volume usage (represented by showers), and a consumption of less than or equal to 50 min is regarded as a low volume usage. Using weekday data only, we derived probability distributions of the starting time for showers and low volume usages.

Figure 3.4 shows the probability distribution of starting time for showers, after applying the moving average method to smooth the data. Two distinctive peaks in the morning and in the evening are observed in the figure. This characteristic indicates high number of showers and hence high hot water loads occur during these two peak periods.

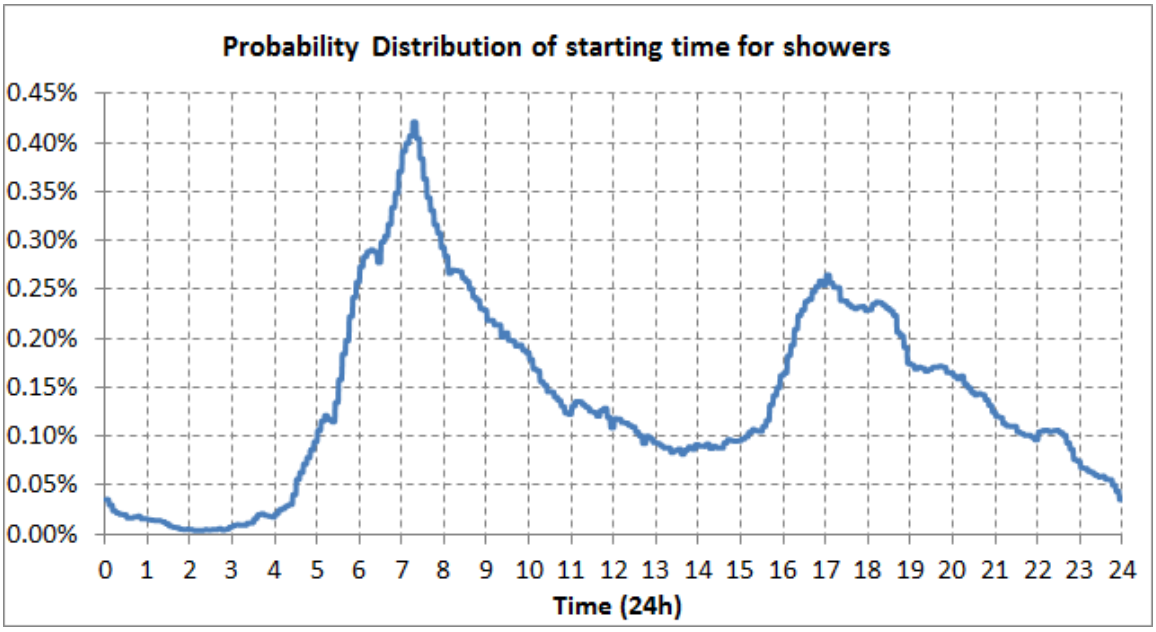


Figure 3.4 Probability distribution of the starting time for showers, smoothed by moving average.

Moving averages are calculated as in ( 3.1 ):

$$Y_S(i) = \frac{1}{2N+1} \cdot \sum_{j=-N}^{N} Y(i+j) \qquad (3.1)$$

where $Y_S(i)$ is the smoothed value of $Y$ at time interval $i$; $Y$ is the probability of starting time for showers derived from the energy metering data, before the smoothing method is applied; $N$ is the number of neighboring data points on either side of interval $i$; the term $(2N+1)$ is the averaging window.

We applied $N$ equals 5 and implemented ( 3.1 ) in a circular manner where the averaging window wraps around at the beginning and at the end of the list to yield uniform averaging across the entire list of data.

Deriving the probability distribution of starting time for low volume usages is not a straight forward task due to the following reasons:

- Depending on the operating conditions of the hot water storage tank (e.g. initial temperature, hot water flow rate etc.), a continuous draw of hot water for about two minutes or longer will usually trigger the thermostat to recharge the tank. Any shorter draws will not be recorded in the energy metering data.
- The energy metering data also records the energy consumption due to standing heat losses after the storage tank idles for a long period. This recharge period lasts for about 20 to 30 minutes, depending on the initial state of the storage tanks.
- Any low volume draws that occur during the recharging period of a hot water tank are not detectable in the recorded energy metering data.

The probability distribution of starting time for low volume usages derived directly from the energy metering data is shown in Figure 3.5.

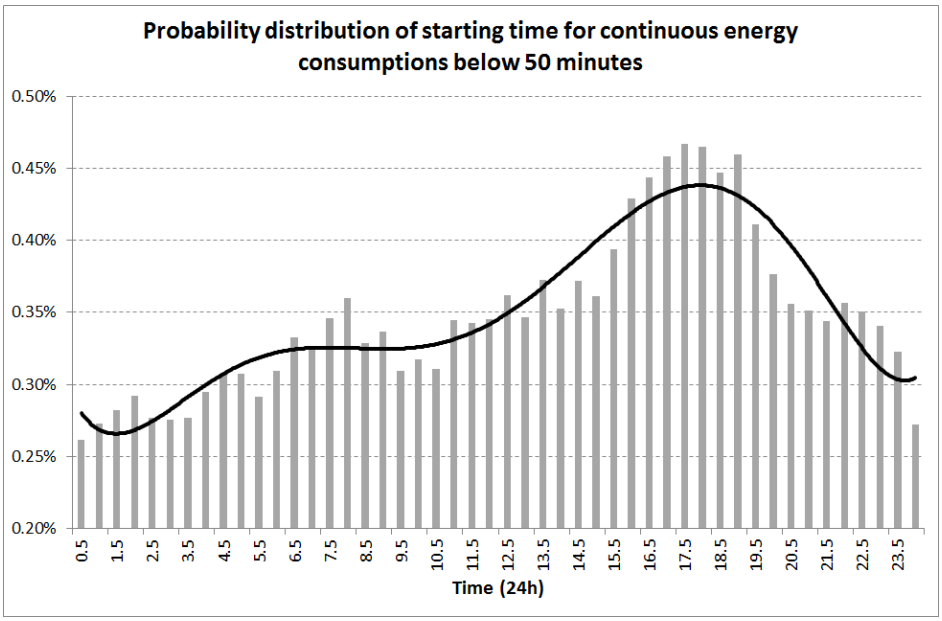


Figure 3.5 Probability distribution of starting time for low volume usages derived directly from energy metering data.

The probabilities are averaged for every 30 minutes. The solid curve depicts the trend line of the probability distribution, which indicates a peak period from around 16:00 to around 21:00.

To simplify the estimation of probability distribution of the starting time for low volume usages, we made the following assumptions:

- An average low volume usage is equivalent to a single 5 minute draw of hot water.
- Any periodic energy consumptions lasting 20–30 minutes and repeating every 11–16 hours are regarded as standing loss recharges. These energy consumption records are not related to hot water usages.
- The probabilities of low volume usages are averaged for every 30 minutes, and rounded to the nearest 0.025%.

The second assumption is based on ( 3.2 ) where $\tau_h$ is the time period (hours) between two consecutive recharges due to heat losses from the hot water storage tank alone; $M$ is the mass of water in the storage tank (kg); $C$ is the specific heat of water (J/kg·K); $U$ is the heat loss coefficient of the hot water storage tank (W/K); $T_{on}$ and $T_{off}$ are respectively the thermostat's turn-on and turn-off temperatures ($^oC$); and $T_a$ is the average ambient temperature ($^oC$).

$$\tau_h = \frac{M \cdot C}{U \cdot 3600} \cdot ln\left[\frac{T_{off} - T_a}{T_{on} - T_a}\right] \qquad (3.2)$$

Based on the results obtained from the modelling of DHWS (described in Chapter 4), a 20 – 30 minute recharge period is required to recover the heat energy lost through standing losses. The value of $\tau_h$ may vary over a wide range due to variations in the parameters used in ( 3.2 ). We considered two sets of common values for DHWSs in Tasmania, as shown in Table 3.2. Hence, any continuous energy consumptions lasting 20–30 minutes and repeating every 11–16 hours are regarded as standing loss recharges, and they are not associated with hot water usages.

Table 3.2 Time intervals between two consecutive recharges due to standing heat losses from the hot water storage tank, for two sets of common parameter values

| $\tau_h$ (hours) | $M$ (kg) | $C$ (J/kg·K) | $T_{on}$ (°C) | $T_{off}$ (°C) | $T_a$ (°C) | $U$ (W/K) |
|---|---|---|---|---|---|---|
| 16 | 165 | 4185 | 52 | 60 | 8 | 2.0 |
| 11 | 165 | 4185 | 53 | 60 | 8 | 2.5 |

The third assumption produces 48 average probabilities of starting time for low volume usages, corresponding to every half an hour in a day.

After filtering and processing the energy metering data with the above assumptions, we obtained the probability distribution of starting time for low volume usages, as presented in Figure 3.6.

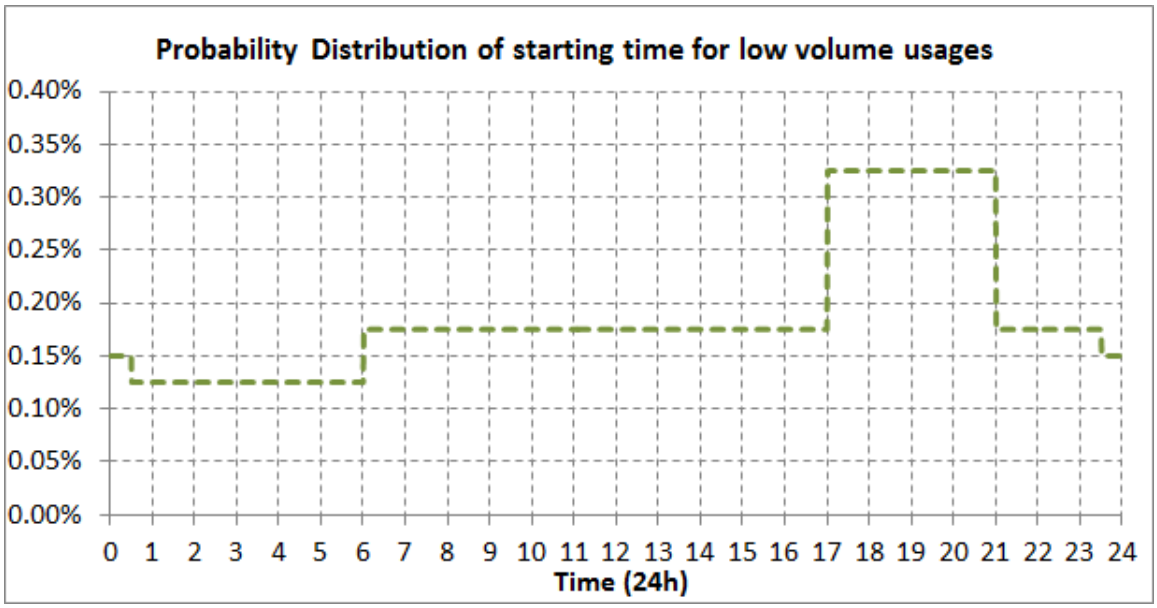


Figure 3.6 Filtered and processed probability distribution of starting time for low volume usages.

## 3.2 Hot water consumption generator

The hot water consumption generator is a module that produces realistic hot water consumption profiles for individual households. Figure 3.7 shows the block diagram of the hot water consumption generator that produces domestic hot water consumption profiles. Numbered blocks are inputs and the grey block is the output from this module.

The hot water consumption profile of a household is specified by four main

parameters:

- the number of hot water usages
- the length of each hot water usage
- the gaps between successive hot water usages
- the starting time of each hot water usage

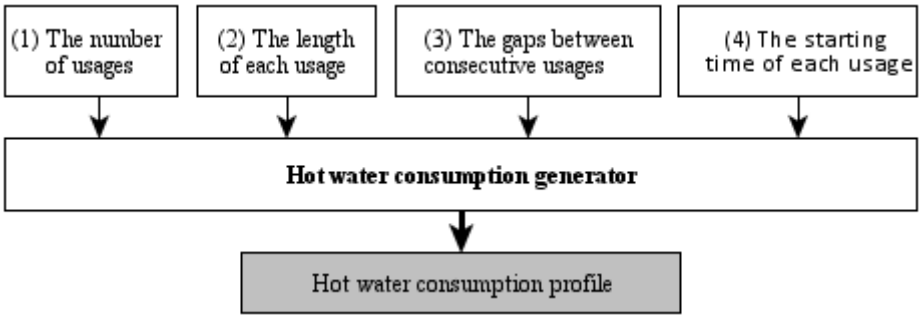


Figure 3.7 Block diagram of the hot water consumption generator.

In our studies, the hot water consumption profile of a household consists of two shower schedules and a number of low volume usages randomly occurring between these two schedules. A shower schedule refers to a number of showers (each shower with a different length) taken in successive sequence, with short gaps between each of them. Each household is expected to have either zero or one shower schedule in the morning and in the evening. The morning and evening shower schedules may contain different numbers of showers. A typical hot water consumption profile of a household is shown in Figure 3.8.

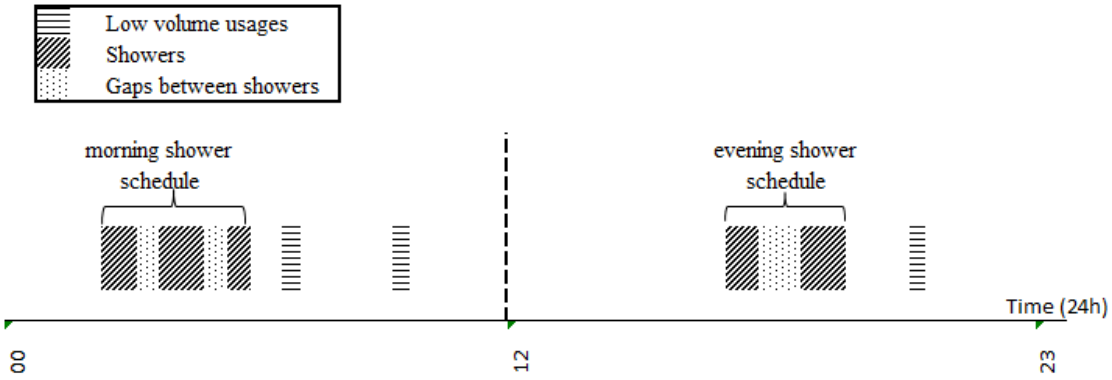


Figure 3.8 A typical hot water consumption profile of a household.

Both survey results and energy metering data revealed that domestic hot water consumption depends mostly on the family size. Therefore, we have divided all households in a controlled area into four family types based on the number of residents in a household. Table 3.3 shows a typical distribution of families in a controlled area.

Table 3.3 Family types and their distributions in a controlled area

| **Family Type** | **1** | **2** | **3** | **4** |
|---|---|---|---|---|
| Family size | Very small | Small | Average | Large |
| Number of residents | 1 | 2 to 3 | 4 to 5 | 6 and above |
| Distribution in a population | 25% | 50% | 22.5% | 2.5% |

We also specify probabilities of morning shower schedule only, evening shower schedule only or both, occurring in a household. The typical probabilities are shown in Table 3.4. Demographic data [53] and household energy consumption records are used to estimate probabilities shown in Table 3.5, which determine the number of showers each family type takes in individual shower schedules (morning, evening, or morning and evening).

Table 3.4 Probabilities for shower schedules to occur in the morning only, evening only and both

| | **Morning showers only** | **Evening showers only** | **Morning and evening showers** |
|---|---|---|---|
| Probability | 0.3 | 0.3 | 0.4 |

Table 3.5 Probabilities of number of showers in a shower schedule for each family type

| | **Number of showers** | | | | | |
|---|---|---|---|---|---|---|
| **Family type** | **0** | **1** | **2** | **3** | **4** | **5** |
| Type 1 | 5% | 95% | 0% | 0% | 0% | 0% |
| Type 2 | 0% | 41% | 53% | 6% | 0% | 0% |
| Type 3 | 0% | 20% | 60% | 19% | 1% | 0% |
| Type 4 | 0% | 7% | 40% | 47% | 5% | 1% |

Similarly to showers, the probability of a low volume usage depends on the family size of a household. The tool uses multipliers to scale this probability up based on the

family type. Default values of the multipliers are 1.0, 1.2, 1.6 and 2.0 for family type 1, type 2, type 3 and type 4, respectively. The tool user can redefine these values, if required. Figure 3.6 gives the probability of a low volume usage occurring in a household at a given time.

Shower lengths and gaps between consecutive showers are specified by their mean, maximum and minimum values. We define minimum and maximum to discard unrealistic values (e.g., a one-minute shower) in probabilistic simulations. Normal distributions are assumed for these two parameters. Default values used by the tool are shown in Table 3.6. On the other hand, a low volume usage is denoted as a single 5 minute draw. If required, the tool user can redefine these values.

Table 3.6 Default values for shower lengths and gaps between consecutive showers

| Parameter | Minimum (min) | Maximum (min) | Mean (min) | Standard deviation (min) |
|---|---|---|---|---|
| Shower length | 5 | 15 | 8 | 4 |
| Shower gap | 5 | 7 | 6 | 1 |

The probability distributions of starting time for shower schedules and low volume usages are shown in Figure 3.4 and Figure 3.6, respectively. We derive from Figure 3.4 the cumulative probability distribution curves shown in Figure 3.9, and use it to determine starting times of morning and evening shower schedules in a household. The curves from 00:00 to 11:59 and from 12:00 to 23:59 are used to determine the starting times of morning shower schedules and evening shower schedules, respectively.

The tool employs a Monte Carlo approach to generate hot water consumption profiles for each household. First, the tool generates random values to determine specific parameters for a single household:

- family type
- shower schedules (morning, or evening, or morning and evening)
- number of showers in each shower schedule
- number of low volume usages

- length of each shower and each gap between consecutive showers
- starting time for each shower schedule and each low volume usage

Next, using these parameters, the tool generates a 24 hour hot water consumption profile for a single household (similar to the one shown in Figure 3.8). The tool then repeats the profile generation process for a specified number of households using a new set of random values each time. Finally, the whole process is repeated for the required number of Monte Carlo iterations.

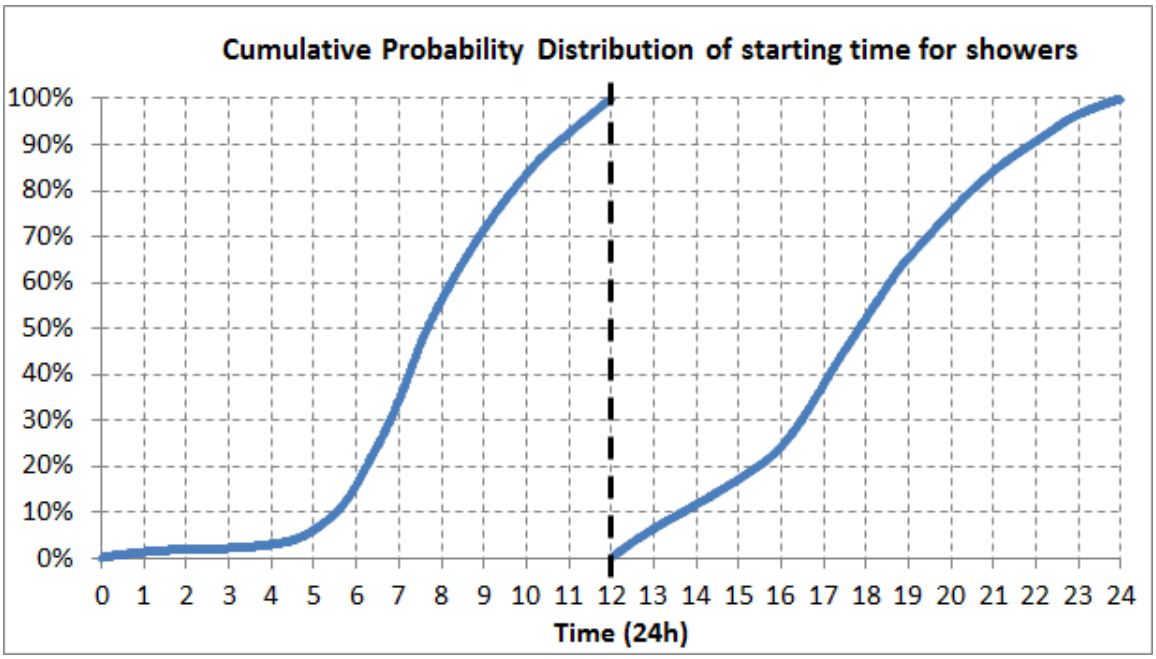


Figure 3.9 Cumulative probability distribution of starting time for showers.

The flowchart in Figure 3.10 outlines the main operations of the hot water consumption generator in creating the hot water consumption profile for a household in each iteration. Individual functional blocks shown in Figure 3.10 are presented as flowcharts in Appendix 3.

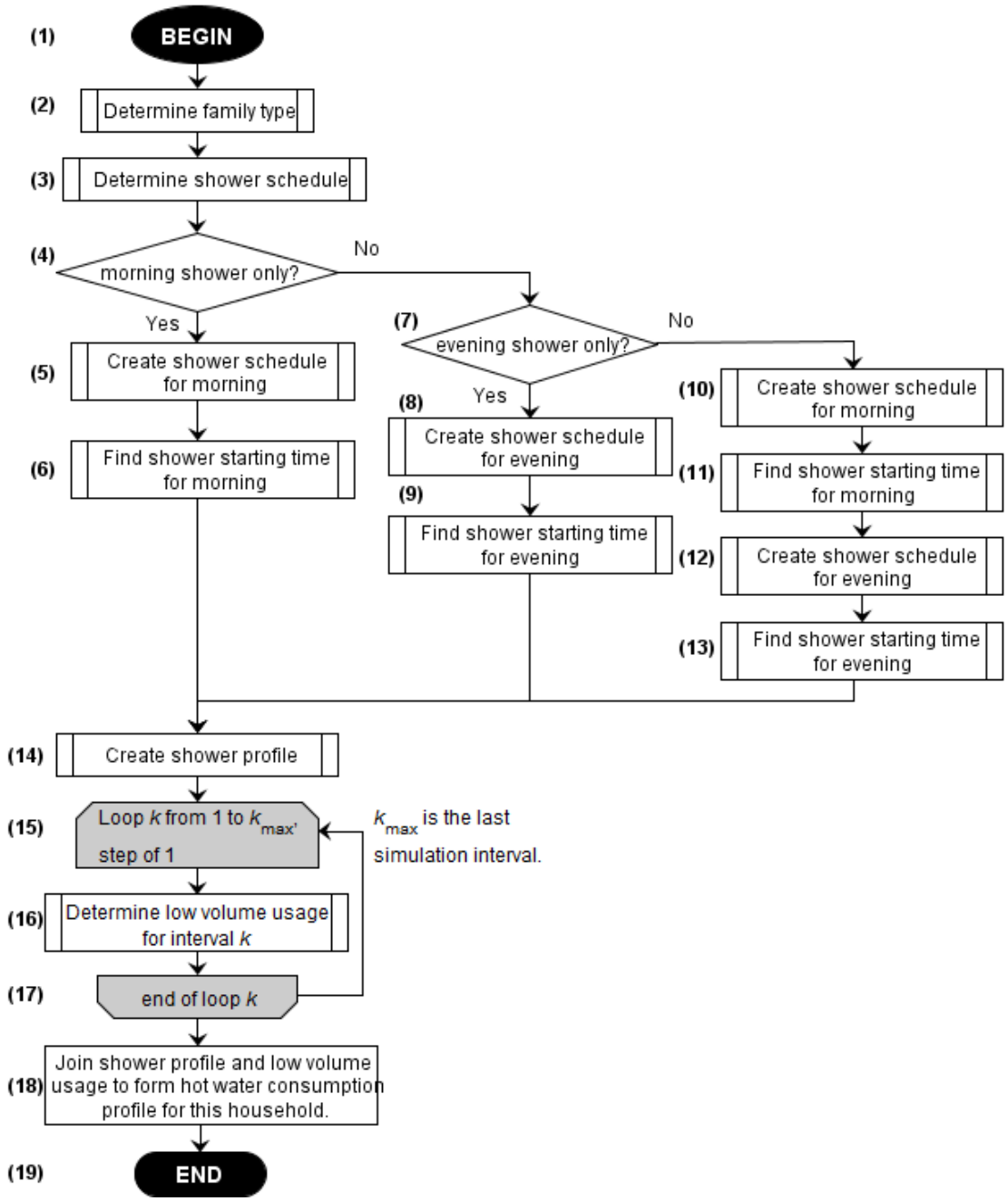


Figure 3.10 Flow chart showing main operations of the hot water consumption generator.

### 3.2.1 Hot water consumption profile

The hot water consumption generator creates a time-based hot water consumption profile for each household per Monte Carlo iteration. A hot water consumption profile is a sequence of "0"s and "1"s. A "0" indicates no hot water usage while a "1" indicates hot water is being drawn from the hot water storage tank at the current time interval. The average hot water profile of a household is obtained by averaging its hot

water consumption profiles over the specified number of iterations. Aggregating the average hot water consumption profile of all households forms the aggregate hot water consumption profile of the controlled area. The calculation is shown in ( 3.3 ).

$$\bar{W} = \sum_{i=1}^{N_H} \frac{1}{N_S} \cdot \sum_{j=1}^{N_S} w(i,j) \qquad (3.3)$$

where $\bar{W}$ is the aggregate hot water consumption profile of the controlled area; $N_H$ is the total number of households; $N_S$ is the total number of Monte Carlo iterations; and $w(i, j)$ is the hot water consumption profile of household $i$ in iteration $j$.

## 3.3 Example of domestic hot water consumption profiles

Figure 3.11 shows the average hot water consumption profiles for family type 1 to type 4. The hot water consumption generator uses the parameters provided in Section 3.2 and produces these results for 500 households in 1000 Monte Carlo simulations. The graphs depict average number of households using hot water over 24 hours, in 5 minute intervals.

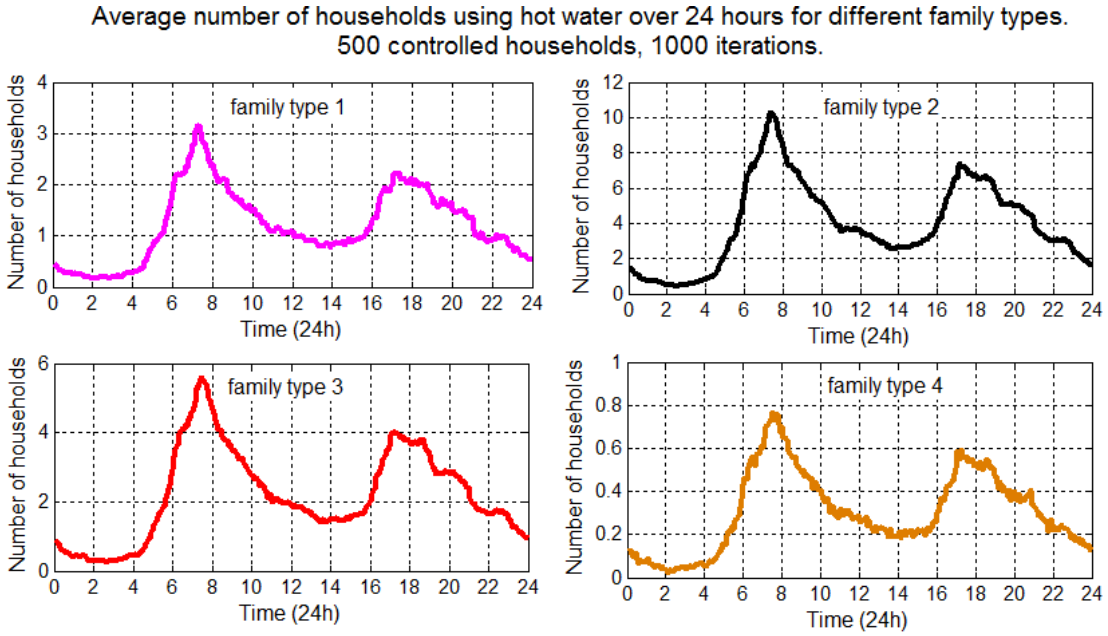


Figure 3.11. Average hot water consumption profiles for family type 1 to type 4.

The majority of hot water usages occur in small families (family type 2), while only a small fraction of usages occur in large families (family type 4). For example, on average, there are about 10 small families using hot water during the peak period at around 07:30, whereas there are only about 0.8 large families using hot water in the

same period. This result is consistent with the distribution of family types as shown in Table 3.3. However, large families consume more hot water per household compared to small families.

Figure 3.12 shows the aggregate hot water consumption profile for 500 households representing all family types in the simulation.

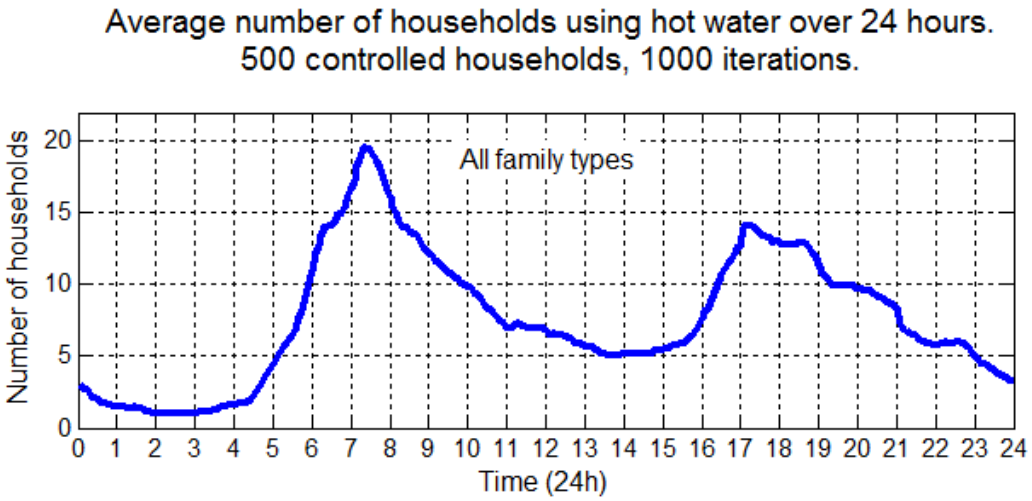


Figure 3.12 Aggregate hot water consumption profile for all family types.

## 3.4 Conclusion

This chapter has described the processes in the estimation of domestic hot water consumption in Tasmania, Australia. Survey data and actual energy metering data were used to determine key characteristics in domestic hot water usage. A positive correlation has been found between the family size and the average number of showers taken daily. Moreover, the operation of a hot water consumption generator has been outlined in detail, and the main parameters used to specify the hot water consumption profile of a household have been discussed. This chapter has also described the Monte Carlo probabilistic simulation employed in the hot water consumption generator. In addition, simulation results representing the hot water consumption profiles for four family types have been presented as an example.

The succeeding chapters will present the other modules under the simulation block shown in Figure 2.1.

# Chapter 4

## Domestic Hot Water System Modeling

This chapter aims to present the modeling of the most common DHWS found in the majority of households in Tasmania, Australia. This model is depicted as the hot water system model in Figure 2.1. Section 4.1 gives a brief description of the operation of a DHWS. Section 4.2 presents the mathematical modeling of a thermally stratified DHWS with heat energy equation. Section 4.3 presents results of comparative analyses between the model and experimental data. Discussions on the results are presented in Section 4.4, and a conclusion is provided in Section 4.5

## 4.1 Operation of a domestic hot water system

Figure 4.1 shows the simplified block diagram of a typical DHWS.

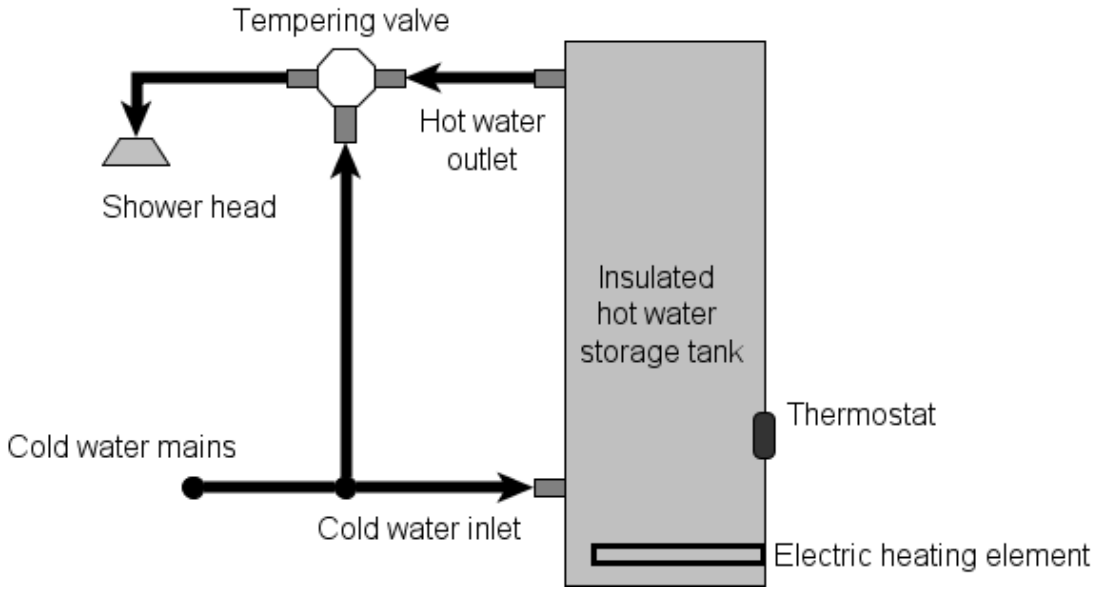


Figure 4.1 Simplified block diagram of DHWS.

A DHWS is made up of the following main components:

- An insulated cylindrical hot water storage tank usually made of stainless steel.
- An electric heating element located at the bottom of the tank. To enhance hot water supply capacity, some models are equipped with a booster heating element

located at the upper section of the storage tank. However, DHWSs with a single heating element are the most common models in Tasmania.

- A cold water inlet and a hot water outlet.
- A thermostat that controls the operation of the heating element, based on the temperature inside the tank.
- A tempering valve that regulates the water temperature at the usage outlets.
- A pressure relief valve as safety measure.

During a shower, cold water at mains pressure flows into the bottom part of the storage tank, while hot water flows through the outlet at the top of the tank and enters the tempering valve. The tempering valve regulates the water temperature at its outlet to a preset value by mixing the right amount of hot (from hot water storage tank) and cold water (from mains supply). A thermostatic element immersed in the mixed water contracts or expands to move a piston that regulates the flow of hot and cold water entering the valve [54]. Figure 4.2 shows the schematic diagram of a typical tempering valve.

As drawing of hot water continues, the water temperature inside the storage tank drops progressively from bottom to top. When the thermostat, located in the lower part of the tank, detects a temperature below the preset turn-on temperature, it switches on the heating element which starts heating up water in the tank. The same thermostat switches off the heater when the water temperature reaches the preset turn-off temperature. In other words, the thermostat maintains the water temperature between the turn-on and turn-off temperatures.

Heat energy is also lost through the insulated wall of the storage tank at a very slow rate. Over a long period of standing time, the water temperature inside the tank will gradually drop below the turn-on temperature, which causes the thermostat to start the heating cycle.

The operating temperatures of the DHWS in Australia are governed by Australian Standard AS 3498. The standard requires heating the water to at least $60^{o}C$ to inhibit Legionella bacteria growth in the storage tank. At the same time, hot water coming

out from any outlet and having direct contact with consumers must be below 50$^{o}$C to prevent scalding and injury [55].

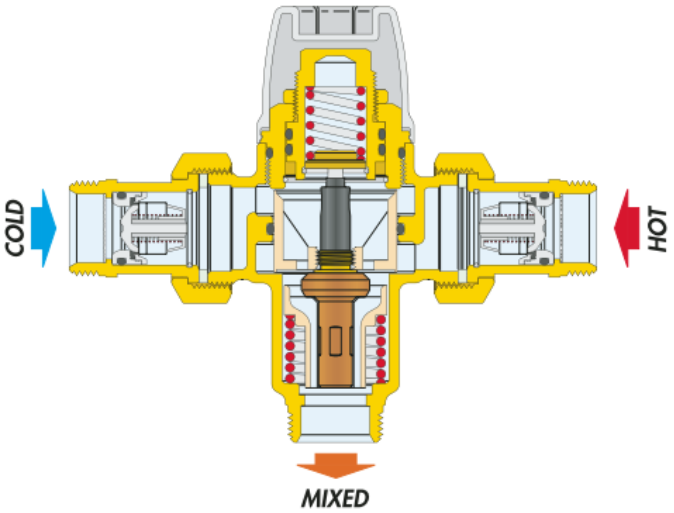


Figure 4.2 Schematic diagram of a tempering valve [54].

The pressure relief valve is required as a safety feature. It relieves any excessive pressure build-up inside the concealed storage tank.

## 4.2 Modeling of a thermally stratified DHWS

This section presents the model of a thermally stratified DHWS that predicts the power consumption, shower temperature and temperature profile inside the storage tank along the vertical axis.

Based on actual measurements and results published in literature [56]–[58], the thermal dynamics of the hot water storage tank is highly complex. Domestic hot water storage tanks are designed to produce thermal stratification along the vertical axis. The tank can be visualized as having multiple horizontal layers of water with different temperatures. Hot water with lower density resides in the upper part of the tank while colder water with higher density stays in the lower part. Thermal stratification effect in a hot water storage tank is illustrated in Figure 4.3 (a).

In principle, the total heat energy content of a thermally stratified tank (Figure 4.3 (a)) is the same as a well-mixed tank (Figure 4.3 (b)) with a uniform temperature [59]. However, thermal stratification in a storage tank increases the system

performance significantly [60]. A thermally stratified hot water storage tank has the following two advantages compared to a well-mixed tank:

- Hot water supply capacity is enhanced as a higher volume of hot water is available in the upper part of the tank.
- The heating element is switched on earlier since colder water near the bottom will trigger the thermostat earlier than in the case of a well-mixed tank.

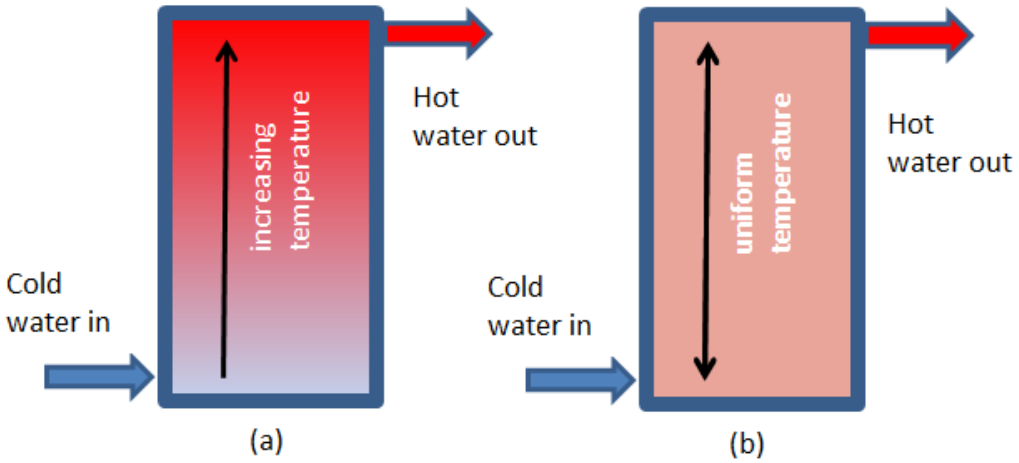


Figure 4.3 (a) thermally stratified hot water storage tank; (b) well-mixed hot water storage tank.

Thermal stratification is a highly complex phenomenon and its full analysis requires extensive computing time [56], [57], [60]. Hence, to have an accurate representation of a DHWS, the developed model must include the thermal stratification effect. At the same time, it must be sufficiently simplified so that a group of hundreds or thousands of DHWSs can be simulated and analyzed within acceptable computing time.

### 4.2.1 Review of models used in published literature

Different models developed to represent the electric hot water storage system have been reported in the literature [34], [37], [38], [61], [62]. The oversimplified models in [34] and [37] do not predict thermal stratification in the hot water storage tank. These models allow uniform mixing of cold and hot water, which produces an average temperature for the entire tank. Both [61] and [62] use a sectionalized temperature model to predict the internal temperatures and the power consumption of the electric hot water system. The hot water storage tank is divided into several

horizontal sections of equal volume and each section is assumed to have a different average temperature. Three sections are used in [61], whereas [62] uses six sections. The average temperature of every section is obtained by solving simultaneous differential equations representing basic heat energy flows in the sections. The heat energy flow of section *j* is represented as in ( 4.1 )

$$E^j = E^j_{\text{inflow}} - E^j_{\text{outflow}} - E^j_{\text{loss}} + E^j_{\text{heater}} \qquad (4.1)$$

where $E_{\text{inflow}}$ is the inflow of energy into section *j* from the section immediately below it; $E_{\text{outflow}}$ is the outflow of energy from section *j* into the section immediately above it; $E_{\text{loss}}$ is the standing heat loss of section *j*; $E_{\text{heater}}$ is the heat energy gained in section *j* from the heating element located in this section; $E_{\text{heater}}$ of a section equals zero if there is no heating element in this section.

The models described above produce thermally stratified sections of equal volume in the hot water storage tank. However, we found that having a constant number of equal-volume sections does not accurately represent the vertical temperature profile seen in actual measurements.

On the other hand, the hot water storage tank model proposed in [38] introduces the concept of thermocline in a mixing layer between two layers of water with different temperatures. However, this paper simplifies the model by assuming only two sections of water exist in the entire tank, with a zero volume mixing layer. These assumptions do not represent the vertical temperature profile inside a hot water storage tank observed in measurements. Furthermore, the operation of the tempering valve in temperature regulation is not included in any of the above models. Hence, we need to develop a new model to represent the thermal dynamics of a DHWS.

### 4.2.2 Thermally stratified model of DHWS

For accurate predictions of the water temperature and power consumption of a DHWS, we have studied the models used in the literature and developed a novel thermally stratified model of DHWS. Similarly to the models used in [59] and [62], our model employs a one-dimensional heat transfer mechanism in a vertically stratified storage tank and assumes negligible heat transfer via conduction and radiation. However, it uses a variable number of stratified layers and assumes

negligible mixing between them. In addition, our model includes the temperature regulating operation of a tempering valve.

As shown in Figure 4.4, the developed model divides the hot water storage tank into two physical zones: a mixing zone, and a layer zone.

The mixing zone is the part of the storage tank located below the cold water inlet. Uniform mixing of incoming cold and existing warm water is assumed in the mixing zone. The layer zone is the remaining part of the storage tank above the mixing zone. This zone consists of multiple horizontal layers of water with stepped temperature distribution [59]. The widths of the shaded areas in Figure 4.4 indicate the average temperatures of the layers; a wider shaded area implies a higher temperature.

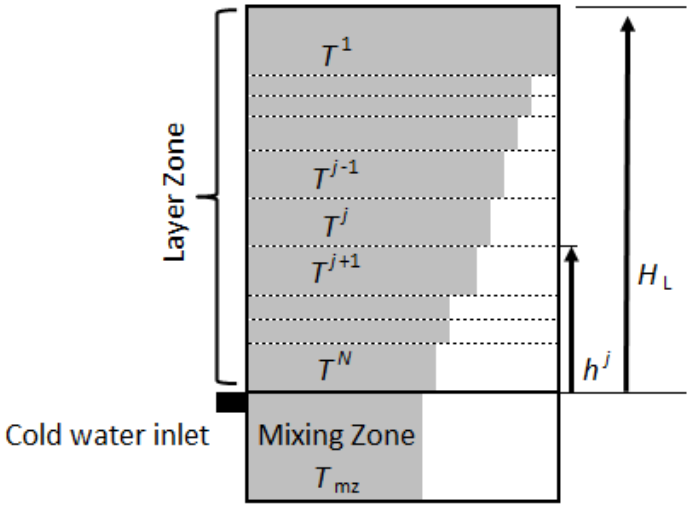


Figure 4.4 Block diagram of a hot water storage tank divided into mixing zone and layer zone.

The temperature $T$ inside the layer zone is expressed as

$$T = \begin{cases} T^1, & H_L \geq h > h^1 \\ T^2, & h^1 \geq h > h^2 \\ \dots & \\ T^N, & h^{N-1} \geq h \geq 0 \end{cases} \quad (4.2)$$

where $H_L$ is the height of the entire layer zone measured from the top of the mixing zone; $T^j$ represents the temperature of layer $j$ in the layer zone; $N$ is the total number of layers in the layer zone; $h$ is measured from the top of the mixing zone, and is constrained as follows:

$$0 \leq h^{N-1} \dots \leq h^2 \leq h^1 \leq H_L \quad (4.3)$$

The temperature of a given layer is always higher than the temperature of the layer below it, and lower than the temperature of the layer above it. The average temperature in the mixing zone is always lower or equal to the temperature of the bottommost layer in the layer zone. The temperatures of the mixing zone and layer zone can be expressed as:

$$T_{\mathrm{mz}} \leq T^{N} \ldots \leq T^{2} \leq T^{1} \qquad (4.4)$$

where $T_{\mathrm{mz}}$ is the mean temperature of the mixing zone.

### 4.2.3 Formulation of a DHWS model

We have developed a thermally stratified model of DHWS in MATLAB and the flowcharts representing the model are shown in Appendices 1 and 2. The developed model predicts the vertical temperature profile inside the storage tank, shower temperature and power consumption of a DHWS. The formulation of this model is presented in the following sections [63]. Table 4.1 summarizes the assumptions applied in the model.

Table 4.1 Assumptions applied in the formulation of the DHWS model

| | **Assumptions applied in the model** |
|---|---|
| 1 | One dimensional heat transfer along the vertical axis. |
| 2 | Temperature variations in the radial direction are ignored. |
| 3 | Uniform mixing of incoming cold water and existing warm water within the mixing zone. |
| 4 | Negligible mixing between the layers within the layer zone. |
| 5 | Stepped temperature distribution along the vertical axis. |
| 6 | Turbulence effect caused by heating is not considered. |
| 7 | Heat transfers via conduction and radiation inside the storage tank are ignored. |
| 8 | In calculations of the mass of water in each layer, the water in the entire storage tank is assumed to have an average density value. |
| 9 | The storage tank is cylindrical and has a uniform radius along its entire height. |
| 10 | The storage tank has a uniform heat loss coefficient along the vertical axis. Heat losses from the top and bottom walls are not considered. |

**Modeling of the tempering valve**

As described in Section 4.1, the main function of a tempering valve is to regulate

the maximum temperature of water at shower heads or tap outlets. Hot water from the top layer of a hot water storage tank is mixed with cold water from the supply mains to produce mixed water at a regulated temperature. Figure 4.5 shows the block diagram of a tempering valve where $m_h$, $m_c$ and $m_{out}$ are respectively the flow rates (kg/s) of hot water, cold water and mixed water on the tempering valve; $T_h$ is the hot water temperature ($^oC$); $T_c$ is the cold water temperature ($^oC$); $T_{out}$ is the regulated temperature ($^oC$) of the mixed water. In the case of a shower, $T_{out}$ is regarded as the preferred shower temperature $T_{shwr}$.

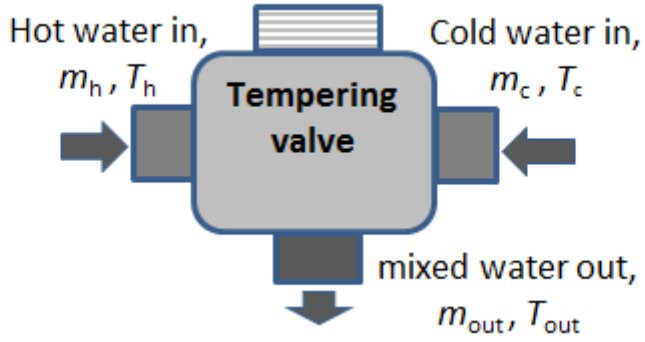


Figure 4.5 Block diagram of a tempering valve.

Applying the law of conservation of energy and mass, and assuming negligible heat loss in the valve, we have the following equations:

$$m_h + m_c = m_{out} \quad (4.5)$$

$$E_h + E_c = E_{out} \quad (4.6)$$

where $E_h$, $E_c$ and $E_{out}$ are the heat energies (J) in the hot water, cold water and mixed water, respectively. The equation ( 4.6 ) can be written as:

$$m_h \cdot T_h + m_c \cdot T_c = m_{out} \cdot T_{out} \quad (4.7)$$

Substituting ( 4.5 ) in ( 4.7 ) gives

$$\alpha = \frac{m_h}{m_{out}} = \frac{T_{out} - T_c}{T_h - T_c} \quad (4.8)$$

$$\alpha = \begin{cases} \alpha, & if\ \alpha \le \alpha_{max} \\ \alpha_{max}, & if\ \alpha > \alpha_{max} \end{cases} \quad (4.9)$$

where $\alpha$ is defined as the ratio of hot water flow to mixed water flow of the tempering valve; $\alpha_{max}$ is the maximum value of $\alpha$ and it is always less than unity (a typical value

is 0.86). The value of $\alpha_{max}$ depends on the design of the tempering valve. The amount of hot water drawn from the storage tank can be determined with ( 4.10 ) if the values of $\alpha$ and $m_{out}$ are known. The tempering valve keeps $T_{out}$ as a constant by varying $\alpha$, as shown in ( 4.11 ).

$$m_h = m_{out} \cdot \alpha \quad (4.10)$$

$$T_{out} = T_c + (T_h - T_c) \cdot \alpha \quad (4.11)$$

In the case of a shower, $T_{shwr}$ equals $T_{out}$. As hot water is consumed, the temperature inside the storage tank drops progressively. The tempering valve can no longer maintain $T_{out}$ as a constant if the value for $\alpha$ (calculated in ( 4.8 )) exceeds $\alpha_{max}$.

**Modeling of the hot water storage tank**

The vertical temperature profiles of the hot water storage tank before and after a hot water draw event are shown in Figure 4.6 (a) and (b), respectively. Discrete time interval is represented by the variable *k*. The superscript represents the position of a layer within the layer zone, where the numbering begins from the topmost layer in ascending order.

At time interval *k*, the layer zone consists of $N(k)$ layers of water. Layer *j* has height $Z^j$ (m) and temperature $T^j$ ($^o$C). The last layer immediately above the mixing zone has height $Z^{N(k)}$ (m) and temperature $T^{N(k)}$ ($^o$C). The mixing zone has a constant height, $Z_{mz}$ (m), and a time dependent temperature, $T_{mz}(k)$ ($^o$C). At time interval $(k+1)$, hot water is drawn from the top layer. An equal volume of cold water enters and mixes with the existing warm water in the mixing zone. Temperature in the mixing zone becomes $T_{mz}(k+1)$. Consequently, the number of layers in the layer zone changes from $N(k)$ to $N(k+1)$. A new layer with height $Z^{N(k+1)}$ and temperature $T^{N(k+1)}$ is formed at the bottom of the layer zone by water displaced from the mixing zone; and $T^{N(k+1)}$ equals $T_{mz}(k)$. The layer zone can be visualized as being shifted up vertically by the introduced cold water. With negligible mixing between the layers, the model maintains the vertical temperature profile of the storage tank. The only changes happen in the top and bottom layers in the layer zone.

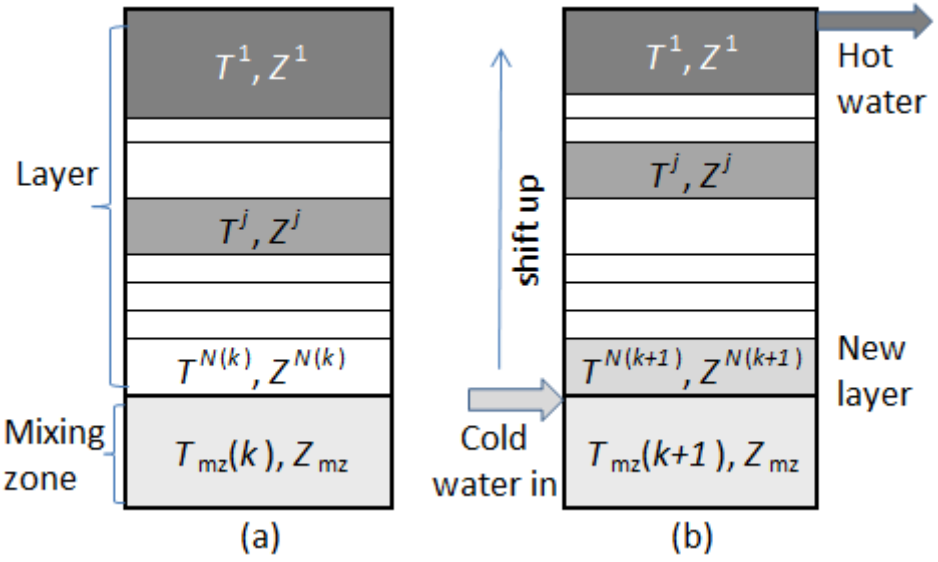


Figure 4.6 Vertical temperature profiles of a hot water storage tank: (a) before a draw, (b) after a draw [63].

As the draw continues, new layers with lower temperatures are formed at the bottom of the layer zone, while upper layers with higher temperatures are extracted from the top. When the thermostat detects a temperature lower than the turn-on temperature $T_{on}$, it switches on the heater to recharge the storage tank until the turn-off temperature $T_{off}$ is reached.

The energy flow in the mixing zone can be represented by a first order differential equation [63] shown below.

$$M_{mz} \cdot C \cdot \frac{dT_{mz}}{dt} = J \cdot P + m_h \cdot C \cdot (T_c - T_{mz}) - U_{mz} \cdot (T_{mz} - T_a) \qquad (4.12)$$

where $M_{mz}$ is the mass of water in the mixing zone (kg); $C$ is the specific heat of water (J/kg·K); $T_{mz}$ is the mean temperature ($^oC$) of the mixing zone; $P$ is the rated power of the heater (W); $U_{mz}$ is the heat loss coefficient of the mixing zone (W/K); $m_h$ is the flow rate of hot water (kg/s); $T_a$ and $T_c$ are the ambient and cold water temperatures ($^oC$), respectively; and $J$ is the thermostat's state governed by the following rules:

$$J(k+1) = \begin{cases} 1, & if\ T_t(k) \le T_{on} \\ 0, & if\ T_t(k) \ge T_{off} \\ J(k), & if\ T_{off} > T_t(k) > T_{on} \end{cases} \qquad (4.13)$$

where $T_t(k)$ is the temperature detected by the thermostat at time $k$. The heater is

turned on if the thermostat detects a temperature below or equal to $T_{on}$; it is turned off if the thermostat detects a temperature above or equal to $T_{off}$. If the detected temperature is between $T_{on}$ and $T_{off}$, the heater retains its operational state of the previous time interval.

We assume the heat loss coefficient is uniform for the entire storage tank, and ignore heat losses through the top and bottom of the storage tank. Hence, the heat loss coefficient for the mixing zone can be calculated as

$$U_{\mathrm{mz}} = \frac{Z_{\mathrm{mz}}}{H} \cdot U_{\mathrm{mean}} \qquad (4.14)$$

where $H$ is the height (m) and $U_{mean}$ the average heat loss coefficient of the storage tank.

The equation ( 4.12 ) can be solved numerically with the fourth order Runge-Kutta method for every time interval $k$ [64].

In the developed model, the heater is located at the bottom of the mixing zone. Heating of water is approximated by assuming uniform distribution of heat energy in the mixing zone and in layers above it that have temperatures lower than $T_{mz}$. In this way, heating is modeled as a heat transfer mechanism that begins in the mixing zone and gradually progresses to the top. This heating model eliminates the occurrence of temperature inversion and produces a vertically stratified temperature profile in the storage tank where hotter water is always above cooler water. When the temperature of the mixing zone is higher than the temperature of layers immediately above it, the mass weighted average temperature of these layers and the mixing zone is used as the mean temperature for all these layers and the mixing zone [62]. This mass weighted average temperature $T_{mean}$ is calculated in the following equation.

$$T_{\mathrm{mean}}(k) = \frac{(\sum_{i=j}^{N(k)} m^i \cdot T^i) + M_{\mathrm{mz}} \cdot T_{\mathrm{mz}}(k)}{(\sum_{i=j}^{N(k)} m^i) + M_{\mathrm{mz}}} \qquad (4.15)$$

where $m^i$ and $T^i$ are the mass (kg) and temperature ($^o$C) of layer $i$, respectively; $M_{mz}$ is the mass of the mixing zone (kg); $T_{mz}$ is the mean temperature ($^o$C) of the mixing zone, calculated in ( 4.12 ); $N(k)$ represents the total number of layers in the layer zone at time interval $k$; $j$ represents the topmost layer in the layer zone where its temperature is below $T_{mz}(k)$, before the heating mechanism is applied. The operating

temperature of a DHWS usually ranges from 10°C to 60°C. As a result, the density of water varies from 999.7 kg/m$^3$ for cold water to 983.2 kg/m$^3$ for hot water [65]. To calculate the mass of water, we assume an average density of 992 kg/m$^3$ (corresponding to 40°C) for water in the entire storage tank and ignore the insignificant error (less than 1%) introduced by this assumption.

If we assume a uniform cross sectional area for the storage tank, and an average density for the water in the storage tank, ( 4.15 ) can be simplified to

$$T_{\text{mean}}(k) = \frac{(\sum_{i=j}^{N(k)} Z^i \cdot T^i) + Z_{\text{mz}} \cdot T_{\text{mz}}(k)}{(\sum_{i=j}^{N(k)} Z^i) + Z_{\text{mz}}} \qquad (4.16)$$

where $Z^i$ represents the height of layer $i$; and $i = j, \ldots, N(k)$.

Figure 4.7 (a) shows the state of the hot water storage tank before the heating model is applied. The temperatures of layer $j$ and layers below it are less than $T_{\text{mz}}$. After applying the heating model, the total number of layers in the layer zone reduces from $N(k)$ to $j$; the temperature in layer $j$ and the mixing zone becomes $T_{\text{mean}}$. This state is illustrated in Figure 4.7 (b). The following equations are applied in the heating model:

$$Z^j = \sum_{i=j}^{N(k)} Z^i \qquad (4.17)$$

$$N(k) = j \qquad (4.18)$$

$$T^j = T_{\text{mz}} = T_{\text{mean}}(k) \qquad (4.19)$$

We use ( 4.20 ) to calculate the standing heat losses of the layers in the layer zone.

$$M^j \cdot C \cdot \frac{dT^j}{dt} = -U^j \cdot \left(T^j - T_{\text{a}}\right) \qquad (4.20)$$

where $M^j$, $T^j$ and $U^j$ are the mass (kg), temperature (°C) and heat loss coefficient (W/K) of layer $j$, respectively; $C$ is the specific heat of water (J/kg·K); and $T_{\text{a}}$ is the ambient temperature (°C).

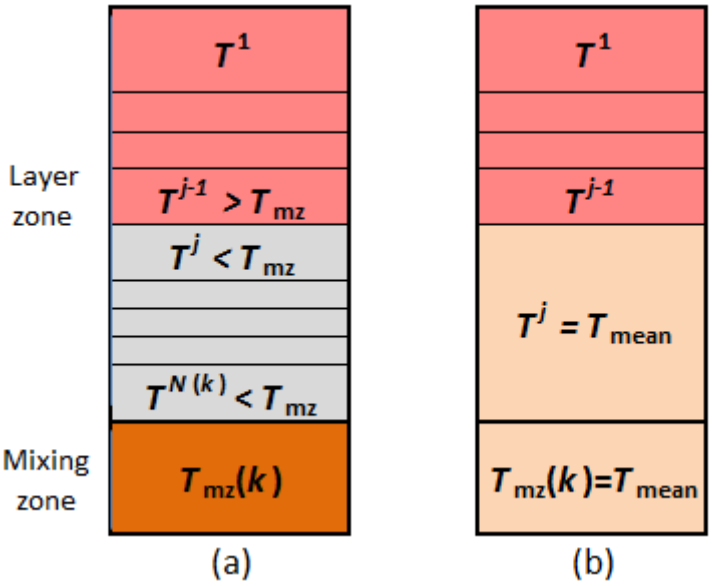


Figure 4.7 States of the hot water storage tank, (a) before heating model is applied, (b) after heating model is applied.

## 4.3 Model Validation

We set up a test system in the university's laboratory to tune and validate the developed model for a DHWS. This setup, as shown in Figure 4.8, is based on the most commonly installed DHWS in Tasmania, which has a 165 liter storage tank and a single 2.4 kW heating element.

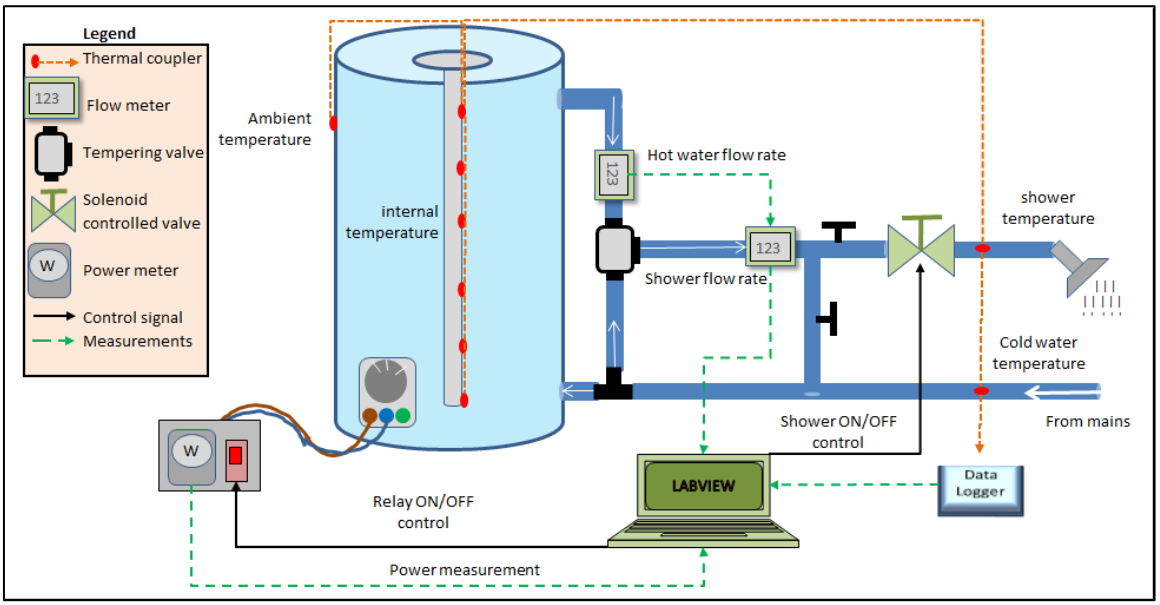


Figure 4.8 Test system setup for model tuning and validation.

### 4.3.1 Controls

Automated data acquisitions and instrument controls are implemented on a computer I/O card controlled by a LabVIEW program. To simulate actual shower events, the program controls a solenoid-controlled valve according to a user-defined shower schedule. In addition, user defined power cycle schedules can be applied to the test DHWS by controlling an optical relay.

### 4.3.2 Measurements

The test system was set up to measure three different quantities:

- Power consumption of the test DHWS
- Flow rate of hot water from the storage tank, and flow rate of showers measured after the tempering valve
- Temperature at various points in the test system:
    - Ambient temperature on the side of the storage tank
    - incoming cold water temperature
    - shower temperature
    - vertical temperature profile inside the storage tank, measured at six different points along the vertical axis of the storage tank

We conducted measurements on the test system under two different test conditions:

- dynamic test
- static test

In the dynamic tests, we applied a series of shower schedules to the test system and logged all the measurements over a period of 48 hours. A shower schedule consisted of four 7 minute draws with a four minute gap between two consecutive draws. There were four such shower schedules in the 48 hour period. The second shower schedule was 12 hours behind the first and 12 hours ahead of the third, and the last shower schedule was 5 hours behind the third. Figure 4.9 illustrates the shower schedules used in the tests.

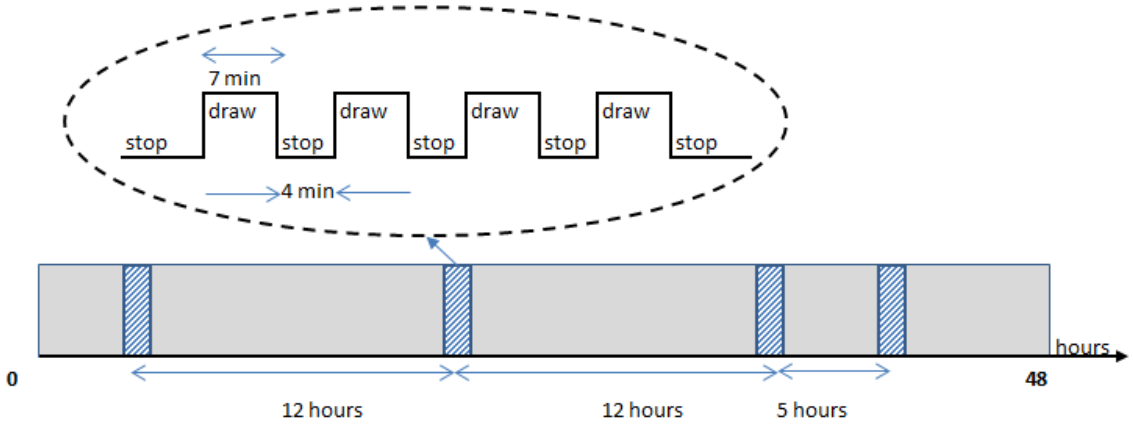


Figure 4.9 Illustration of shower schedules in 48 hours.

In the static test, we logged all the measurements over 24 hours without drawing any hot water from the storage tank.

### 4.3.3 Parameters of the DHWS and operating conditions for simulations

We calibrated the instruments after the test system was installed and commissioned. Then we collected sets of data from the test system and used them to tune and validate the developed DHWS model. After that, we used the tuned DHWS model to simulate the behavior of a DHWS with a configuration similar to the test system, and operated under comparable operating conditions. Subsequently, we performed comparative analyses on the measured and predicted time-based profiles of the following parameters:

- shower temperature
- temperatures of the top and bottom layers inside the storage tank
- cumulative power consumption
- state (on or off) of the DHWS thermostat
- cumulative volume of hot water consumption

Three sets of measurements were taken under different configurations and operating conditions, as shown in Table 4.2. Measurement 1 and Measurement 2 were taken from dynamic tests, whereas Measurement 3 was taken from the static test.

Table 4.2 Operating conditions and configurations of the test system in three measurements

| | **Measurement 1 (dynamic)** | **Measurement 2 (dynamic)** | **Measurement 3 (static)** |
|---|---|---|---|
| Initial conditions | Hot water depleted. Average temperature in the tank at about 22°C. | Hot water still available. Average temperature in the tank at about 50°C. | Hot water depleted. Average temperature in the tank at about 22°C. |
| Measured shower temperature | 45°C–47°C | 42°C–44°C | Not applicable |
| Measured average cold water temperature | 10.1°C | 9.8°C | Not applicable |
| Measured average ambient temperature | 19.5°C | 19.4°C | 20.4°C |

We then ran three simulations and compared the predictions with the respective values obtained in Measurements 1, 2 and 3. For meaningful comparisons, the physical parameters of the DHWS model must closely match the configuration of the test system. Similarly, the operating conditions used in the simulations must be as close as possible to the values measured in the test system. The physical parameters used in the DHWS model and the operating conditions of the simulations are shown in Table 4.3 and Table 4.4, respectively.

Table 4.3 Physical parameters of the DHWS model used for Simulations 1, 2 and 3

| **Parameter** | **Value** |
|---|---|
| Tank size (liter) | 165 |
| Tank height (m) | 1.6 |
| Cold inlet position from the base of the storage tank (m) | 0.15 |
| Heater power (W) | $P_{\text{mean}}$ |
| Thermostat turn on temperature (°C) | 53.5 |
| Thermostat turn off temperature (°C) | 58.3 |
| Maximum unbalanced dynamic supply ratio on tempering valve | 6:1 |
| Heat loss coefficient (W/°C) [66] | 2.0 |

Table 4.4 Operating conditions of the DHWS model in Simulations 1, 2 and 3

| Parameter | Value |
|---|---|
| Cold water temperature ($^{o}$C) | Use measured values |
| Ambient temperature ($^{o}$C) | Use measured values |
| Set shower temperature on tempering valve ($^{o}$C) | 45.5 $^{o}$C for simulation 1.<br>43.0 $^{o}$C for simulation 2. |
| Shower flow rate (liter/min) | Use measured values |

Cold inlet position represents the height of the mixing zone $Z_{mz}$ (described in Section 4.2.3) and it is about 0.15 m measured from the base of the storage tank. $P_{mean}$ in Table 4.3 is the time weighted average value of the power consumptions measured on the test system. We found considerable variations in the measured power consumption of the test system, which varied from 2.2 kW to 2.4 kW. This variation was mainly due to voltage fluctuations of the power supply for the test system. Hence, for a close comparison with the measurements, we used $P_{mean}$ as the heater power in the DHWS model instead of the specified 2.4 kW rated power. Table 4.5 shows the values of $P_{mean}$ for Simulations 1, 2 and 3, calculated from the power consumptions of Measurements 1, 2 and 3, respectively.

Table 4.5 Values of $P_{mean}$ used in Simulations 1, 2 and 3

| | Simulation 1 | Simulation 2 | Simulation 3 |
|---|---|---|---|
| $P_{mean}$ | 2.31 kW | 2.32 kW | 2.32 kW |

We set a higher shower temperature in Measurement 1 compared to Measurement 2. However, the tempering valve on the test system was only able to regulate shower temperature within ± 3% of the set value [54]. To cater for the variations in the measured shower temperature values, we used 45.5$^{o}$C and 43$^{o}$C as the shower temperatures in Simulation 1 and Simulation 2, respectively. According to the technical data found in [54], the tempering valve has a maximum unbalanced dynamic supply ratio of 6:1. This parameter denotes the maximum mixing ratio of hot and cold water, and determines the value of $\alpha_{max}$ in ( 4.9 ). The tempering valve can no longer regulate its output temperature if the hot water temperature drops to a level such that a mixing ratio higher than 6:1 is required.

To match the actual variations in cold water temperature, ambient temperature and shower flow rate, we directly applied the measured values of these parameters for every interval in Measurements 1, 2 and 3 to Simulations 1, 2 and 3, respectively.

### 4.3.4 Results of case study 1

In this case study, the results from Simulation 1 were compared with the measured values in Measurement 1. Figures 4.10–4.12 show the comparisons of top layer temperatures, normalized power consumptions and normalized cumulative hot water consumptions, respectively.

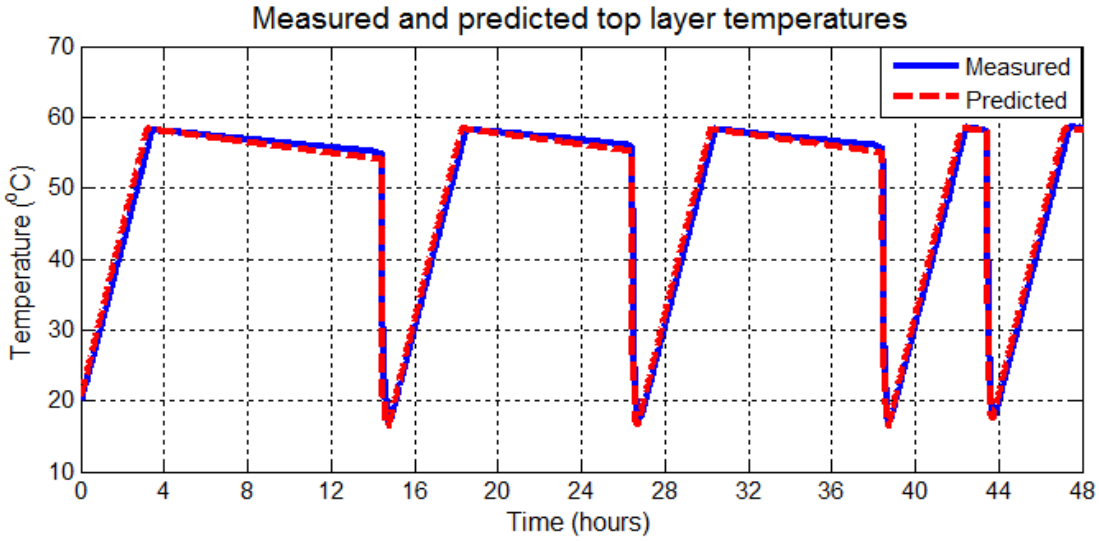


Figure 4.10 Top layer temperatures over 48 hours for Measurement 1 and Simulation 1.

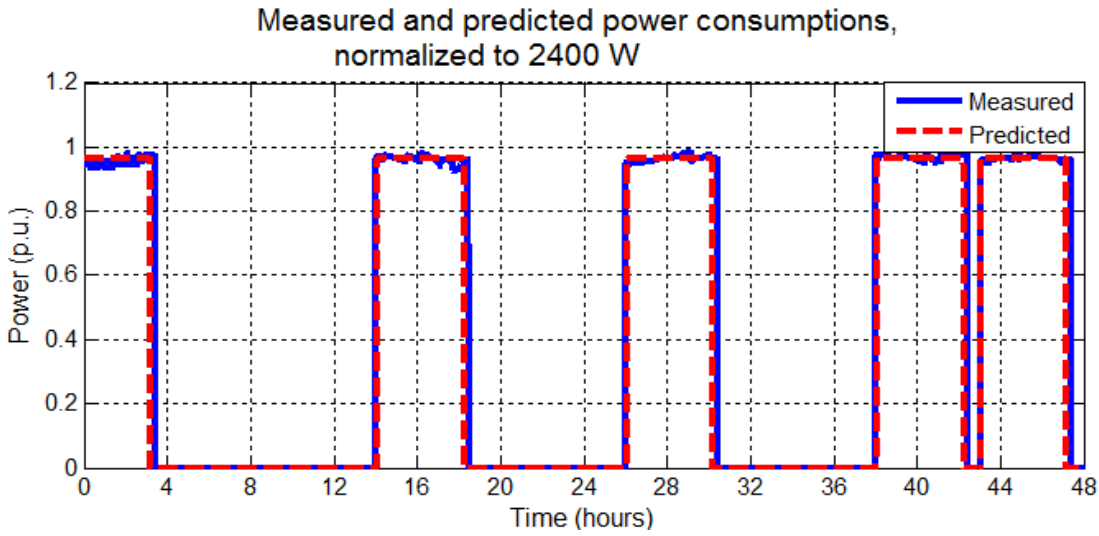


Figure 4.11 Normalized power consumptions over 48 hours for Measurement 1 and Simulation 1.

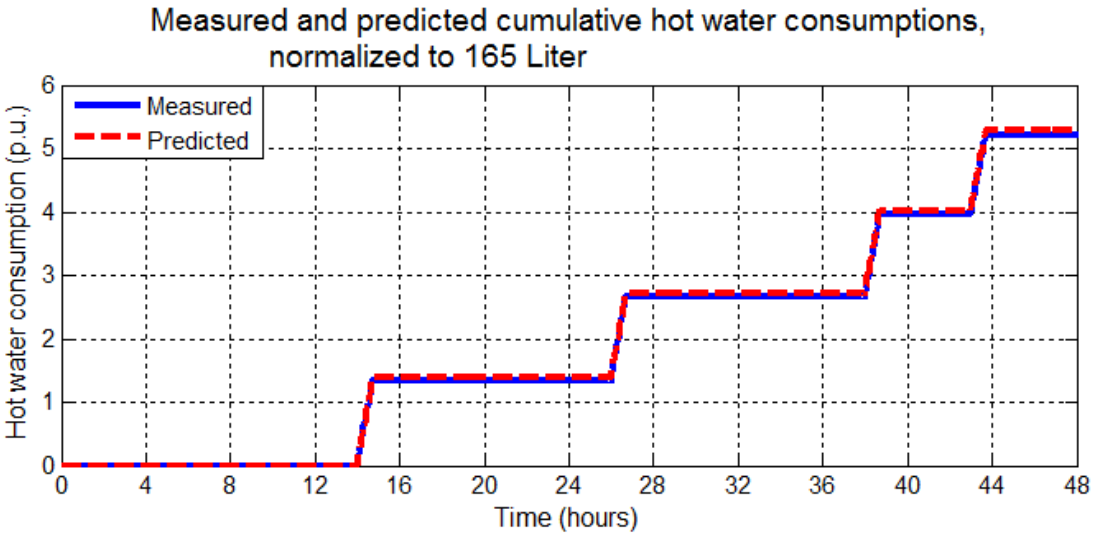


Figure 4.12 Normalized cumulative hot water consumptions over 48 hours for Measurement 1 and Simulation 1.

Figures 4.13–4.16 show the comparisons of shower temperatures of each shower schedule in smaller time scales for Measurement 1 and Simulation 1.

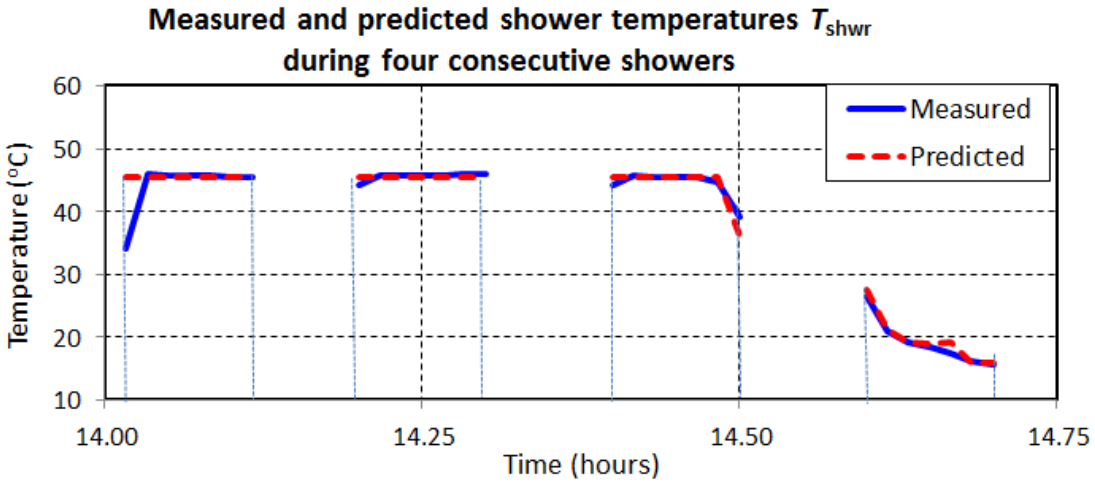


Figure 4.13 Shower temperatures in shower schedule 1 for Measurement 1 and Simulation 1.

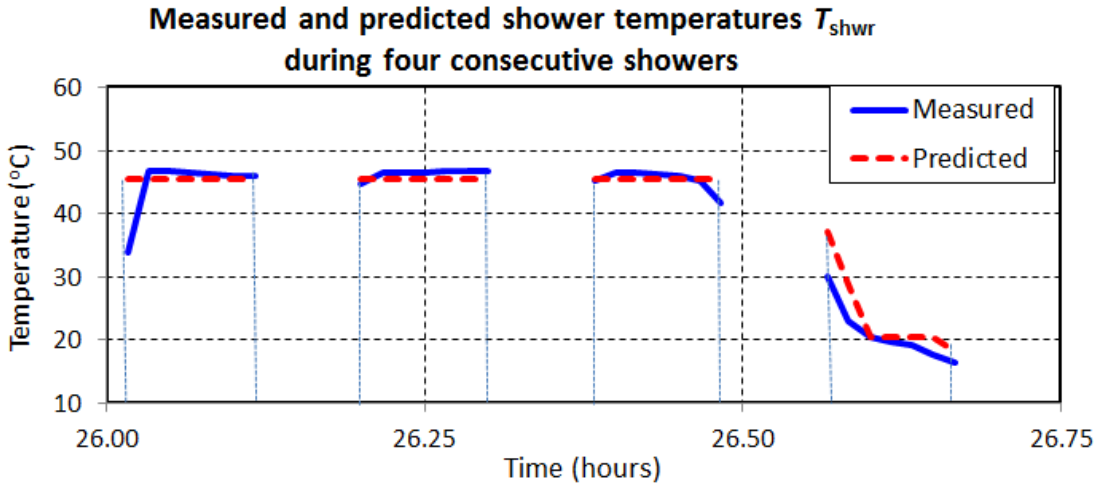


Figure 4.14 Shower temperatures in shower schedule 2 for Measurement 1 and Simulation 1.

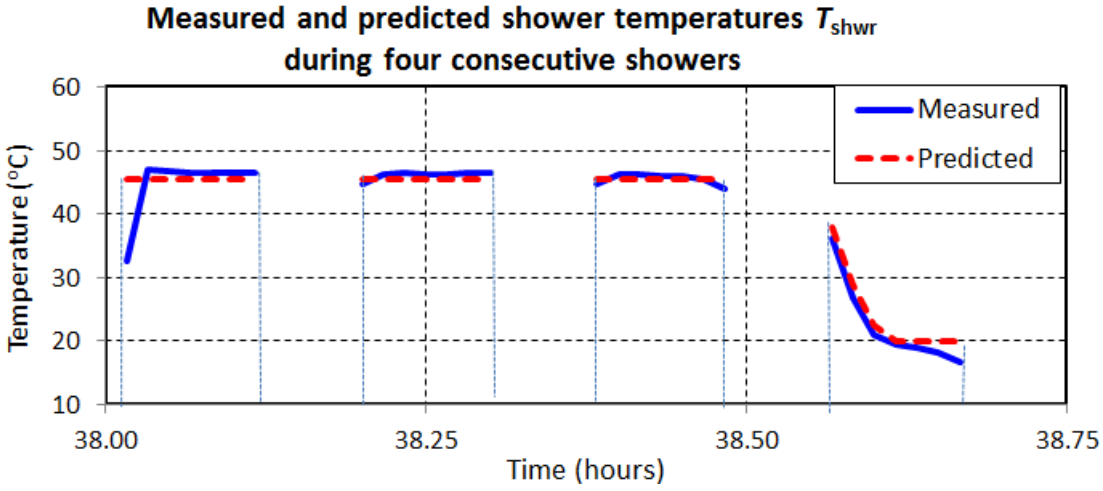


Figure 4.15 Shower temperatures in shower schedule 3 for Measurement 1 and Simulation 1.

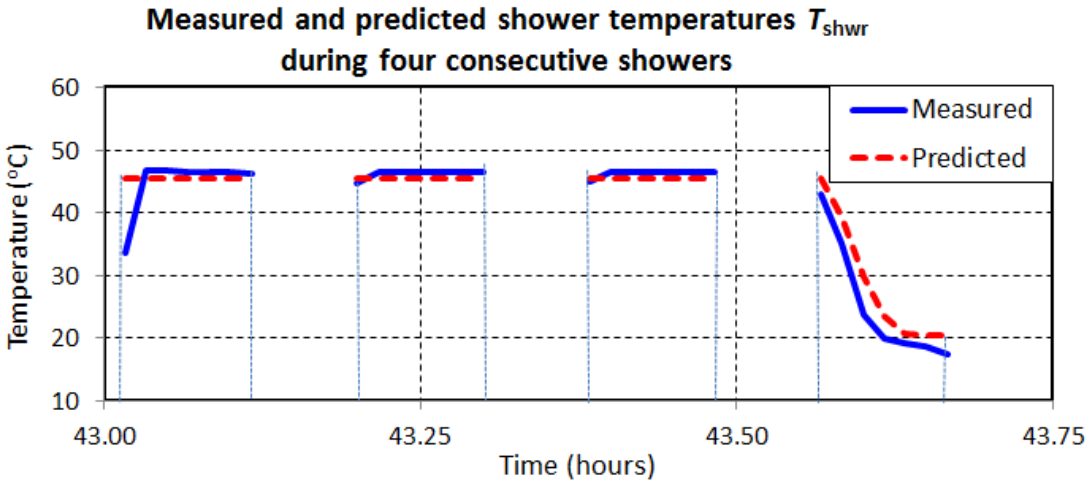


Figure 4.16 Shower temperatures in shower schedule 4 for Measurement 1 and Simulation 1.

### 4.3.5 Results of case study 2

In this case study, the results obtained from Simulation 2 were compared with Measurement 2. Figures 4.17–4.19 show the comparisons of top layer temperatures, normalized power consumptions and normalized cumulative hot water consumptions, respectively.

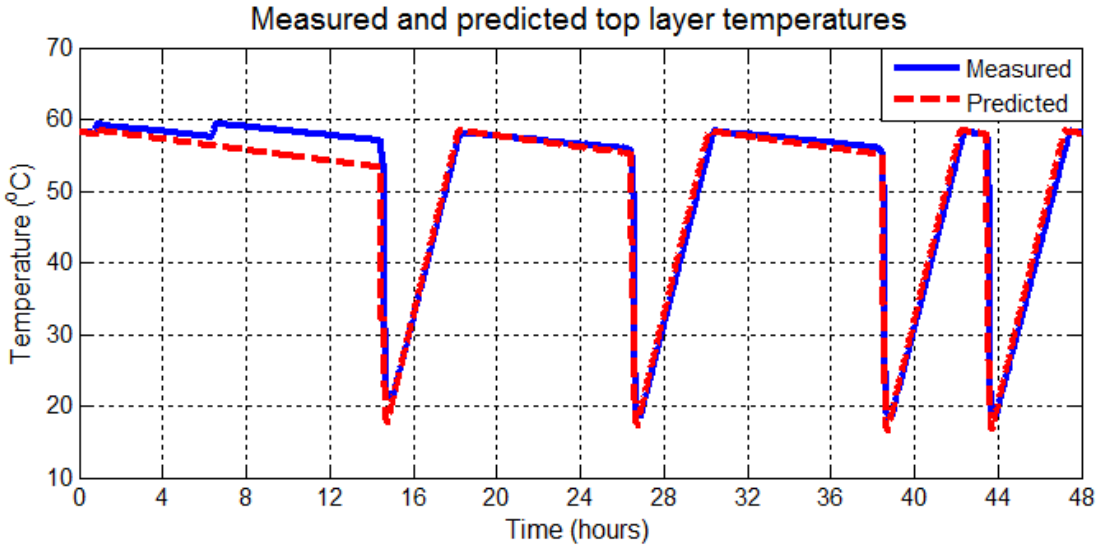


Figure 4.17 Top layer temperatures over 48 hours for Measurement 2 and Simulation 2.

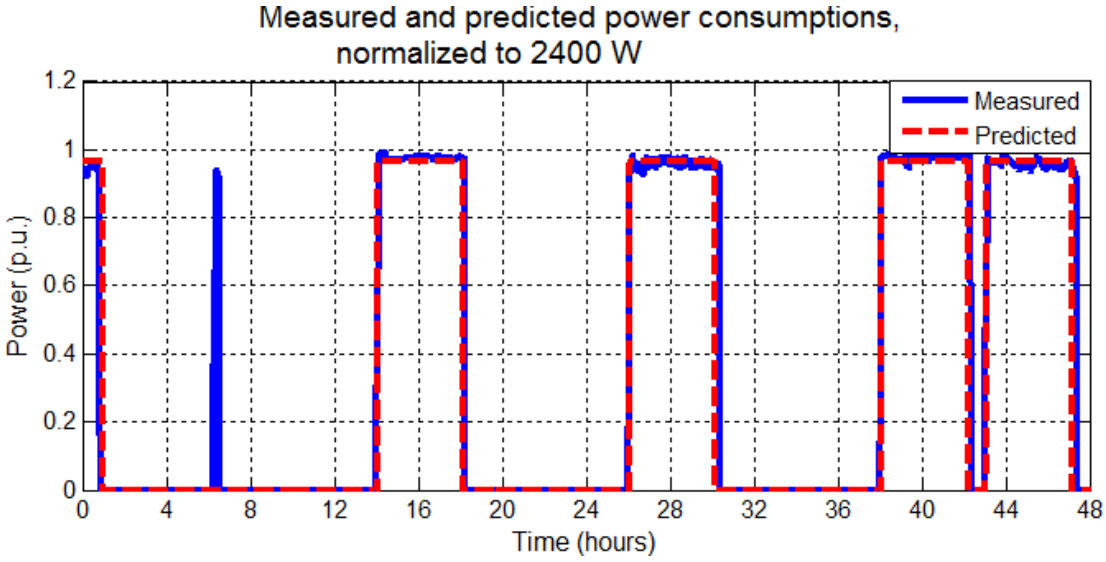


Figure 4.18 Normalized power consumptions over 48 hours for Measurement 2 and Simulation 2.

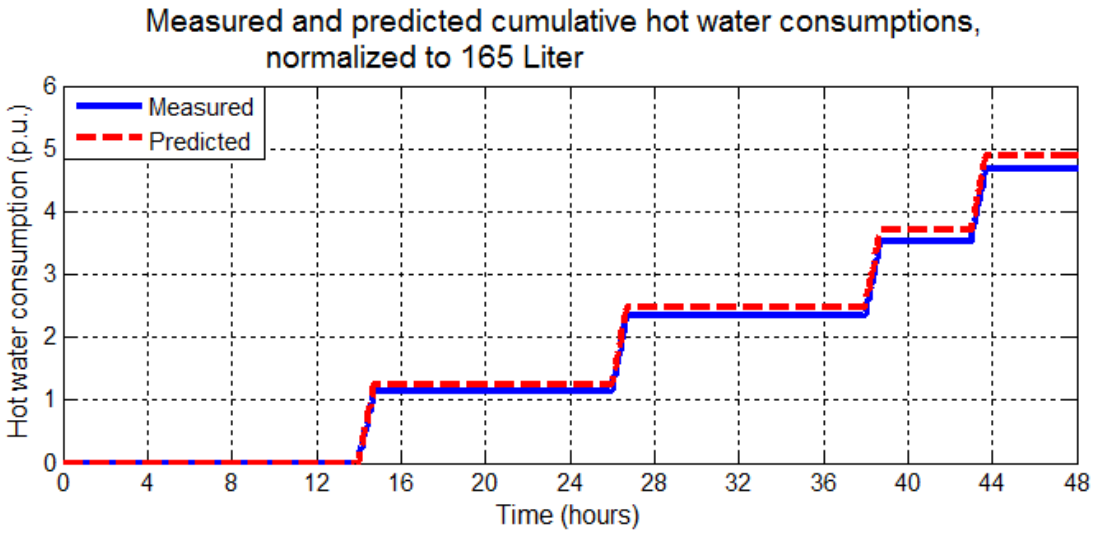


Figure 4.19 Normalized cumulative hot water consumptions over 48 hours for Measurement 2 and Simulation 2.

Figures 4.20–4.23 show the comparisons of shower temperatures of each shower schedule in smaller time scales for Measurement 2 and Simulation 2.

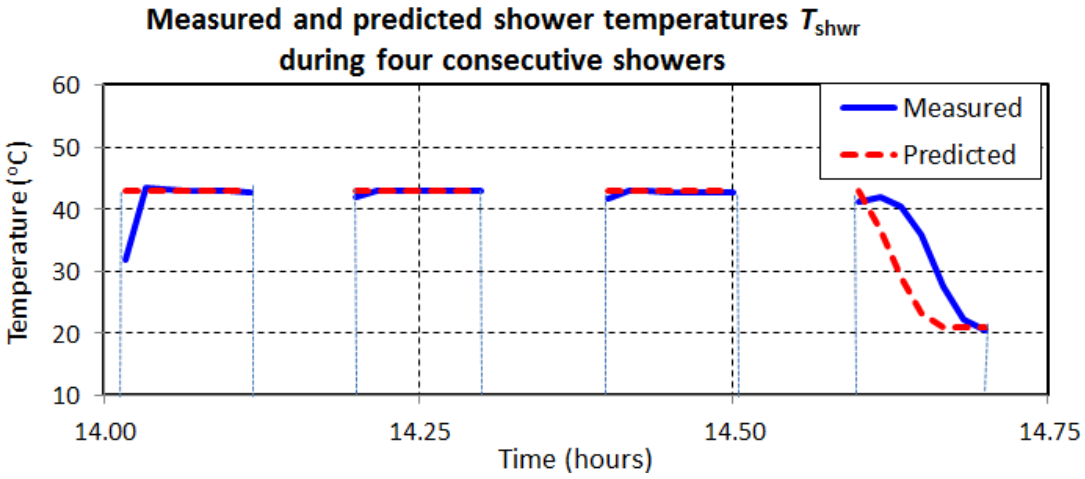


Figure 4.20 Shower temperatures in shower schedule 1 for Measurement 2 and Simulation 2.

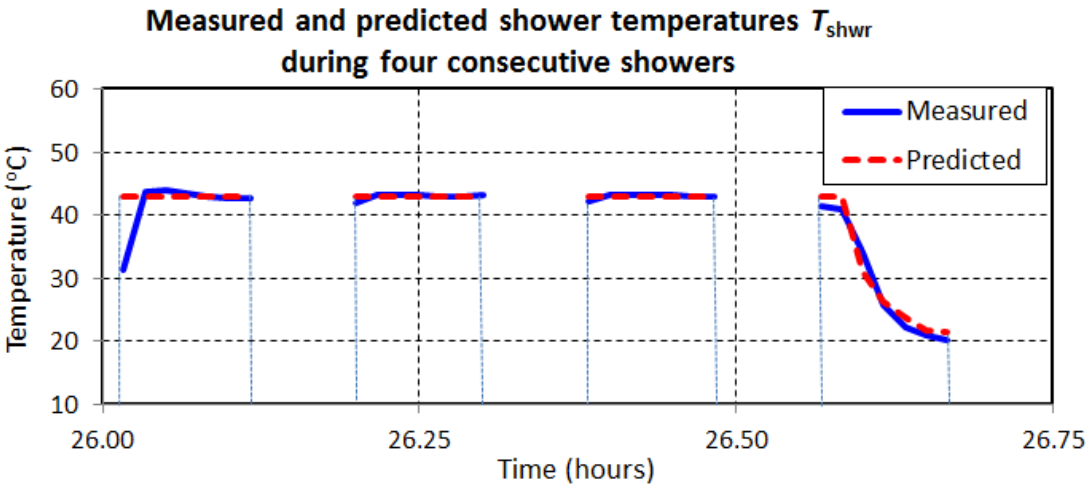


Figure 4.21 Shower temperatures in shower schedule 2 for Measurement 2 and Simulation 2.

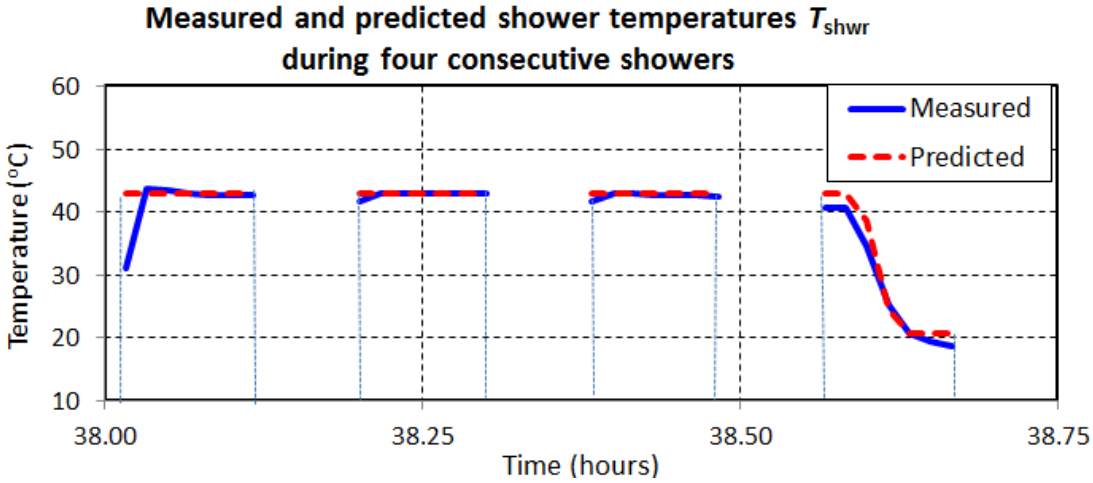


Figure 4.22 Shower temperatures in shower schedule 3 for Measurement 2 and Simulation 2.

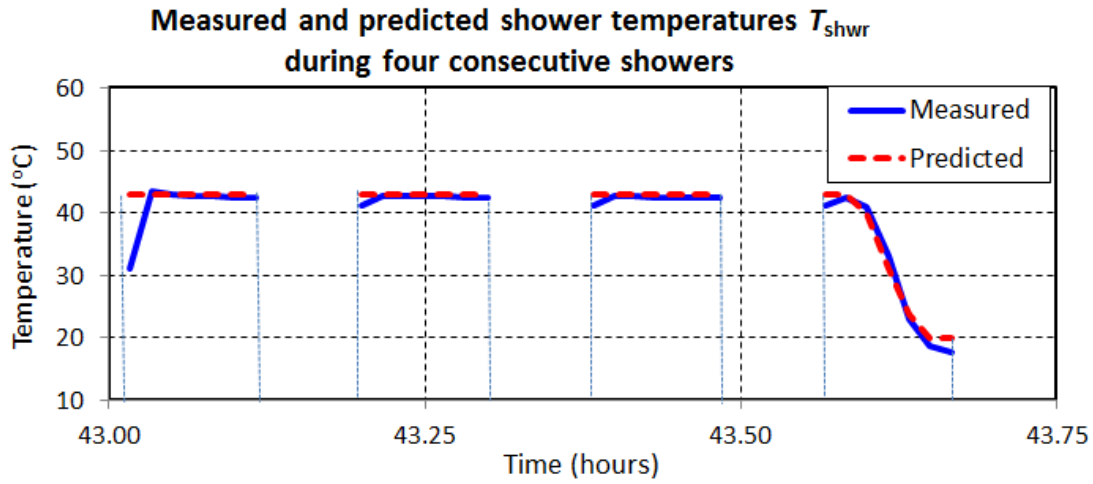


Figure 4.23 Shower temperatures in shower schedule 4 for Measurement 2 and Simulation 2.

### 4.3.6 Results of case study 3

The results obtained from Simulation 3 were compared with the measured values of Measurement 3. Figures 4.24–4.26 show the comparisons of normalized power consumptions, bottom and top layer temperatures, respectively. The bottom layer temperature was measured at about 0.25 m above the base of the storage tank, and it was assumed as the temperature detected by the thermostat.

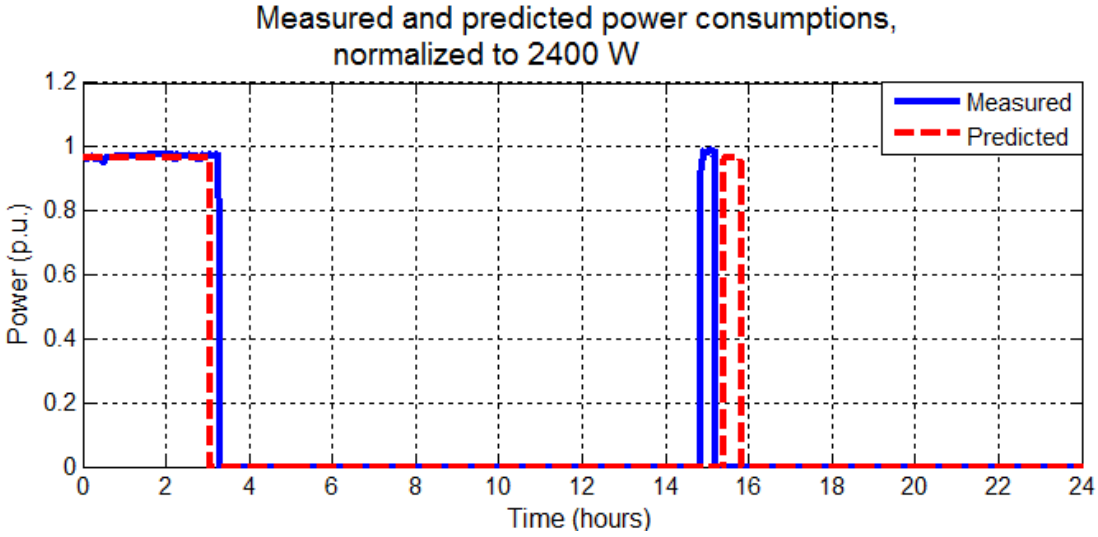


Figure 4.24 Normalized power consumptions over 24 hours for Measurement 3 and Simulation 3.

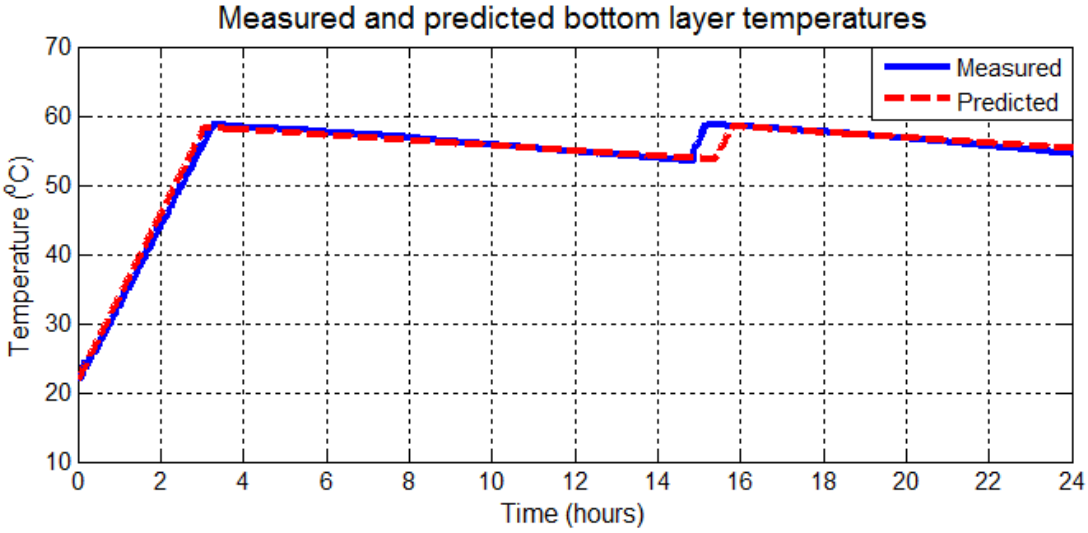


Figure 4.25 Bottom layer temperatures over 24 hours for Measurement 3 and Simulation 3.

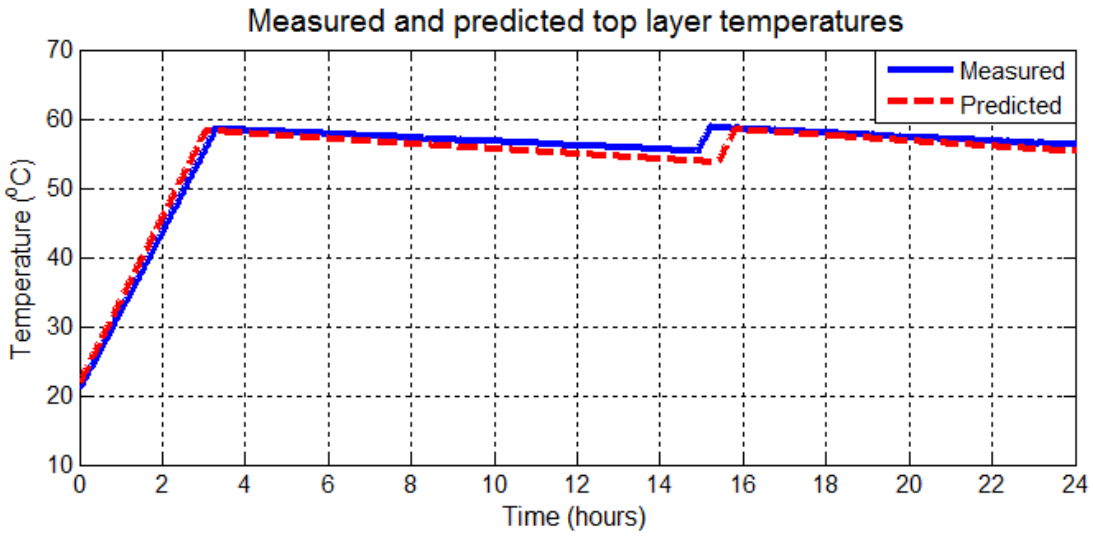


Figure 4.26 Top layer temperatures over 24 hours for Measurement 3 and Simulation 3.

### 4.3.7 Comparative analyses and summaries

Table 4.6 shows the prediction errors of the DHWS model with respect to actual measurements, after comparative analyses were performed on the results.

Table 4.6 Prediction errors of Simulations 1, 2 and 3 compared to Measurements 1, 2 and 3, respectively

| | **Simulation 1** | **Simulation 2** | **Simulation 3** |
|---|---|---|---|
| Error in total energy consumption (%) | 5.5 | 4.6 | 5.1 |
| Mismatch in thermostat state (%) | 2.3 | 2.0 | 4.0 |
| Error in hot water consumption (%) | -1.2 | -4.5 | N/A |
| MAE in shower temperature ($^{o}$C) | 1.6 | 1.4 | N/A |
| RMSE in shower temperature ($^{o}$C) | 2.8 | 3.1 | N/A |
| MAE in top layer temperature ($^{o}$C) | 1.1 | 1.5 | 1.0 |
| RMSE in top layer temperature ($^{o}$C) | 1.7 | 2.7 | 1.3 |
| MAE in bottom layer temperature ($^{o}$C) | 0.7 | 1.0 | 0.5 |
| RMSE in bottom layer temperature ($^{o}$C) | 1.0 | 1.5 | 0.9 |

For all the calculations presented in this section, $i$ represents the simulation intervals: from the first interval to the last interval $K$. We used an interval of one minute in all the simulations conducted. Thus, the values of $K$ are 1440 and 2880 for 24 hour and 48 hour simulation periods, respectively.

**Error in total energy consumption**

Total energy consumption is calculated as the total area under the power consumption curve over the entire measurement period, and the corresponding error is calculated as:

$$\textit{Error in total energy consumption} = 100\% \times (E_{\mathrm{m}} - E_{\mathrm{p}})/E_{\mathrm{m}} \qquad (4.21)$$

where $E_{\mathrm{m}}$ and $E_{\mathrm{p}}$ are the measured and predicted total energy consumptions of the DHWS, respectively.

**Mismatch in thermostat state**

This index measures the total number of mismatches between measured and predicted thermostat states, and expresses it as a percentage of the total number of thermostat states over the entire measurement period. It is calculated in the following equations.

$$J_{\mathrm{err}}^{i} = \begin{cases} 0 \;\; if \;\; J_{\mathrm{m}}^{i} = J_{\mathrm{p}}^{i} \\ 1 \;\; if \;\; J_{\mathrm{m}}^{i} \neq J_{\mathrm{p}}^{i} \end{cases} \qquad (4.22)$$

where $J_{\mathrm{m}}$ and $J_{\mathrm{p}}$ are the measured and predicted thermostat states, respectively; $J_{\mathrm{err}}$ is the counter for mismatches in the thermostat state between measured and predicted results; and the superscript $i$ represents the time interval.

$$\textit{Error in thermostat state} = 100\% \cdot \frac{1}{K} \cdot \sum_{i=1}^{K} J_{\mathrm{err}}^{i} \qquad (4.23)$$

**Error in hot water consumption**

This index is calculated as:

$$\textit{Error in hot water consumption} = 100\% \times (V_{\mathrm{m}} - V_{\mathrm{p}})/V_{\mathrm{m}} \qquad (4.24)$$

where $V_{\mathrm{m}}$ and $V_{\mathrm{p}}$ are the measured and predicted total volumes of hot water drawn from the DHWS, respectively.

**Error in temperatures**

In Table 4.6, RMSE is the root mean square error and MAE the mean absolute error [67]. The calculations of MAE and RMSE are given as below:

$$MAE = \frac{1}{K} \cdot \sum_{i=1}^{K} \left| (T_{\mathrm{m}}^{i} - T_{\mathrm{p}}^{i}) \right| \qquad (4.25)$$

$$RMSE = \frac{1}{\sqrt{K}} \cdot \sqrt{\sum_{i=1}^{k} (T_{\mathrm{m}}^{i} - T_{\mathrm{p}}^{i})^2} \qquad (4.26)$$

where $T_{\mathrm{m}}$ and $T_{\mathrm{p}}$ are the measured and predicted temperatures, respectively; the superscript $i$ represents the time interval; and $|x|$ represents the absolute value of $x$.

## 4.4 Discussion

By comparing the dynamic tests and simulation results, we found that the predicted shower temperatures closely matched the measurements (Figures 4.13–4.16, and Figures 4.20–4.23). The highest MAE between measurements and predictions was 1.6°C over a period of 48 hours. At the same time, the corresponding RMSE was 2.8°C.

RMSE squares prediction errors and hence amplifies large deviations. The closer the value of RMSE to MAE, the more uniform is the distribution of prediction errors. The lower and upper limits of RMSE are functions of the MAE, as given below [68]:

$$MAE \leq RMSE \leq \sqrt{K} \cdot MAE \qquad (4.27)$$

If all the prediction errors are uniformly distributed (i.e. all errors are the same), RMSE is equal to MAE.

Hence, the error analysis of predicted shower temperatures demonstrated that the deviations from measured values were reasonably uniform and with acceptable accuracy (MAE < 2°C).

Similar error analyses can be applied to the predictions of temperature profile inside the storage tank. The top layer temperature profile of Simulation 2 showed the highest prediction error with 1.5°C of MAE and a corresponding 2.7°C of RMSE. Compared to the top layer temperature predictions, lower magnitudes of error were found in predictions for the bottom layer temperature profile in all the simulations. As the calculated RMSE and MAE of the internal temperature profiles were rather close to each other, we deduced that the majority of the deviations between the predictions and measurements were reasonably uniform. This deduction is evident in the graphs showing comparisons of temperature profiles in the previous sections (Sections 4.3.4–4.3.6).

As the actual temperature on the thermostat was not directly measurable in our test system, we assumed it equaled the temperature recorded by the bottommost thermo coupler positioned at about the same height as the thermostat inside the storage tank (about 0.25 m from the base of the storage tank). Meanwhile, in the simulations, the temperature of the layer at this height was used as the temperature detected by the thermostat. Moreover, the thermostat on a DHWS is not a precision device and the margin of error can be as high as ± 4$^{o}$C according to the manufacturer data sheet [69]. For example, a power spike is observed at about hour 6 in Figure 4.18. This spike causes a step increase in the top layer temperature, as can be seen in Figure 4.17. This power spike was not predicted because the model is based on a one-dimensional heat transfer mechanism, and thus temperature variations in the redial direction are not considered. As a result, the actual temperature decrease detected by the thermostat was not predicted by the model. In addition, the rate of temperature drop inside a well insulated storage tank is rather slow (less than 0.5$^{o}$C per hour). As a result, slight deviations between the predicted and actual temperatures can produce mismatches in the thermostat state. In the case of an idling DHWS, if the prediction is 0.5$^{o}$C above the actual temperature, the thermostat in the simulation will turn on after about an hour of delay. This phenomenon is shown in Figure 4.25 and it is the cause of the mismatches seen in Figure 4.24.

In the experimental setup, the metal piping between the shower head and the hot water tank is not insulated. Hence, water in the piping continually loses heat energy to the environment. At the beginning of a shower schedule, cooler water in the piping flows through the shower head before hot water from the tank does. As a result, the measured shower temperature at the starting time of a shower schedule is below the preferred shower temperature set on the tempering valve. On the other hand, heat losses from the metal piping are not considered in predictions. Thus, the preferred shower temperature is predicted at the starting time of a shower schedule. This discrepancy between measured and predicted shower temperatures at the starting time of a shower schedule can be observed in Figure 4.13–4.16, 4.20– 4.23.

Table 4.6 shows that the measured total energy consumption is always higher than the prediction, with the highest error of 5.5%. This prediction error is mainly due to

two reasons:

- The actual turn-on and turn-off temperatures on the thermostat of the test system were not known. Besides, as explained above, the thermostat is not very accurate and it may not trigger at the same set temperature in every cycle. A small deviation from the set temperature will cause an observable deviation from the expected energy consumption. For example, a deviation from 60$^{o}$C to 60.5$^{o}$C in the turn-off temperature will increase the energy consumption by about 1.1%, assuming the test DHWS recharges from an initial average temperature of 15$^{o}$C.
- Several factors ignored in the developed DHWS model may contribute to higher energy consumption in the actual system. Some such factors are: the thermal mass of the stainless steel wall of the storage tank, the deviation in heat loss coefficient between the model and actual value, and heat losses through conduction in the metal pipes.

The errors in predicted hot water consumptions were mainly due to prediction errors in the top layer temperature, and the fluctuations in actual shower temperature. Referring to ( 4.5 ) – ( 4.8 ), variations in the hot water temperature and shower temperature will change the ratio of hot water flow over shower flow.

As a summary, we conclude that the developed DHWS model is able to predict the behavior of an actual DHWS with acceptable accuracy. The error in power consumption is less than 6%, while the MAE in temperature prediction is less than 2$^{o}$C. Thus, the developed DHWS model can be used in our research on DSM of DHWSs in the Tasmanian power distribution system.

## 4.5 Conclusion

This chapter has described the general operation of the most common DHWS in Tasmania, Australia. The development of a DHWS model to represent the thermal behavior of a thermally stratified DHWS has been presented from the basis of a unique one dimensional heat transfer mechanism and heat energy equations. The model assumes two different zones in the storage tank, namely the mixing zone and the layer zone. Incoming cold and existing warm water mix uniformly in the mixing

zone with a constant volume. The layer zone contains a variable number of layers, each with a variable volume of water. A stepped temperature distribution with negligible mixing between layers is assumed for the layer zone. In addition, this model also includes a tempering valve model and a mechanism that models the heating of water in the storage tank.

Predictions made with the developed model were compared with experimental data obtained from a test system. Comparative analyses demonstrated that predicted results closely matched the measured data. Over a period of 48 hours, less than 6% of prediction error was found in the total energy consumption while the highest mean absolute error in temperature prediction was less than $2^{o}$C. At the same time, the majority of the deviations between the predicted and measured temperatures were reasonably uniform. Hence, the accuracy of the developed model is acceptable to be used in further research work.

The succeeding chapters will present the other modules under the simulation block shown in Figure 2.1.

# Chapter 5

## Performance Calculation and Optimization of DLC Switching Programs

This chapter presents the calculation of performance and the optimization of DLC programs for controlling DHWSs. The performance calculator, as depicted in Figure 2.1, determines the KPIs of implementing a DLC switching program on the participating households in an area. It has two main functions: calculating peak reductions in the hot water load and estimating the consumer comfort level. Meanwhile, the optimization process is performed by the switching program optimizer module, which has been briefly described in Chapter 2.

Section 5.1 describes the calculations of two KPIs used to measure, evaluate and compare the performance of implementing DLC switching programs in a controlled area. Section 5.2 outlines the structure of the switching program optimizer, as well as its required I/Os. Subsequent sections describe its key components in detail. Section 5.3 describes the switching program generator and the control management system parameters. The operation of the load estimator is presented in Section 5.4. Section 5.5 presents the optimizer and the operation of two different optimization methods. A conclusion is provided in Section 5.6.

Power consumption is normalized to 2.4 kW in examples presented in this chapter.

## 5.1 Performance calculator

### 5.1.1 Peak load reduction

To calculate the peak load reduction, the performance calculator firstly determines an average uncontrolled hot water load profile for each household. The average uncontrolled load profile for a household represents an average profile of the household obtained over a specified number of Monte Carlo iterations. Then, it determines an aggregate uncontrolled hot water load curve $L_U$ by aggregating uncontrolled hot water load profiles for all households. An aggregate controlled hot

water load curve $L_C$ is obtained in a similar manner after a DLC switching program is applied to the uncontrolled hot water loads of individual households. Equations ( 5.1 ) and ( 5.2 ) are used to calculate $L_U$ and $L_C$, respectively.

$$L_U = \sum_{i=1}^{N_H} \frac{1}{N_S} \cdot \sum_{j=1}^{N_S} l_U(i,j) \quad (5.1)$$

$$L_C = \sum_{i=1}^{N_H} \frac{1}{N_S} \cdot \sum_{j=1}^{N_S} l_C(i,j) \quad (5.2)$$

where $N_H$ is the total number of households; $N_S$ is the total number of Monte Carlo iterations, which produce the hot water consumption profiles for the controlled households; $l_U(i, j)$ and $l_C(i, j)$ represent the uncontrolled and controlled hot water load profiles for household $i$ in Monte Carlo iteration $j$, respectively.

The peak load reduction $R(\tau)$ of the control period $\tau$ is defined as

$$R(\tau) = 1 - \frac{max[L_C(\tau)]}{max[L_U(\tau)]} \cdot 100\% \quad (5.3)$$

where $max[L_C(\tau)]$ and $max[L_U(\tau)]$ are the peaks of $L_C$ and $L_U$ in the control period $\tau$, respectively.

### 5.1.2 Consumer comfort level

The success of any DSM program depends heavily on the acceptance of consumers. As a result, any domestic DSM program must be designed to limit impacts on consumer comfort level, in order to gain widespread acceptance and participation. In the case of direct load control applied to domestic hot water systems, the comfort level is profoundly dependent on the hot water temperature during consumption.

The first step to characterize consumers' comfort level is to find the hot water temperature range that is preferable to the consumers in general. The authors in [70] find that the preferred shower temperature has a negative correlation with the mean body temperature. The test subjects prefer a hotter shower after submerging their bodies in cold water (25$^o$C) for 30 minutes. This paper reveals that the preferred range of shower temperature is from 40$^o$C to about 44$^o$C under different situations. A comparable temperature range from 39$^o$C to about 42$^o$C is reported in [71], while [72] uses 40.6$^o$C (105$^o$F) as the average comfortable shower temperature in their study.

On the other hand, Australian Standard AS 3498 dictates that the water temperature at the shower head or tap outlet must be below 50$^{o}$C, for safety reasons.

In the Tasmanian distribution network, domestic demand peaks in the winter months. According to the results in [70], consumers prefer hotter showers during this colder period. Hence, we assume the preferred hot water temperature ranges from 41$^{o}$C to 43$^{o}$C in our studies.

A consumer's comfort level depends on the frequency (or probability) of getting a "cold shower"—an event when the shower temperature drops below the preferred temperature (e.g. 43$^{o}$C). In our developed tool, the preferred temperature is specified by the tool user. Hence, probabilities of cold showers are used as the performance indicator for consumer comfort level in our studies. Using ( 5.4 ) and ( 5.5 ), the performance calculator estimates the probability of cold showers for each family type, as well as an overall probability of cold showers for all the families in a controlled area. These probabilities are calculated over the specified number of Monte Carlo iterations.

$$P_{\text{cold}}(j) = \sum_{k=1}^{N_S} N_{\text{cold}}(j,k) \,/\, \sum_{k=1}^{N_S} N_{\text{shwr}}(j,k) \qquad (5.4)$$

where $P_{\text{cold}}$ is the probability of cold showers; $N_{\text{cold}}$ is the number of cold shower events; $N_{\text{shwr}}$ is the total number of showers; $j$ indicates the family type; $k$ represents the Monte Carlo iteration; and $N_S$ is the total number of Monte Carlo iterations.

$$P_{\text{cold}}(all) = \sum_{j=1}^{N_F} \sum_{k=1}^{N_S} N_{\text{cold}}(j,k) \,/\, \sum_{j=1}^{N_F} \sum_{k=1}^{N_S} N_{\text{shwr}}(j,k) \qquad (5.5)$$

where $P_{\text{cold}}(all)$ is the overall probability of cold showers for all families; $k$ represents the Monte Carlo iteration; $j$ indicates the family type; and $N_F$ is the total number of family types.

Because of a large number of households in a controlled area, we can assume the same preferred temperature for all hot water consumers. The tool allows its user to change the preferred temperature if required.

## 5.2 Structure of the switching program optimizer

Figure 5.1 shows the block diagram of the switching program optimizer module.

I/Os are depicted as numbered blocks. I/O 1 represents parameters of the control management system, I/O 2 optimization parameters, I/O 3 uncontrolled hot water loads generated by the DHWS model, and I/O 4 denotes optimized switching programs. The tool user specifies I/O 1 and I/O 2.

The switching program optimizer produces switching programs iteratively, optimizing them in successive iterations. First, it configures the optimizer and switching program generator modules with user-specified parameters (I/O 1 and I/O 2). Next, the switching program generator produces a switching program (I/O 4) that the load estimator applies to the uncontrolled hot water loads (I/O 3) to produce estimated controlled loads. The optimizer then uses these estimated controlled loads and optimizes turn-off periods of the current switching program, which are subsequently used by the switching program generator to produce the switching program for the next iteration in optimization.

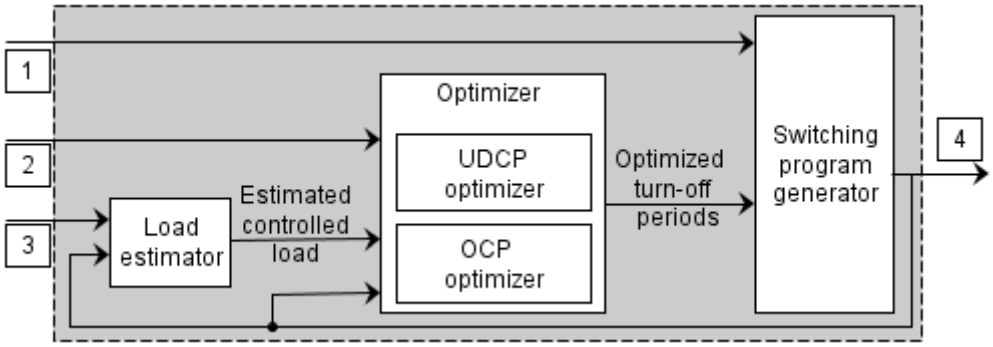


Figure 5.1 Block diagram of switching program optimizer.

## 5.3 Switching program generator

The switching program generator uses user-specified control management system parameters and optimized turn-off periods produced by the optimizer to create switching programs, as shown in Figure 5.2. The control management system parameters that define a switching program are listed and described below:

- A control step $\tau_{\text{step}}$ is the smallest switching time interval. All other switching program parameters must be in multiples of a control step.
- A turn-off period $\tau_{\text{off}}$ is the time interval when the DHWS is turned off for several

consecutive control steps, whereas a turn-on period $\tau_{on}$ is the time interval when the DHWS is turned on for several consecutive control steps. The smallest turn-off or turn-on period equals one control step.

- A switching cycle $\tau_{sc}$ consists of a turn-off period followed by a turn-on period. The lengths of switching cycles are uniform in a switching program.
- A control period $\tau$ contains multiple switching cycles, and it is defined by the starting time $t_s$ and finishing time $t_f$ of the period. There are two control periods in a switching program; one for the morning peak period and another for the evening peak period. The length of the morning control period may be different from the evening control period.
- Control groups are formed by shifting the switching cycles by one or more control steps. As shown in Figure 5.2, to ensure the time shifted switching cycles are contained in a control period, each control group has one switching cycle less than the control period. To prevent unwanted high peaks on the controlled hot water load curve, turn-off periods of the control groups must overlap with each other in such a way that all the controlled DHWSs do not turn on simultaneously within a control period. To satisfy this condition for overlapping, the number of control groups $N_G$ must be at least equal to the number of control steps in a switching cycle.

$$N_G \geq \tau_{SC}/\tau_{step} \qquad (5.6)$$

- Results in [73] demonstrate that division of households based on the family type does not significantly affect the comfort level of household residents. Thus, the entire set of households can be divided into control groups of approximately equal size, regardless of the family type of a household.

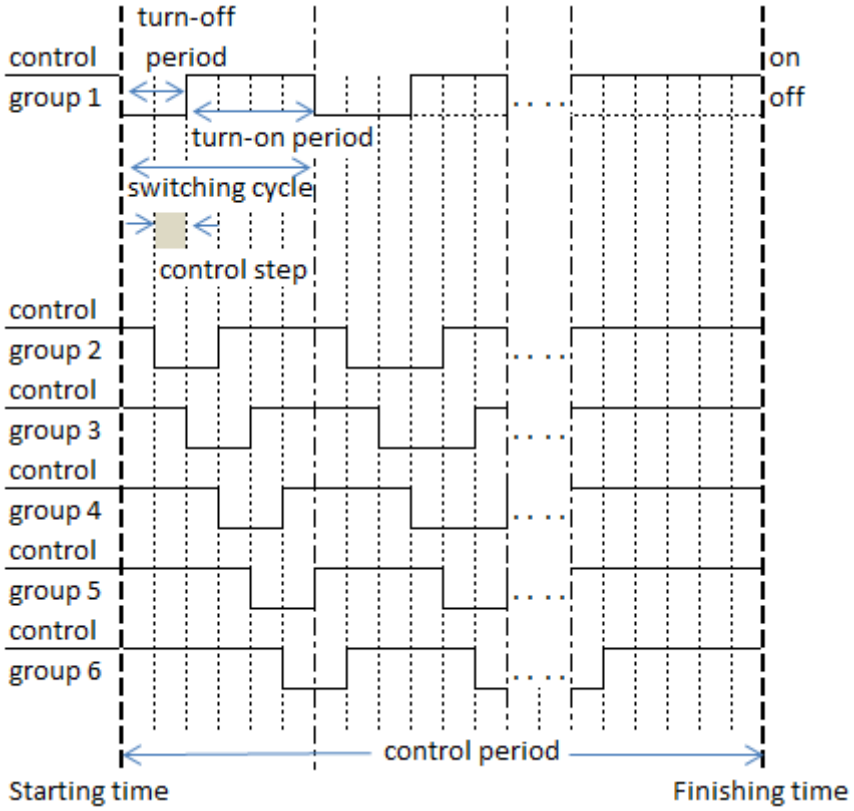


Figure 5.2 A typical switching program and its control management system parameters.

## 5.4 Load estimator

The load estimator estimates controlled hot water loads by applying a switching program to uncontrolled loads of individual households. It sets the load to zero during the turn-off periods of the applied switching program and restores the deferred load during the turn-on periods. This operation is performed on all uncontrolled hot water load profiles for every household.

On the other hand, water temperatures of the DHWSs are not considered in the load estimator.

## 5.5 Optimizer

The main function of the optimizer is to optimize turn-off periods of a switching program so that the aggregate controlled load is below or as close as possible to the user-defined target value. The tool implements two methods of optimization:

- The user defined control period (UDCP) optimizer.

- The optimized control period (OCP) optimizer.

### 5.5.1 UDCP optimizer

The UDCP optimizer determines turn-off periods based on user-defined control periods and the peak load reduction target. The control periods remain unchanged throughout the optimization process. This optimizer implements an iterative process to minimize the mean error between the user-defined target value $L_T$ and the estimated aggregate controlled load $L_C$, in each switching cycle of a switching program. To calculate required changes in the turn-off period for each switching cycle, the optimizer applies proportional and integral (PI) functions to the mean errors [74].

In Figure 5.3, $\tau_{off}(j,k)$ is the turn-off period of switching cycle $j$ in optimization iteration $k$; e$(j,k)$ is the average error between $L_C$ and $L_T$ in switching cycle $j$ and iteration $k$; $K_P$ is the proportional gain and $T_I$ the integral time of the PI functions.

The proportional function multiplies the error by $K_P$. The integral function sums the mean errors of switching cycle $j$ from the previous ($S$-1) iterations to the current one, and multiplies the result by $K_P/T_I$. The sum of the current turn-off period and outputs from the PI functions is converted by the limiter function into an integer between the minimum and maximum values. The final result is the turn-off period for the next iteration.

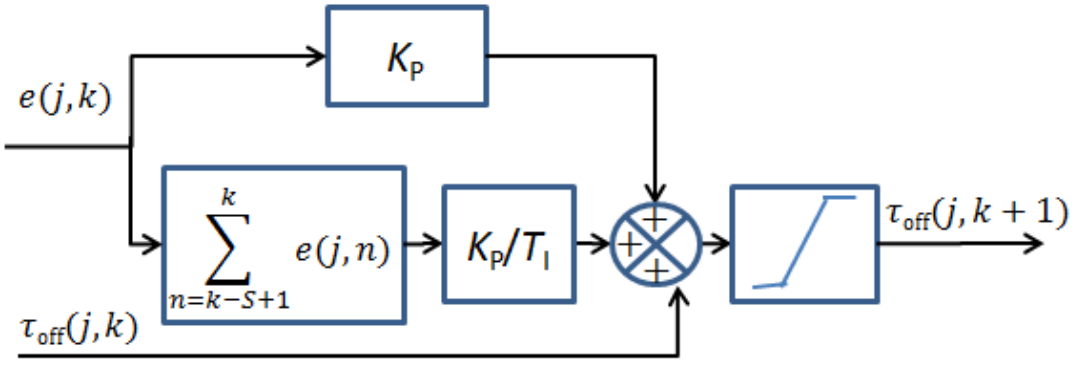


Figure 5.3 Block diagram of the UDCP optimizer.

The performance of the UDCP optimizer is dependent on parameters of the PI functions and the control management system. Thus, the tool allows its users to

modify these parameters to find switching programs that meet their requirements. Setting a high value for $K_P$ may create oscillations on $L_C$, as shown in Figure 5.4. In this case, $K_P$ is set to 2.0 and the integral function is disabled by setting $T_I$ to a very large value relative to $K_P$. Table 5.1 shows the value of control management system parameters used in the simulations. We find that $L_C$ alternates its shape in every other iteration. Furthermore, the difference between the lowest point and the highest point on $L_C$ increases if a higher value of $K_P$ is used.

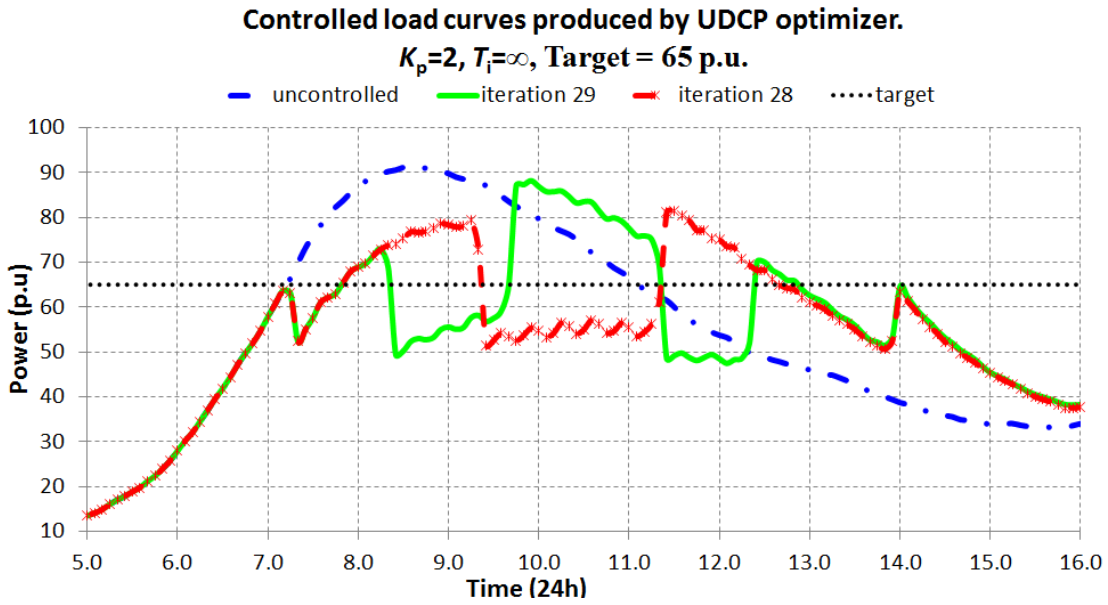


Figure 5.4 Oscillations in aggregate controlled load curves produced by the UDCP optimizer.

Table 5.1 Control management system parameters

| Number of control group | Control Period | Switching cycle | Control step |
|---|---|---|---|
| 6 | 07:15 to 14:15 | 30 min | 5 min |

By reducing the value of $K_P$ to 1.4 while using the same control management system parameters (Table 5.1), the aggregate controlled load curves converge after several iterations. The converged curve alternates around the user-specified target line, as shown in Figure 5.5. With this configuration, we achieve about 17.5% of peak load reduction.

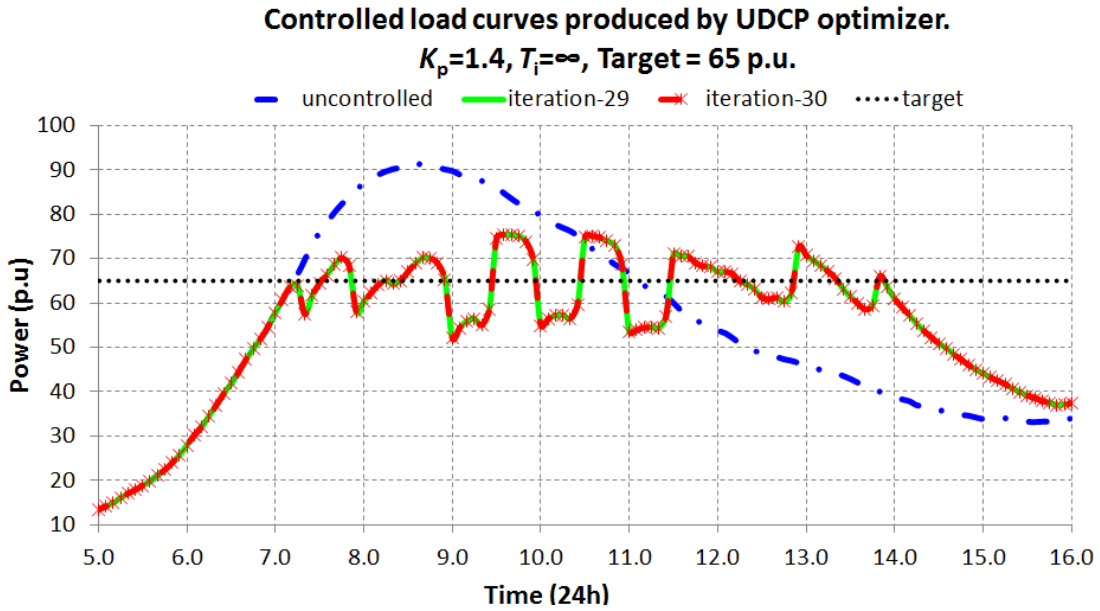


Figure 5.5 Aggregate controlled load curve without oscillations produced by UDCP optimizer.

The performance of the UDCP optimizer improves when the integral function is included, as shown in Figure 5.6. The values for $K_P$, $T_I$ and $S$ are set to 1.2, 5 and 4, while the target remains at 65 p.u. (power) and the same control management system parameters are used (Table 5.1). Compared to the previous two curves, the one shown in Figure 5.6 is smoother and more closely matches the target line. It also has a lower peak, which is about 20% below the peak of the uncontrolled load curve.

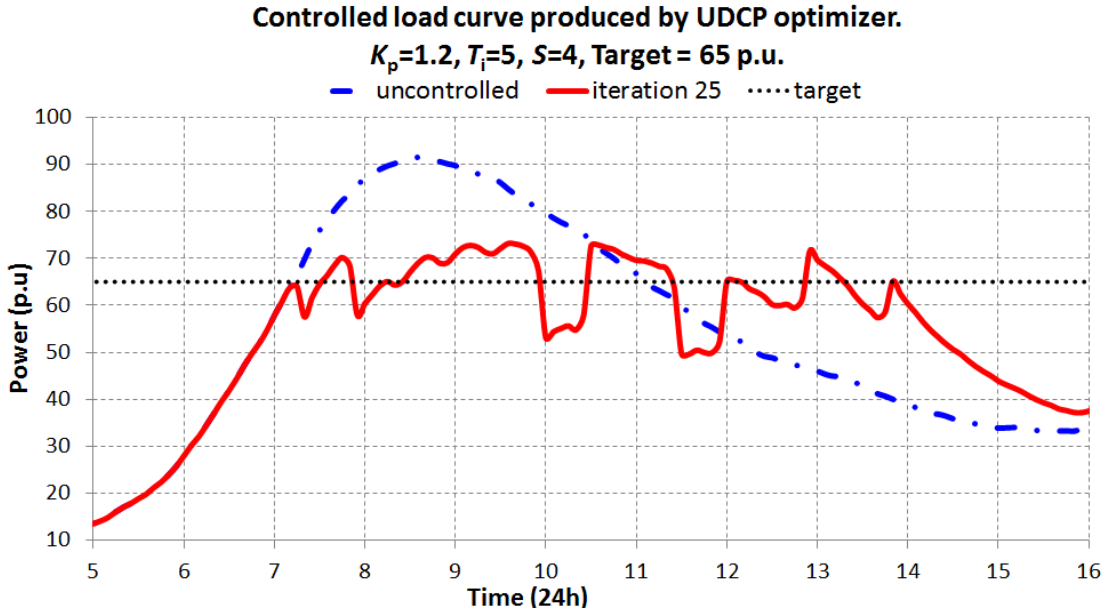


Figure 5.6. Aggregate controlled load curve produced with PI functions in UDCP optimizer.

### 5.5.2 OCP optimizer

Switching programs can be further optimized by implementing OCP optimization. The OCP optimizer determines turn-off periods and control periods of a switching program based on the user-defined peak load reduction target $L_T$. First, it finds the starting time $t_s$ and finishing time $t_f$ of the initial control period. The time $t_s$ is found as the first intersection of the aggregate uncontrolled load curve $L_U$ and the target $L_T$, as shown in Figure 5.7. To avoid a high payback peak after the control period, the finishing time $t_f$ is found by solving the following equation:

$$\int_{t_s}^{t_f} L_U(t) \cdot dt = L_T \cdot (t_s - t_f) \qquad (5.7)$$

where the left hand term represents the total uncontrolled energy consumption between $t_s$ and $t_f$, which is the area under $L_U$ (red solid curve) between $t_s$ and $t_f$ in Figure 5.7; the right hand term represents the area under $L_T$ (blue dotted line) between $t_s$ and $t_f$ in Figure 5.7.

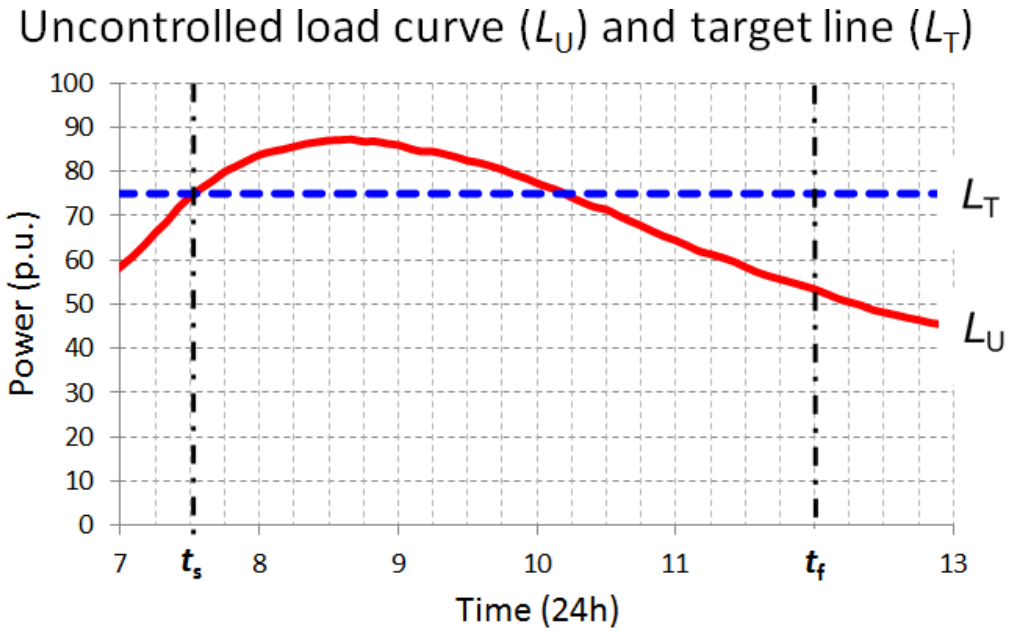


Figure 5.7. Initial control period in relation to $L_T$ and $L_U$.

To further minimize the error between $L_C$ and $L_T$, the OCP optimizer iteratively tunes the switching program optimized by the UDCP optimizer. The OCP optimizer increases or decreases the turn-off period $\tau_{off}$ of each switching cycle to minimize the error between $L_T$ and $L_C$. We define three tolerance levels:

- $L_1$ is 1% above $L_T$;
- $L_2$ is 2% above $L_T$;
- $L_3(j)$ is the difference between $L_T$ and the estimated load (in addition to the existing load) that would be restored in switching cycle $j$, if $\tau_{off}(j)$ is decreased by one control step. It is calculated as:

$$L_3(j) = L_T - max[L_U(j-2), L_U(j-1), L_U(j)] \cdot \frac{\tau_{step}}{\tau_{sc}} \qquad (5.8)$$

where $\tau_{step}$ is the control step; $\tau_{sc}$ is the switching cycle; $max[L_U(j–2), L_U(j–1), L_U(j)]$ is the maximum value of the aggregate uncontrolled load $L_U$ over three switching cycles ($j$-2), ($j$-1) and $j$.

The OCP optimizer tunes the $\tau_{off}$ of all but the last switching cycle within a control period, based on the three scenarios shown below, where $L_C(j)$ denotes values of $L_C$ within switching cycle $j$. Figure 5.8 graphically illustrates these scenarios.

- Scenario 1. The peak of $L_C(j)$ is above $L_2$.
- Scenario 2. $L_C(j)$ stays between $L_1$ and $L_2$ for more than 15 min.
- Scenario 3. The peak of $L_C(j)$ is below $L_3(j)$.

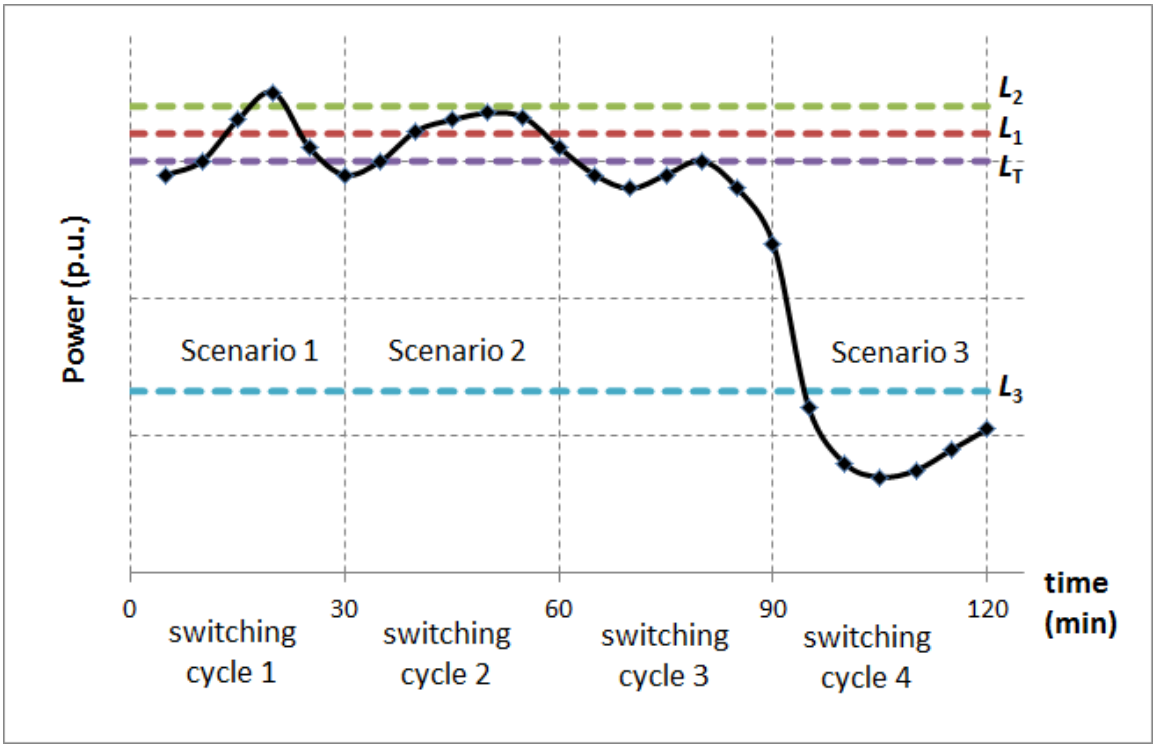


Figure 5.8 Scenario 1, 2 and 3 used in OCP optimization.

Scenarios 1 and 2 represent overshooting, whereas Scenario 3 indicates over-

control that can potentially create higher payback peaks. The OCP optimizer reduces $L_C(j)$ by increasing $\tau_{off}(j)$ by one $\tau_{step}$, if either Scenario 1 or Scenario 2 is met. If Scenario 3 is met, $\tau_{off}(j)$ is decreased by one $\tau_{step}$ to restore some deferred loads while keeping $L_C$ below $L_T$. No change is made on $\tau_{off}(j)$ if none of the above conditions are met.

Before changing $\tau_{off}(j)$, the OCP optimizer considers the current value of $\tau_{off}$ (expressed as the number of control steps) and the location of the peak of $L_C(j)$ within switching cycle $j$. For a peak located within the first $n$ control steps of a given switching cycle, the OCP optimizer imposes the following conditions to accept only the changes in $\tau_{off}$ that are effective in reducing (or increasing) the peak in this switching cycle:

- If $\tau_{off}$ is to be increased and the current value of $\tau_{off}$ is below or equal to ($n$-1), then increase $\tau_{off}$ by one $\tau_{step}$. No change is made otherwise
- If $\tau_{off}$ is to be decreased and the current value of $\tau_{off}$ is below or equal to $n$, then decrease $\tau_{off}$ by one $\tau_{step}$. No change is made otherwise

where $\tau_{off}$ is expressed as the number of control steps ($\tau_{step}$).

If $j$ is the last switching cycle of a control period, and either Scenario 1 or Scenario 2 is met, the control period is extended by one switching cycle; $\tau_{off}(j)$ is then set to a value equal to a multiple of $\tau_{step}$ and proportional to the error between the peak of $L_C(j)$ and $L_T$. Through iterations, the OCP optimizer tunes the switching program so that the aggregate controlled load stays below or as close as possible to the user-defined target.

The operation of the OCP optimizer is illustrated in Figure 5.9. In this case, a hot water load profile with a dominant evening peak is used, which is represented as the blue dotted curve in Figure 5.9. After the first iteration, we can still find several overshooting peaks on the aggregate controlled load curve. Through iterations, the OCP optimizer reduces these peaks to values less than or very close to the required target lines. In the 6$^{th}$ iteration, the OCP optimizer has reduced the evening peak

below the intended target line, except for a rather small overshoot at around 22:00. This optimizer has also extended the morning control period to allow for a more gradual load restoration. However, the peaks located at 13:30 and 14:30 cannot be further reduced because the morning control period has reached the maximum limit of 7.5 hours set in the tool.

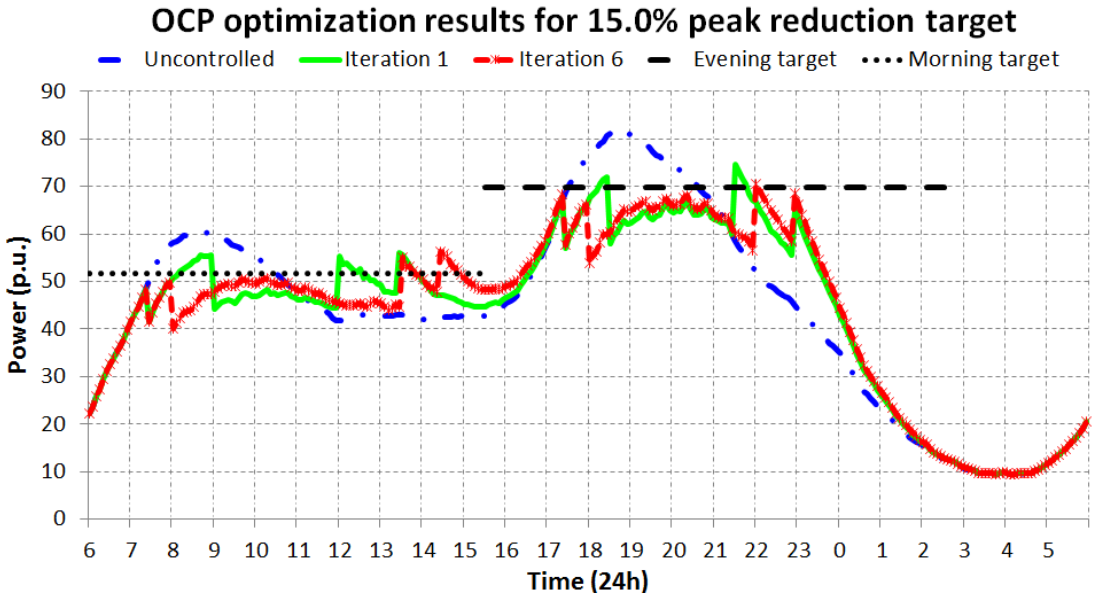


Figure 5.9 OCP optimization results for iteration 1 and iteration 6.

More case studies and detailed analyses on simulation results are provided in Chapter 6.

## 5.6 Conclusion

The chapter has presented the performance calculator and the switching program optimizer modules in the developed hot water evaluation tool (shown in Figure 2.1).

The KPIs produced by the performance calculator are employed by the tool to assess the performance of the switching programs applied to DHWSs in a controlled area. The two KPIs described in this chapter were peak load reduction and probabilities of cold showers. The former is used to evaluate the effectiveness of a DLC switching program in reducing peak load, while the latter is used to assess the impact of a DLC switching program on consumer comfort level.

Meanwhile, the operation of the switching program generator has been described

with the control management system parameters clearly defined. Functions of the load estimator have also been outlined. At the same time, two optimization methods implemented in the optimizer to produce optimized switching programs have been presented in detail. To produce optimized DLC switching programs, the UDCP optimizer requires the control periods and the peak load reduction target to be specified by the tool user. On the other hand, the OCP optimizer uses the peak load reduction target specified by the tool user to iteratively determine the optimized control periods and subsequently produces optimized DLC switching programs. The operations of the optimizers have been demonstrated through simulation examples presented in this chapter.

The next chapter presents a number of case studies that use the developed hot water evaluation tool to investigate the performance of different DLC switching programs under various operating scenarios.

# Chapter 6

## Case Studies

This chapter presents a number of case studies performed with the developed hot water evaluation tool, as well as discussions on the results obtained in these studies.

First, we investigate the scalability of the results obtained from the tool. In other words, we wish to find out how well the results scale when different numbers of households are used in simulations. For example, we want to find out if it is possible to perform simulations for 300 households and scale up the results to represent 3000 households in an area. Performing simulations on a scaled down number of households requires lower computing resources and drastically reduces simulation time.

Next, we study the potential impacts of using average values of ambient temperature and cold water temperature on simulation results. We wish to determine if constant average values can be used to represent the actual values for these two parameters, and produce results that accurately approximate the actual results. Ambient and cold water temperatures not only change according to climate zone, they also vary throughout the day. Hence, using average values in place of actual values simplifies the simulation process.

In the subsequent case study, we evaluate the effect of using common values for thermostat settings on simulation results. Thermostat settings on a DHWS determine its turn-on temperature $T_{on}$ and turn-off temperature $T_{off}$. Practically, these two parameters are different from one household to another. We wish to find out if common values for $T_{on}$ and $T_{off}$ can be used for all households without significantly affecting the results. Being able to do this will simplify the simulation process.

In succeeding case studies, we use the tool to generate optimized switching programs and assess their performance in terms of the peak load reduction and consumer comfort level. Several operating scenarios are considered in these studies.

Power consumption is normalized to 2.4 kW in all the studies presented in this

chapter.

## 6.1 Case study 1: scalability of results

We performed six simulations in this case study. First, we used the tool to randomly generate hot water consumption profiles with a dominant morning peak for 300 households and obtained an aggregate uncontrolled hot water load curve ($L_{300}$). Then, the aggregate uncontrolled load curves for 1500 households ($L_{1500}$) and 3000 households ($L_{3000}$) were determined using the same set of configuration parameters. Next, we scaled up $L_{300}$ by factors of 5 and 10, and compared them with $L_{1500}$ and $L_{3000}$, respectively. After that, the above process was repeated for a hot water consumption profile with a dominant evening peak.

Figures 6.1 and 6.3 show the uncontrolled load curves for hot water consumption profiles with dominant morning peak; Figures 6.2 and 6.4 show the uncontrolled load curves with dominant evening peak. The dotted curves in Figures 6.1 and 6.2 depict $L_{1500}$ and the solid curves depict $L_{300}$ scaled up by a factor of 5; the dotted curves in Figures 6.3 and 6.4 depict $L_{3000}$ and the solid curves depict $L_{300}$ scaled up by a factor of 10.

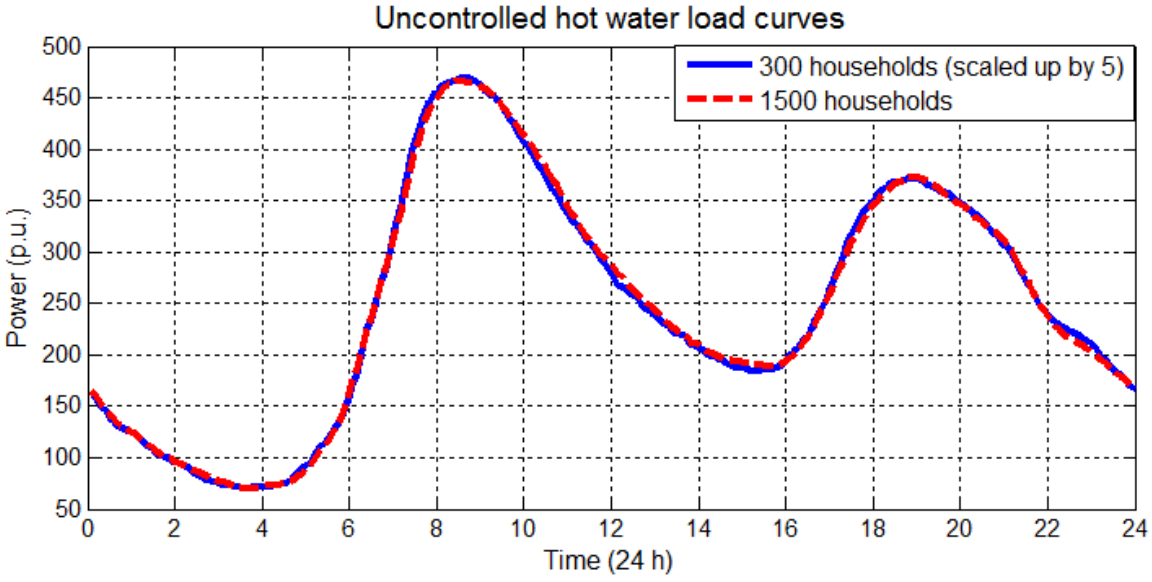


Figure 6.1 Uncontrolled load curves with dominant morning peak for 1500 households.

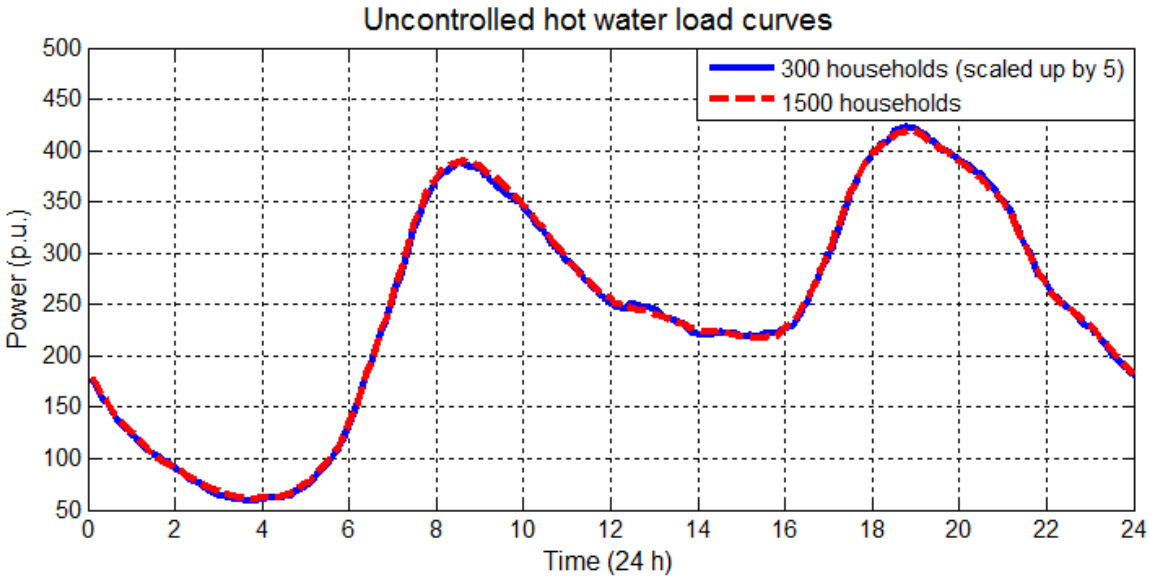


Figure 6.2 Uncontrolled load curves with dominant evening peak for 1500 households.

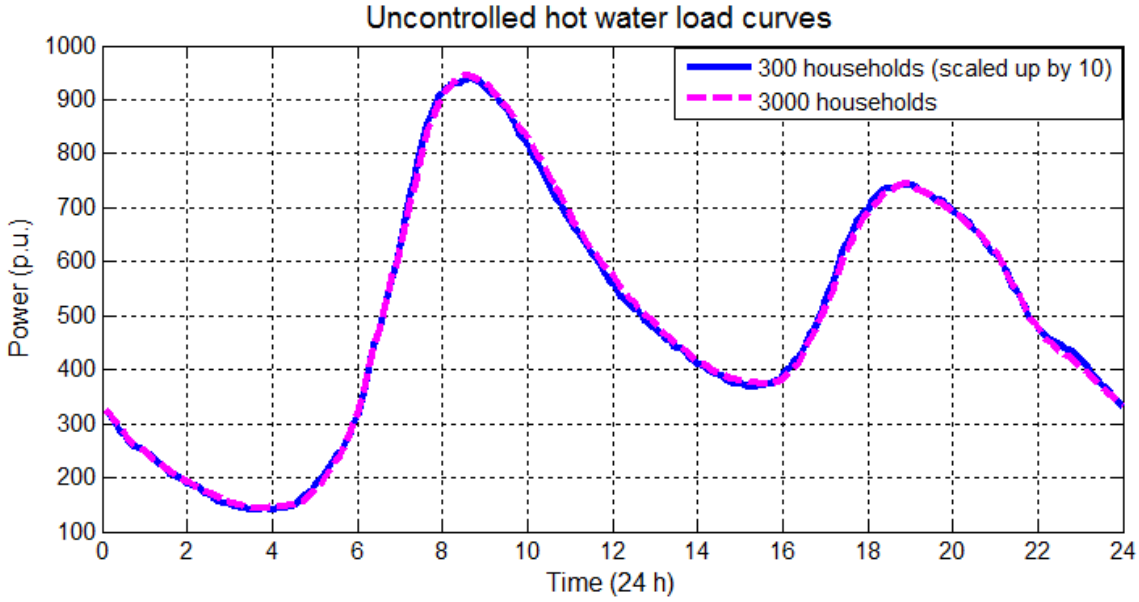


Figure 6.3 Uncontrolled load curves with dominant morning peak for 3000 households.

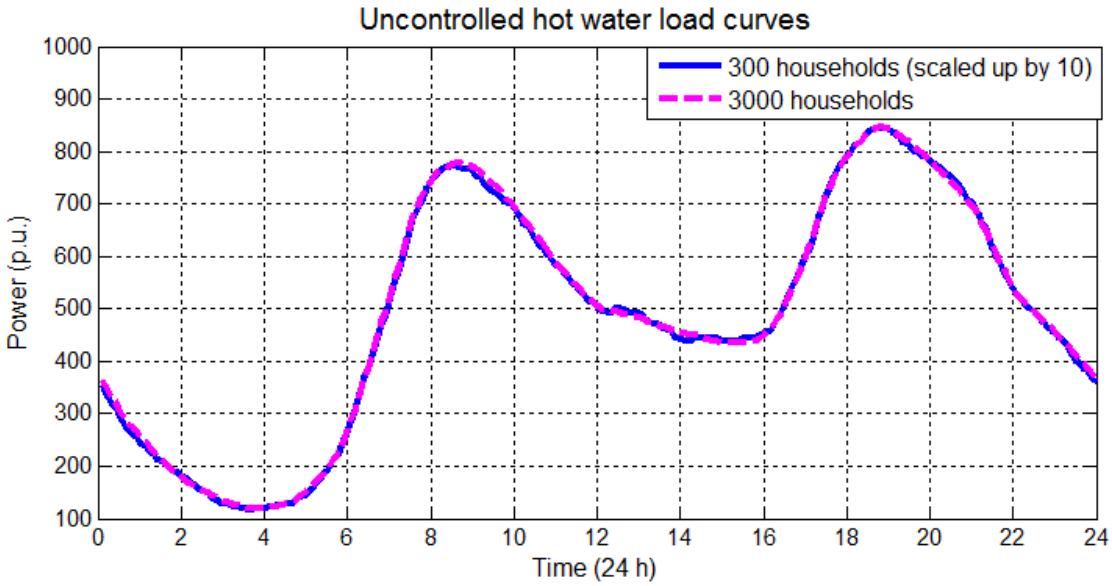


Figure 6.4 Uncontrolled load curves with dominant evening peak for 3000 households.

We performed comparative analyses on the load curves shown in Figures 6.1–6.4 and tabulated the results in Table 6.1.

Table 6.1 Results of comparative analyses

| | **Difference in total energy consumption over 24 hours** | **MAE** | **MAPE** |
|---|---|---|---|
| **Between $L_{1500}$ and $L_{300}$ x5 (Figure 6.1)** | 0.1% | 3.5 p.u. | 1.6% |
| **Between $L_{1500}$ and $L_{300}$ x5 (Figure 6.2)** | 0.3% | 2.2 p.u. | 1.1% |
| **Between $L_{3000}$ and $L_{300}$ x10 (Figure 6.3)** | 0.1% | 6.4 p.u. | 1.4% |
| **Between $L_{3000}$ and $L_{300}$ x10 (Figure 6.4)** | 0.5% | 4.5 p.u. | 1.1% |

MAE is the mean absolute error and MAPE the mean absolute percentage error. The calculations of MAE and MAPE are given below.

$$MAE = \frac{1}{N} \cdot \sum_{i=1}^{N} |v_i - u_i| \qquad (6.1)$$

$$MAPE = \frac{1}{N} \cdot \sum_{i=1}^{N} \left| \frac{v_i - u_i}{v_i} \right| \qquad (6.2)$$

where $N$ is the total number of data points; $u$ and $v$ are the respective data to be compared; and $|x|$ denotes absolute value of variable $x$.

The above results demonstrate that the simulation results scale very well. Hence, we can use a smaller number of households in simulations and scale up the results to represent a higher number of households without introducing significant errors.

## 6.2 Case study 2: ambient and cold water temperatures

This case study compared results of two simulations. In the first simulation, we used actual values of ambient temperature $T_a$ and cold water temperatures $T_c$ of Tasmania during the winter period, shown in Figure 6.5.

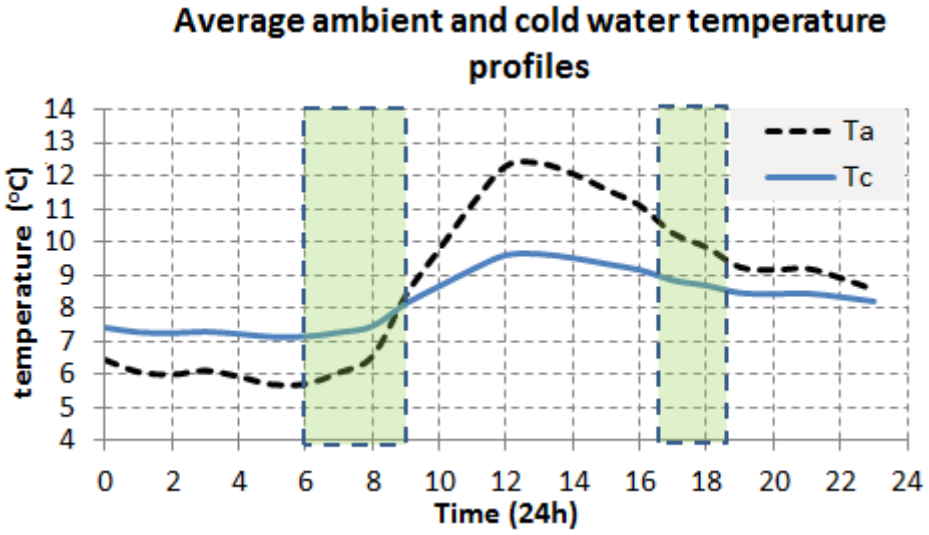


Figure 6.5 Average ambient and cold water temperatures in winter time.

Shaded areas indicate peak periods of hot water usage (06:00 – 09:00 and 16:30 – 18:30). The profile of $T_a$ was obtained from historical climate data for Tasmania [75]; $T_c$ usually has a positive correlation with $T_a$ [61], but has a smaller range of variation. As can be seen in Figure 6.5, values of $T_a$ and $T_c$ vary considerably over the 24 hour period (particularly, values of $T_a$), but their variations during peak periods are rather small. Therefore, in the second simulation, $T_a$ and $T_c$ were set to a constant value of 8°C.

Figure 6.6 shows two aggregate uncontrolled hot water load curves obtained using variable and constant values for ambient and cold water temperatures.

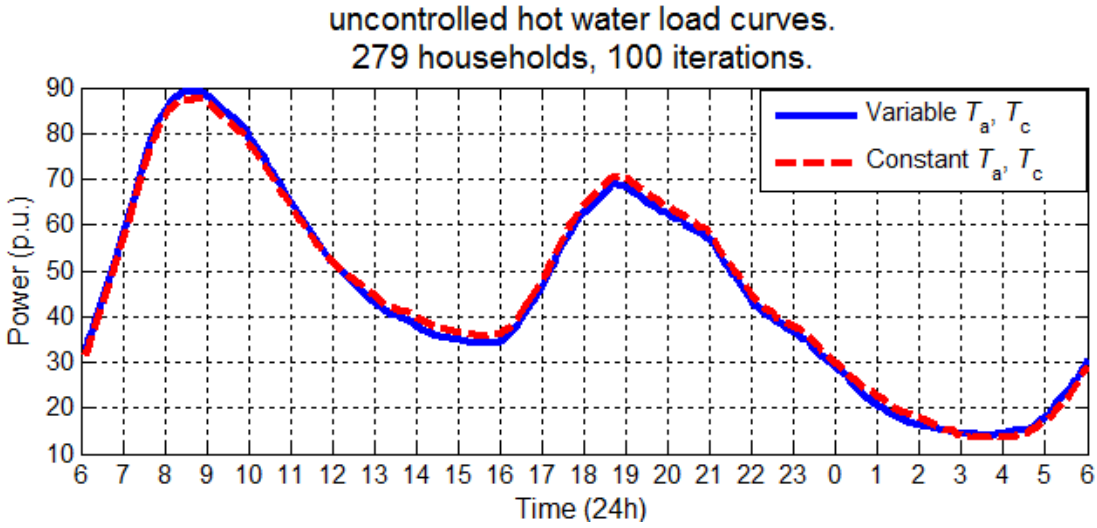


Figure 6.6 Uncontrolled load curves for constant and variable values of ambient and cold water temperatures.

We found insignificant differences between the two curves. Over the 24 hour period, the difference in the total energy consumption was about 1%, and the MAE was about 1.3 p.u. The results can be explained by the fact that a great majority of hot water usages occurred during peak periods when variations of actual cold water temperature were rather small (within ± 1$^{o}$C, in shaded areas of Figure 6.5). On the other hand, although $T_a$ varied significantly during the day, its variation had negligible overall effect on the rate of hot water tank heat losses. An insulated hot water tank idles for a long period (usually from 13 to 15 hours) between two consecutive recharges due to heat losses. During this period, the effect of $T_a$ variation is smoothed, and using the average value of $T_a$ produces results similar to using variable values of $T_a$. Thus, variations of $T_a$ and $T_c$ can be represented with their respective average values in further studies.

## 6.3 Case study 3: thermostat settings

This case study compared the results of using constant versus variable thermostat settings. In the first simulation, we set the thermostat turn-on temperature $T_{on}$ to 52$^{o}$C and the turn-off temperature $T_{off}$ to 60$^{o}$C for all households. In the second simulation, we assumed that $T_{on}$ and $T_{off}$ were variables uniformly distributed from 50$^{o}$C to 54$^{o}$C and from 58$^{o}$C to 62$^{o}$C, respectively [37]. We found no significant difference between the two simulations, as depicted in Figure 6.7. Over the 24 hour period, the difference

in the total energy consumption was about 0.2%, and the MAE was about 1.1 p.u. Thus, common values of $T_{on}$ and $T_{off}$ can be used for all households in simulations without any significant impact on the results.

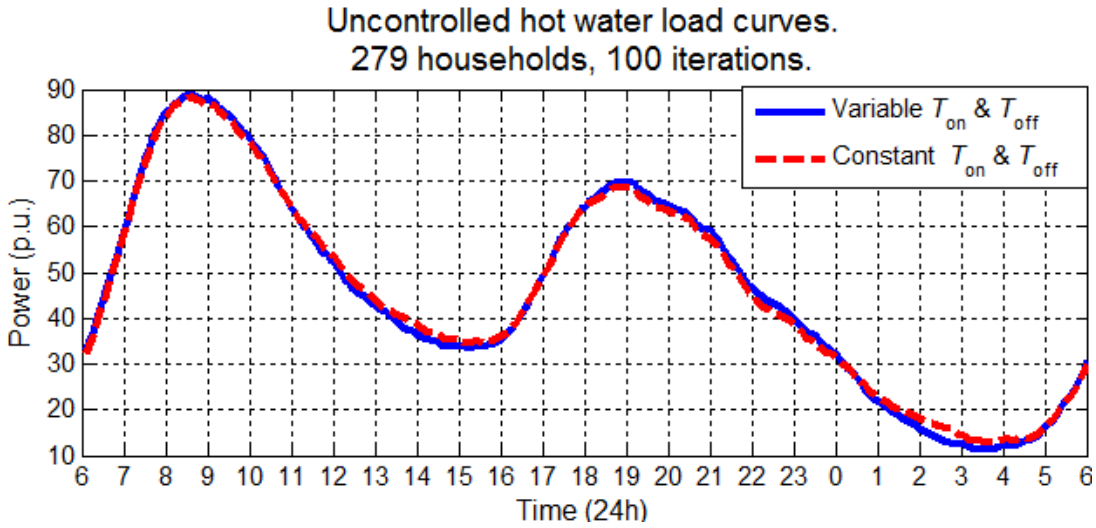


Figure 6.7 Uncontrolled load curves for constant and variable turn-on and turn-off temperatures.

In fact, the thermostat settings are fixed by qualified installers and consumers rarely change them. Obviously, setting higher values for $T_{on}$ and $T_{off}$ results in storing more heat energy in the hot water tank and reduces the probability of getting cold showers. On the other hand, Australian Standard AS 3498 requires heating the water to at least 60$^{o}$C to inhibit Legionella bacteria growth in the storage tank [55]. Thus, to represent the worst case scenario in our simulations, we make the assumption to use 52$^{o}$C as the value of $T_{on}$ and 60$^{o}$C as $T_{off}$ for all controlled households in our further studies.

## 6.4 Case study 4: evaluation of switching programs

This case study consisted of several studies which assessed the performance of switching programs produced by the developed tool for different operating scenarios. We used the tool to randomly generate hot water consumption profiles for 279 households. This set of households provided us the opportunity to use actual energy metering data in our studies. From the hot water consumption profiles generated by the tool, we subsequently obtained an aggregate uncontrolled hot water load curve, which matched the actual data. Then, the optimizer module in the tool optimized and

recommended optimized switching programs to the tool user who would select the switching program that suited his/her objectives. The tool subsequently applied the selected switching program to the uncontrolled hot water loads and obtained the aggregate controlled hot water load curve. Performance was evaluated in terms of the peak load reduction and consumer comfort level.

In all of these studies, we used 43$^{o}$C as the preferred shower temperature for all households. A default switching program configuration as shown in Table 6.2 was used in all the studies, except otherwise stated. It had 30 minute switching cycles and 5 minute control steps. The turn-off period of each switching cycle varied from 5 minutes to 25 minutes in 5 minute steps. The controlled households were divided into six control groups each containing approximately an equal number of households.

Table 6.2 Default switching program configuration

| | **default switching program configuration** |
|---|---|
| Control groups | 6 |
| Switching Cycle | 30 (min) |
| Control Step | 5 (min) |
| Turn-off periods | 5, 10, 15, 20, 25 (min) |

### 6.4.1 Comparison of UDCP and OCP optimizers

This case study compared the performance of the UDCP optimizer and the OCP optimizer. Both optimizers used the default switching program configuration (Table 6.2) to produce optimized switching programs that were applied to the same set of hot water loads. The peak reduction target was 15% in both cases. Figures 6.8 and 6.9 show the aggregate controlled load curves produced by the UDCP and OCP optimizers, respectively. Table 6.3 shows the control periods and peak reductions achieved. The UDCP optimizer does not change the user-specified control periods in its optimization process. Probabilities of cold showers for each family type are shown in Table 6.4 for the uncontrolled scenario, and scenarios controlled by the UDCP-optimized and OCP-optimized switching programs.

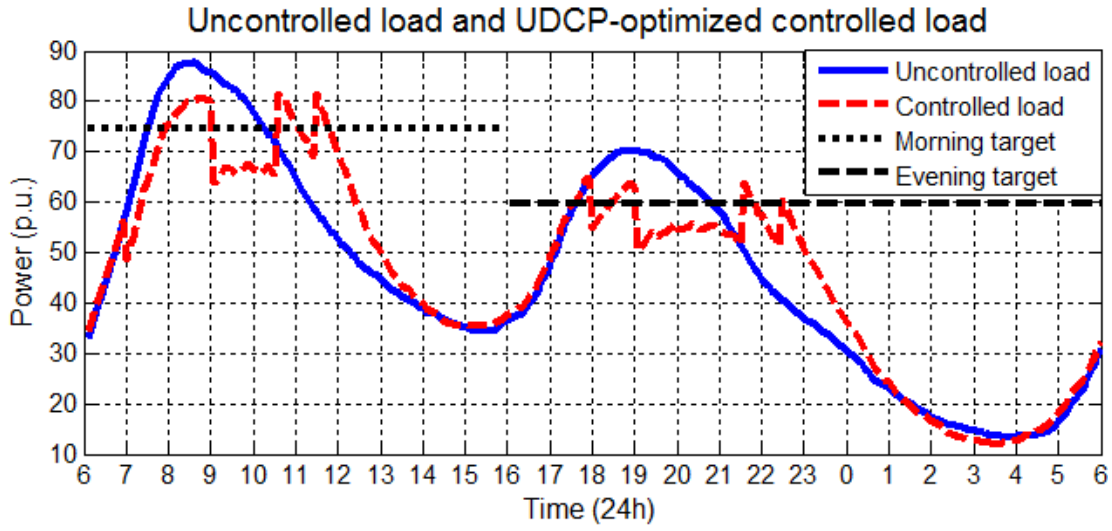


Figure 6.8 Result of the UDCP optimization.

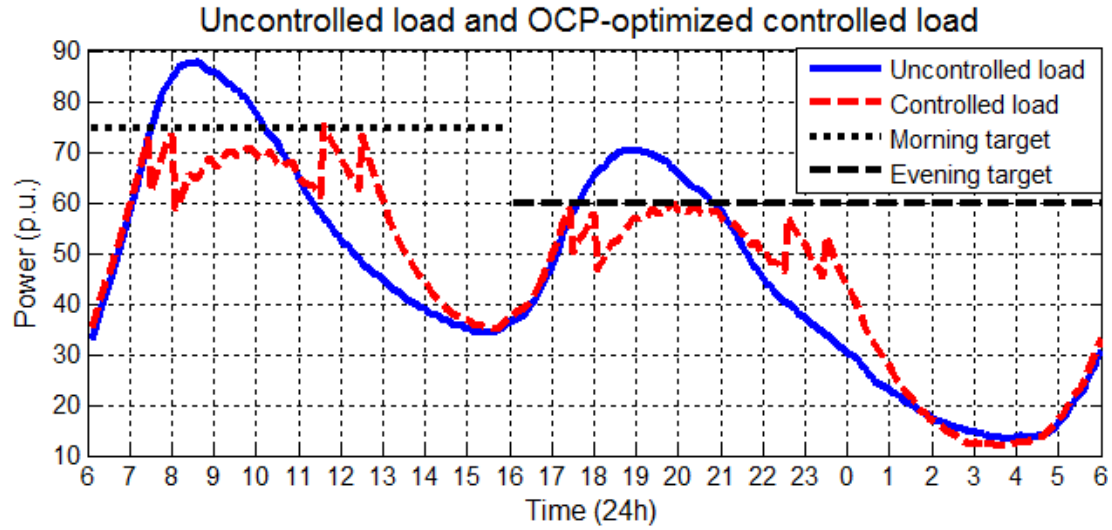


Figure 6.9 Result of the OCP optimization.

Table 6.3 Control periods and peak reductions for UDCP and OCP optimizers

| | Morning | | Evening | |
|---|---|---|---|---|
| | **Control period** | **Peak reduction** | **Control period** | **Peak reduction** |
| **UDCP optimizer** | 07:00-12:00 | 7.1% | 18:00-23:00 | 9.3% |
| **OCP optimizer** | 07:30-13:00 | 14.3% | 17:30-00:00 | 15.0% |

Table 6.4 Probabilities of cold showers for uncontrolled scenario and controlled scenarios

| | Uncontrolled | UDCP optimizer | OCP optimizer |
|---|---|---|---|
| Family type 1 | 0.0% | 0.0% | 0.0% |
| Family type 2 | 4.4% | 4.5% | 4.6% |
| Family type 3 | 8.0% | 8.3% | 8.4% |
| Family type 4 | 13.9% | 14.1% | 14.4% |
| Overall | 5.1% | 5.2% | 5.3% |

Comparing the aggregate controlled load curves produced by both optimizers, we found that the OCP optimizer performed much better in terms of peak load reduction. The starting and finishing times of control periods in a switching program are vital for peak load reduction. A delayed control period produces an initial peak above the target line, as seen in the evening control period of Figure 6.8. Starting a control period too early defers loads needlessly and creates slightly higher peaks in subsequent switching cycles of the same control period, as observed in the morning control period of Figure 6.8. Control periods with sufficient length allow a gradual restoration of loads below the target line. Hence, ending a control period prematurely creates an unwanted high payback peak at the end of the control period, as seen at around 11:30 of Figure 6.8. Similar results were reported in [73] and [76]. As shorter than required control periods were used in the UDCP optimization, reducing the peaks at 10:30 and 21:30 would produce higher payback peaks at the end of the respective control periods.

While both controlled scenarios produced higher probabilities of cold showers than in the uncontrolled scenario, the OCP optimizer degraded the comfort level more than the UDCP optimizer due to its longer control periods (Table 6.4).

### 6.4.2 Switching programs for two different hot water consumption profiles

In this case study, we evaluated the tool's ability to optimize switching programs for two different hot water load profiles. The first one had a dominant morning peak and the second a dominant afternoon peak. The first load profile was used in the case study presented in Section 6.4.1. The default switching program configuration (Table

6.2) was used and the peak reduction target was 15%. Figure 6.10 shows the aggregate uncontrolled load curve of the second hot water load profile, and the aggregate controlled load curve after the OCP-optimized switching program was applied. Table 6.5 shows probabilities of cold showers estimated for each family type under uncontrolled and controlled scenarios.

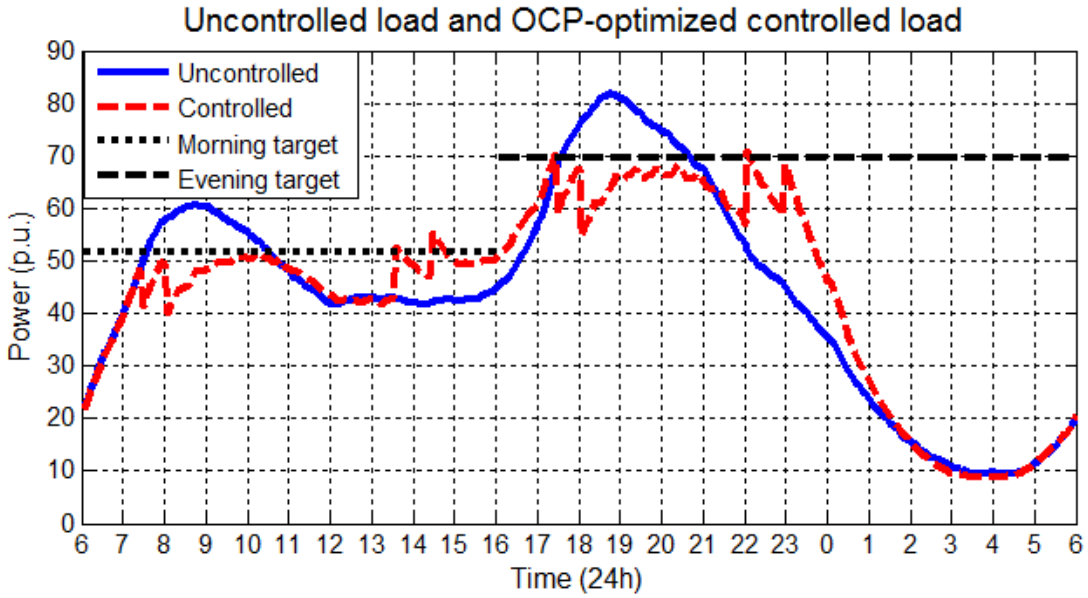


Figure 6.10 The OCP optimization of a hot water load profile with a dominant afternoon peak.

Table 6.5 Probabilities of cold showers for a hot water load profile with dominant afternoon peak under uncontrolled and controlled scenarios

| | **Uncontrolled** | **Controlled** |
|---|---|---|
| Family type 1 | 0.0% | 0.1% |
| Family type 2 | 4.1% | 4.5% |
| Family type 3 | 7.5% | 8.3% |
| Family type 4 | 14.3% | 15.8% |
| Overall | 4.8% | 5.3% |

Optimized morning and evening control periods were from 07:30 to 15:00 and from 17:30 to 23:30, respectively. A 9.1% peak reduction was achieved for the morning control period, and 13.4% for the evening. The morning control period had reached the maximum limit of 7.5 hours. Hence, the tool could not further reduce the

payback peak detected at 14:30 as seen in Figure 6.10.

Comparison of the results produced by the OCP optimizer in the current case study and the one presented in Section 6.4.1 (Table 6.4 and Table 6.5) reveals that consumers experienced similar comfort under different load profiles.

### 6.4.3 Comparison of two different switching program configurations

In this case study, we used the hot water load profiles of the case study presented in Section 6.4.1 and compared the performance of two different switching program configurations represented in Table 6.6. Results produced by the OCP optimizer as presented in Section 6.4.1 represent the implementation of the default configuration. The results of implementing the second switching program (configuration 2) on the same set of hot water loads are shown in Figure 6.11 and Table 6.7.

The optimized control periods were from 07:30 to 13:30 in the morning and from 17:30 to 00:00 in the evening. Peak reductions for morning and evening control periods were 14.8% and 13.2%, respectively.

Table 6.6 Switching program configurations used in the case studies

| | **Configuration 1 (default)** | **Configuration 2** |
|---|---|---|
| Control groups | 6 | 3 |
| Switching Cycle | 30 (min) | 30 (min) |
| Control Step | 5 (min) | 10 (min) |
| Turn-off periods | 5, 10, 15, 20, 25 (min) | 10, 20 (min) |

Table 6.7 Probabilities of cold showers for uncontrolled scenario and controlled scenario employing switching configuration 2

| | **Uncontrolled** | **Controlled** |
|---|---|---|
| Family type 1 | 0.0% | 0.1% |
| Family type 2 | 4.4% | 4.8% |
| Family type 3 | 8.0% | 8.7% |
| Family type 4 | 13.9% | 14.6% |
| Overall | 5.1% | 5.5% |

The default switching program configuration performed slightly better in peak reduction as it had a smaller control step and a higher number of control groups. Switching program configuration 2 degraded the consumer comfort level further as hot water systems were switched off for longer periods of time.

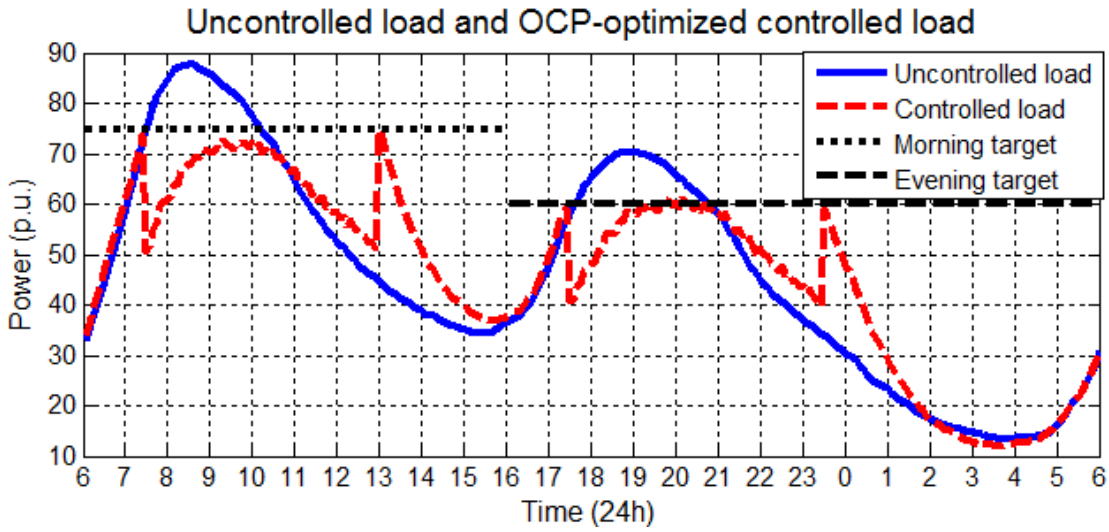


Figure 6.11 The OCP optimization with switching program configuration 2.

### 6.4.4 Maximum peak load reduction

In this case study, we limited the control periods to a maximum of 7.5 hours, and used the tool to find the best achievable peak load reduction under this constraint. For comparison, we used the hot water load profiles of the case study presented in Section 6.4.1 and the default switching program configuration shown in Table 6.2. Figure 6.12 shows the aggregate controlled load curve created by the OCP optimizer.

A 17.4% peak reduction was achieved for the morning control period, and 17.5% for the evening. The optimized control periods were from 07:15 to 14:45 in the morning and from 17:30 to 01:00 in the evening.

From Figure 6.12, we can see that 7.5 hours is a practical limit under the operating conditions used in the simulation. After the morning control period, deferred hot water loads were fully restored just before the beginning of the next control period. Nevertheless, due to the much longer total control period, this switching program significantly degraded the comfort level of all families compared to the previous case studies. The overall probability of cold showers increased from about 5% in the

uncontrolled scenario to over 6% in the controlled scenario. The probabilities of cold showers estimated for each family type are shown in Table 6.8.

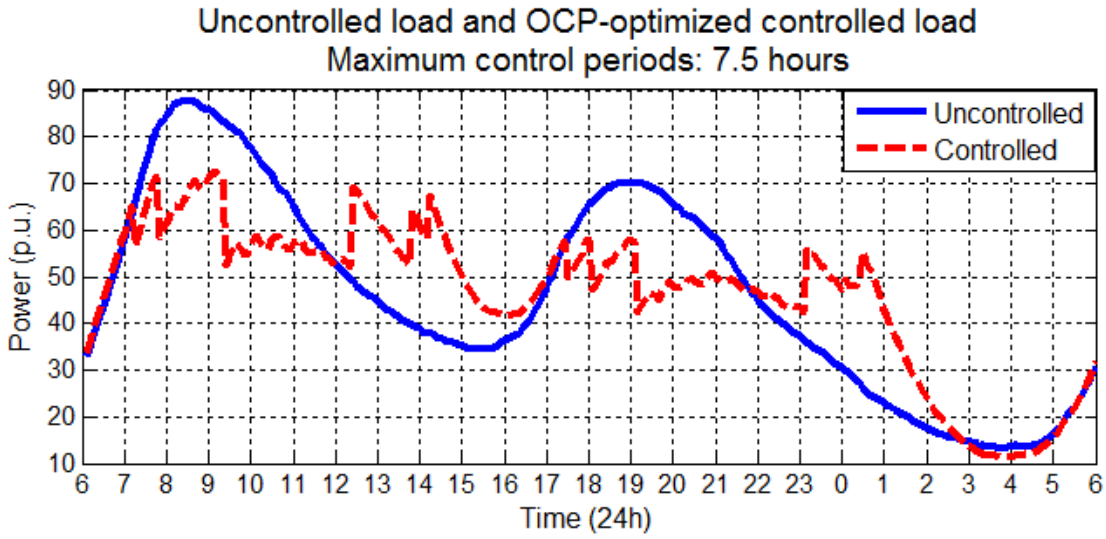


Figure 6.12 The OCP optimization result with control periods limited to 7.5 hours.

Table 6.8 Probabilities of cold showers for uncontrolled scenario and controlled scenario with maximum control periods

| | **Uncontrolled** | **Controlled** |
|---|---|---|
| Family type 1 | 0.0% | 0.1% |
| Family type 2 | 4.4% | 5.7% |
| Family type 3 | 8.0% | 10.0% |
| Family type 4 | 13.9% | 16.0% |
| Overall | 5.1% | 6.4% |

## 6.5 Conclusion

This chapter has presented the case studies conducted with the developed tool. We have demonstrated that simulation results can be scaled without introducing significant errors. The highest MAPE associated with scaling simulation results was below 2%. Hence, the results simulated with a smaller number of households can be scaled up to represent a higher number of households. We have also investigated the potential impacts of using average values of ambient temperature, cold water temperature and thermostat settings on the simulation results. Assuming average ambient and cold water temperatures throughout the day produced an error of

approximately 1% in the total energy consumption, whereas applying common thermostat set point temperatures to all households produced less than 1% of error in the total energy consumption. Thus, we have demonstrated that average values for these parameters could be used to represent actual variable values without sacrificing the accuracy of simulations.

The subsequent case study results have shown that the optimized switching programs produced aggregate controlled load curves that closely matched the user-specified peak reduction targets under various operating scenarios. We have compared the performance of the OCP and UDCP optimizers and discovered that the former performed better in terms of peak reduction. For a 15% peak reduction target, the OCP-optimized switching program successfully reduced the peak by more than 14% while the UDCP-optimized switching program could only achieve less than 10% of peak reduction. However, the former degraded the consumer comfort level slightly more than the latter due to longer control periods.

On the other hand, the tool has worked well to optimize switching programs for two different hot water load profiles. In both cases, peak reductions close to the required target (15%) were achieved and consumers experienced a similar level of comfort. We have also studied different configurations of switching program and found that using smaller control steps and a higher number of control groups will produce a slightly higher peak reduction. In the case study, a configuration that used 5 minute control steps and six control groups improved the peak reduction by about 1%, as compared to a configuration with 10 minute control steps and three control groups.

In general, the results have revealed that the starting time and the length of control periods are crucial in peak reduction. Having a longer control period will potentially result in higher peak reductions. However, the length of control periods must be limited to minimize negative impact on consumer comfort. The results have shown that implementing a 7.5 hour control period in both the morning and evening will cause an additional 1.3% of households to experience cold showers.

# Chapter 7

## Conclusion and Future Studies

### 7.1 Summary of the thesis

This thesis has presented the research work in the development of an evaluation tool for the DSM of domestic hot water load. This tool aims to simulate domestic hot water loads, produce optimized switching programs for direct control of DHWSs and evaluate the performance of these switching programs with simulations. The developed tool has met the two objectives set for this research. It can accurately model the available domestic hot water load and predict the potential peak reduction achievable through direct load control; and it can be used to assist distribution system operators in designing their load management programs. Our research work, as presented in this thesis, is summarized in the following paragraphs.

First, we provided an introduction on DSM in Chapter 1. The main types of DSM initiatives were described together with their respective implementations in power systems around the world. At the same time, a literature review of DSM methods and their results were presented. In this chapter, we also included the values of DSM for modern power systems in a deregulated market.

After reviewing the literature, we proceeded to present the development of individual components of the evaluation tool. Chapter 2 described the structure of the developed tool and the information flows between the main functional modules. The general operation, the user interfaces and the outputs of the tool were also presented.

Then, we provided detailed descriptions of the main functional modules of the tool in subsequent chapters. Chapter 3 was devoted to explaining the operation of the hot water consumption generator, which creates hot water consumption profiles for individual households. To obtain key characteristics of the domestic hot water consumption in Tasmania (Australia), survey results were compiled and actual energy metering data were analyzed. In addition, parameters used in the hot water consumption generator and the Monte Carlo probabilistic simulations employed to

create hot water consumption profiles were also described in this chapter.

In Chapter 4 we developed a unique multi-layer thermally stratified hot water system model to represent the most common DHWS found in Tasmania. This model uses a one-dimensional heat transfer mechanism in a vertically stratified storage tank and assumes negligible heat transfers via conduction and radiation. In addition, we also included the temperature regulating operation of a tempering valve in the model. The accuracy of this model was validated with experimental data.

We presented the performance calculator in Chapter 5. The equations used to determine KPIs were described here. We used two KPIs in our research to evaluate the performance of the switching programs. The first KPI was the peak load reduction of the aggregate controlled load with respect to the aggregate uncontrolled load; the second KPI was the consumer comfort level measured by probabilities of getting cold showers in different types of families.

In Chapter 5, we also described in detail the optimization of switching programs for direct load control of DHWSs. First, we outlined the structure of the switching program optimizer with the information flows between its main components clearly depicted. Then we described the operations of the main components in the switching program optimizer, and explained in detail the operations of the two optimization methods employed in the tool. Simulation examples of each optimization method were given to illustrate their respective operations.

Lastly, Chapter 6 was dedicated to presenting the case studies performed with the developed tool. In this chapter, we evaluated the tool and found that it worked well to meet our research objectives. We used the tool to assess the scalability of the simulation results, the impacts of applying certain variables as constant values, as well as the performance of the switching programs produced by the tool for different operating scenarios.

## 7.2 Major Contributions

Our research has added the following contributions to the main body of knowledge:

- The developed model for a DHWS is unique and novel. It accurately models

the heat transfer mechanism in a thermally stratified hot water storage tank. As a result, the predictions in power consumption, vertical temperature profile inside the storage tank, shower temperature and hot water consumption match actual measurements with acceptable margins of error.

- The developed optimization algorithms are effective in producing switching programs that can be implemented practically.
- The developed tool has the capability to perform system level simulations that include creating realistic domestic hot water loads, proposing practical optimized switching programs and evaluating the results for the implementation of a load management program in a power distribution network. It can be used as a useful tool for engineers to plan and design practical load management programs for a power distribution system.

## 7.3 Suggestions for Future Work

Although our work has fulfilled all the research objectives, further development work may be carried out to improve and extend the scope of the current research. We outline the following suggestions for future researchers to consider:

- A small scale trial system implementing the switching programs proposed by the tool can be deployed to verify the performance of the tool. Field data and customer feedbacks collected in the proposed trial system are valuable information to validate and fine-tune the models in the tool.
- Currently, the hot water system model has been validated for the most common type of DHWS used in Tasmania. The model can be further developed to include other types of hot water system that may operate differently, and have different sizes and rated powers.
- Further research in optimization algorithms should be explored to further improve the effectiveness of the direct load control switching programs. Among other potential optimization methods, artificial neural network and genetic algorithm are two candidates which future research may investigate.

# Bibliography


[1] S. Elphick, P. Ciufo, and S. Perera, "Supply current characteristics of modern domestic loads," in *Australasian Universities Power Engineering Conf.*, 2009, pp. 1-6.

[2] Department of Infrastructure, Energy and Resources of Tasmania. (2013). *Energy in Tasmania* [Online]. Available: http://www.dier.tas.gov.au/energy/energy_in_tasmania

[3] Charles River Associates, "DM Programs for Integral Energy," Integral Energy, Australia, 20 Aug. 2003.

[4] A. Daneshi, N. Sadrmomtazi, H. Daneshi, and M. Khederzadeh, "Wind power integrated with compressed air energy storage," in *IEEE Int. Conf. on Power and Energy (PECon)*, 2010, pp. 634-639.

[5] R. Masiello, "Energy storage activities in the united states electricity grid," Electricity Advisory Committee, May 2011.

[6] S. K. Khator and L. C. Leung, "Power distribution planning: a review of models and issues," *IEEE Trans. Power Syst.,* vol. 12, pp. 1151-1159, 1997.

[7] R. R. M. Witherden, C. Tyler, W. K. G. Seah, "Managing Peak Demand Using Direct Load Monitoring and Control," presented at the Australasian Universities Power Engineering Conf., Hobart, Australia, 2013.

[8] Equipment Energy Efficiency, "CONSULTATION REGULATION IMPACT STATEMENT. Mandating 'Smart Appliance' Interfaces for Air Conditioners, Water Heaters and other Appliances," Equipment Energy Efficiency, Australia, 2012.

[9] Office of Energy, "A smarter energy future for Western Australians," Office of Energy, Government of Western Australia, Mar. 2011.

[10] J. Zhong, C. Kang, and K. Liu, "Demand side management in China," in *Proc. IEEE PES General Meeting*, 2010, pp. 1-4.

[11] F. P. Sioshansi, "Demand-side management: the third wave," *Energy Policy,* vol. 23, pp. 111-114, 1995.

[12] F. P. Sioshansi, "Restraining energy demand: The Stick, the carrot, or the market?," *Energy Policy,* vol. 22, pp. 378-392, 1994.

[13] Y. Yu, "Policy redesign for solving the financial bottleneck in demand side management (DSM) in China," *Energy Policy,* vol. 38, pp. 6101-6110, 2010.

[14] N. Zhou, M. D. Levine, and L. Price, "Overview of current energy-efficiency policies in China," *Energy Policy,* vol. 38, pp. 6439-6452, 2010.

[15] S. Mukhopadhyay and A. K. Rajput, "Demand side management and load control—An Indian experience," in *Proc. IEEE PES General Meeting*, 2010, pp. 1-5.

[16] A. Sinha, S. Neogi, R. Lahiri, S. Chowdhury, S. Chowdhury, and N. Chakraborty, "Role of Demand Side Management for power distribution utility in India," in *Proc. IEEE PES General Meeting*, 2011, pp. 1-8.

[17] S. Carley, "Energy demand-side management: New perspectives for a new era," *Journal of Policy Analysis and Management,* vol. 31, pp. 6-32, 2012.

[18] P. Palensky and D. Dietrich, "Demand side management: Demand response, intelligent energy systems, and smart loads," *IEEE Trans. Ind. Informat.,* vol. 7, pp. 381-388, 2011.

[19] F. Boshell and O. Veloza, "Review of developed demand side management programs including different concepts and their results," in *IEEE Transmission and Distribution Conference and Exposition: Latin America*, 2008, pp. 1-7.

[20] D. Greene and A. Pears, "Policy options for energy efficiency in Australia," *Melbourne: ACRE and The Australian CRC for Renewable Energy Policy Group,* 2003.

[21] M. Colombier and P. Menanteau, "From energy labelling to performance standards: some methods of stimulating technical change to obtain greater energy efficiency," *Energy Policy,* vol. 25, pp. 425-434, 1997.

[22] H. Geller, P. Harrington, A. H. Rosenfeld, S. Tanishima, and F. Unander, "Polices for increasing energy efficiency: Thirty years of experience in OECD countries," *Energy Policy,* vol. 34, pp. 556-573, 2006.

[23] D. J. Crossley, "Tradeable energy efficiency certificates in Australia," *Energy Efficiency,* vol. 1, pp. 267-281, 2008.

[24] K. Heussen, S. You, B. Biegel, L. Hansen, and K. Andersen, "Indirect control for demand side management-A conceptual introduction," in *Proc. 3rd IEEE PES Int.l Conf. and Exhibition on Innovative Smart Grid Technologies (ISGT Europe),* 2012, pp. 1-8.

[25] Origin. (2013, Mar.). *Residential tariffs - electricity* [Online]. Available: http://www.originenergy.com.au/2087/Electricity-tariffs-QLD

[26] M. LeMay, R. Nelli, G. Gross, and C. A. Gunter, "An integrated architecture for demand response communications and control," in *Proc. 41st Annual Hawaii Int. Conf. on System Sciences,* 2008, pp. 174-174.

[27] M. Ilic, J. W. Black, and J. L. Watz, "Potential benefits of implementing load control," in *IEEE Power Engineering Society Winter Meeting*, 2002, pp. 177-182.

[28] J. Wilson, A. Rosenfeld, and M. Jaske, "Using demand responsive loads to meet California's reliability needs," in *ACEEE summer conference*, Asilomar, CA, 2002, pp. 5.305 – 5.316.

[29] I. Khanna, "Smart Grid application: Peak demand management trial-the Western Australian experience," in *Innovative Smart Grid Technologies Asia (ISGT), 2011 IEEE PES*, 2011, pp. 1-6.

[30] Appliance Energy Efficiency Branch, "Information for the Australian Energy Market Commission in response to the Issues Paper: Power of choice – giving consumers options in the way they use electricity," Department of Climate Change and Energy Efficiency, Australia, Aug. 2011.

[31] M. Donnelly, S. Mattix, D. Trudnowski, and J. Dagle, "Autonomous Demand Response for Primary Frequency Regulation," Department of Energy, U.S.A., Jan. 2012.

[32] P. McKelvie, J. Hoddinott, G. Boland, and G. Kahl, "Load Management Tools for Optimal Control of Hot Water Loads," in *Electric Energy Conf.*, 1992, pp. 153–159.

[33] C. Diduch, M. Shaad, R. Errouissi, M. Kaye, J. Meng, and L. Chang, "Aggregated domestic electric water heater control-building on smart grid infrastructure," in *7th Int.Power Electronics and Motion Control Conf. (IPEMC),* 2012, pp. 128-135.

[34] L. Paull, H. Li, and L. C. Chang, "A novel domestic electric water heater model for a multi-objective demand side management program," *Electric Power Systems Research,* vol. 80, pp. 1446-1451, Dec 2010.

[35] I. Lane and N. Beute, "A model of the domestic hot water load," *IEEE Trans. Power Syst.,* vol. 11, pp. 1850-1855, 1996.

[36] M. Orphelin and J. Adnot, "Improvement of methods for reconstructing water heating aggregated load curves and evaluating demand-side control benefits," *IEEE Trans. Power Syst.,* vol. 14, pp. 1549-1555, 1999.

[37] S. Shao, M. Pipattanasomporn, and S. Rahman, "Development of physical-based demand response-enabled residential load models," *IEEE Trans. Power Syst.,* vol. 28, pp. 607-614, 2013.

[38] J. Kondoh, N. Lu, and D. J. Hammerstrom, "An evaluation of the water heater load potential for providing regulation service," in *Proc. IEEE PES General Meeting*, 2011, pp. 1-8.

[39] A. Gomes, A. G. Martins, and R. Figueiredo, "Simulation-based assessment of electric load management programs," *International Journal of Energy Research,* vol. 23, pp. 169-181, Feb 1999.

[40] M. H. Nehrir, R. Jia, D. A. Pierre, and D. J. Hammerstrom, "Power management of aggregate electric water heater loads by voltage control," in *Proc. IEEE PES General Meeting*, 2007, pp. 1-6.

[41] J. C. vanTonder and I. E. Lane, "A load model to support demand management decisions on domestic storage water heater control strategy," *IEEE Trans. Power Syst.,* vol. 11, pp. 1844-1849, Nov 1996.

[42] A. Gomes, C. H. Antunes, and A. G. Martins, "A multiple objective evolutionary approach for the design and selection of load control strategies," *IEEE Trans. Power Syst.,* vol. 19, pp. 1173-1180, May 2004.

[43] S. Lee and C. Wilkins, "A practical approach to appliance load control analysis: a water heater case study," *IEEE Trans. Power App. Syst.,* pp. 1007-1013, 1983.

[44] A. Abhyankar and S. Khaparde, "Introduction to deregulation in power industry," *Indian Institute of Technology, Mumbai*, pp 1-8.

[45] G. Strbac, "Demand side management: Benefits and challenges," *Energy Policy,* vol. 36, pp. 4419-4426, 2008.

[46] G. Strbac, A. Shakoor, M. Black, D. Pudjianto, and T. Bopp, "Impact of wind generation on the operation and development of the UK electricity systems," *Electric Power Systems Research,* vol. 77, pp. 1214-1227, 2007.

[47] T. J. Chang, Y.-T. Wu, H.-Y. Hsu, C.-R. Chu, and C.-M. Liao, "Assessment of wind characteristics and wind turbine characteristics in Taiwan," *Renewable Energy,* vol. 28, pp. 851-871, 2003.

[48] Y. Xie. (2012, Nov. ). Does Taxing Carbon Level the Playing Field for Wind Power? *chicago policy review*. Available: http://chicagopolicyreview.org/2012/11/13/does-taxing-carbon-level-the-playing-field-for-wind-power/

[49] P. Cappers, C. Goldman, and D. Kathan, "Demand response in US electricity markets: Empirical evidence," *Energy,* vol. 35, pp. 1526-1535, 2010.

[50] B. Liscouski and W. Elliot, "Final Report on the August 14, 2003 Blackout in the United States and Canada: Causes and Recommendations," US-Canada Power System Outage Task Force, Apr. 2004.

[51] P. A. Daly and J. Morrison, "Understanding the potential benefits of distributed generation on power delivery systems," in *Rural Electric Power Conf.,* 2001, pp. A2.1-A2.13.

[52] L. Sachs, *Applied statistics : a handbook of techniques*, 2nd ed.: Springer-Verlag, New York, 1984, pp. 382-456.

[53] Australian Bureau of Statistics. (2012). [Online]. Available: www.ausstats.abs.gov.au

[54] *Tempering valve 5213 series* [Online]. Available: http://www.reece.com.au/plumbing/products/109210

[55] *Heated water plumbing* [Online]. Available: http://workplacestandards.tas.gov.au/safety/plumbing/plumbing_technical_advice/heated_water_plumbing

[56] J. Fernandez-Seara, F. J. Uhia, and J. Sieres, "Experimental analysis of a domestic electric hot water storage tank. Part I: Static mode of operation," *Applied Thermal Engineering,* vol. 27, pp. 129-136, Jan 2007.

[57] J. Fernandez-Seara, F. J. Uhia, and J. Sieres, "Experimental analysis of a domestic electric hot water storage tank. Part II: dynamic mode of operation," *Applied Thermal Engineering,* vol. 27, pp. 137-144, Jan 2007.

[58] Y. Han, R. Wang, and Y. Dai, "Thermal stratification within the water tank," *Renewable and Sustainable Energy Reviews,* vol. 13, pp. 1014-1026, 2009.

[59] I. Dincer and M. A. Rosen, *Thermal Energy Storage: Systems and Applications*, 2nd ed., Chichester, U.K: Wiley, 2010, pp. 281–298.

[60] R.-J. Shyu, J.-Y. Lin, and L.-J. Fang, "Thermal analysis of stratified storage tanks," *Journal of solar energy engineering,* vol. 111, pp. 54-61, 1989.

[61] G. van Harmelen and G. J. Delport, "Multi-level expert-modelling for the evaluation of hot water load management opportunities in South Africa," *IEEE Trans. Power Syst.,* vol. 14, pp. 1306-1311, 1999.

[62] A. H. Fanney and B. P. Dougherty, "The thermal performance of residential electric water heaters subjected to various off-peak schedules," *Journal of Solar Energy Engineering-Transactions of the Asme,* vol. 118, pp. 73-80, May 1996.

[63] M. Negnevitsky and K. Wong, "Demand Side Management Evaluation Tool," *IEEE Trans. Power Syst.,* vol. 99, pp. 1-11, 2014.

[64] R. P. Canale and S. C. Chapra, *Numerical Methods for Engineers*, 5th ed. New York: Mc Graw Hill, 2006, pp. 711-716.

[65] *Properties of water* [Online]. Available: http://en.wikipedia.org/wiki/Properties_of_water

[66] Equipment Energy Efficiency. *Standing heat losses from household hot water cylinders* [Online]. Available: http://www.energyrating.gov.au/products-themes/water-heating/electric-water-heaters/meps-and-labelling-electric/

[67] W. Mendenhall, J. E. Reinmuth, and R. J. Beaver, *Statistics for management and economics*: PWS-KENT, MA, 1989, pp. 697-759.

[68] C. J. Willmott and K. Matsuura, "Advantages of the mean absolute error (MAE) over the root mean square error (RMSE) in assessing average model performance," *Climate Research,* vol. 30, pp. 79-82, 2005.

[69] *"ST" hot water thermostats* [Online]. Available: http://stokes.strategyonline.com/documents/productpdf/ST_Thermostat_LR.pdf

[70] T. Ohnaka, Y. Tochihara, and Y. Watanabe, "The effects of variation in body temperature on the preferred water temperature and flow rate during showering," *Ergonomics,* vol. 37, pp. 541-546, 1994.

[71] C. Herrmann, V. Candas, A. Hoeft, and I. Garreaud, "Humans under showers: thermal sensitivity, thermoneutral sensations, and comfort estimates," *Physiology & behavior,* vol. 56, pp. 1003-1008, 1994.

*[72] M. Schuldt and D. Tachibana, "Energy-related water fixture measurements: securing the baseline for Northwest single family homes," Proc. of the 2008 Summer Study on Energy Efficiency in Buildings, pp. 2.235-2.266, 2008.*

[73] K. Wong and M. Negnevitsky, "Development of an evaluation tool for demand side management of domestic hot water load," in *Proc. IEEE PES General Meeting*, 2013, pp. 1-5.

[74] F. Haugen, *PID control*: Tapir academic press, Trondheim, 2004.

[75] Australian Bureau of Meteorology. (2012). [Online]. Available: www.bom.gov.au

[76] K. Wong and M. Negnevitsky, "Optimisation of switching programs for demand side management of domestic hot water load," in *Australasian Universities Power Engineering Conf.,* 2013, pp. 1-6.

# Appendix 1 Main flowchart of the DHWS model

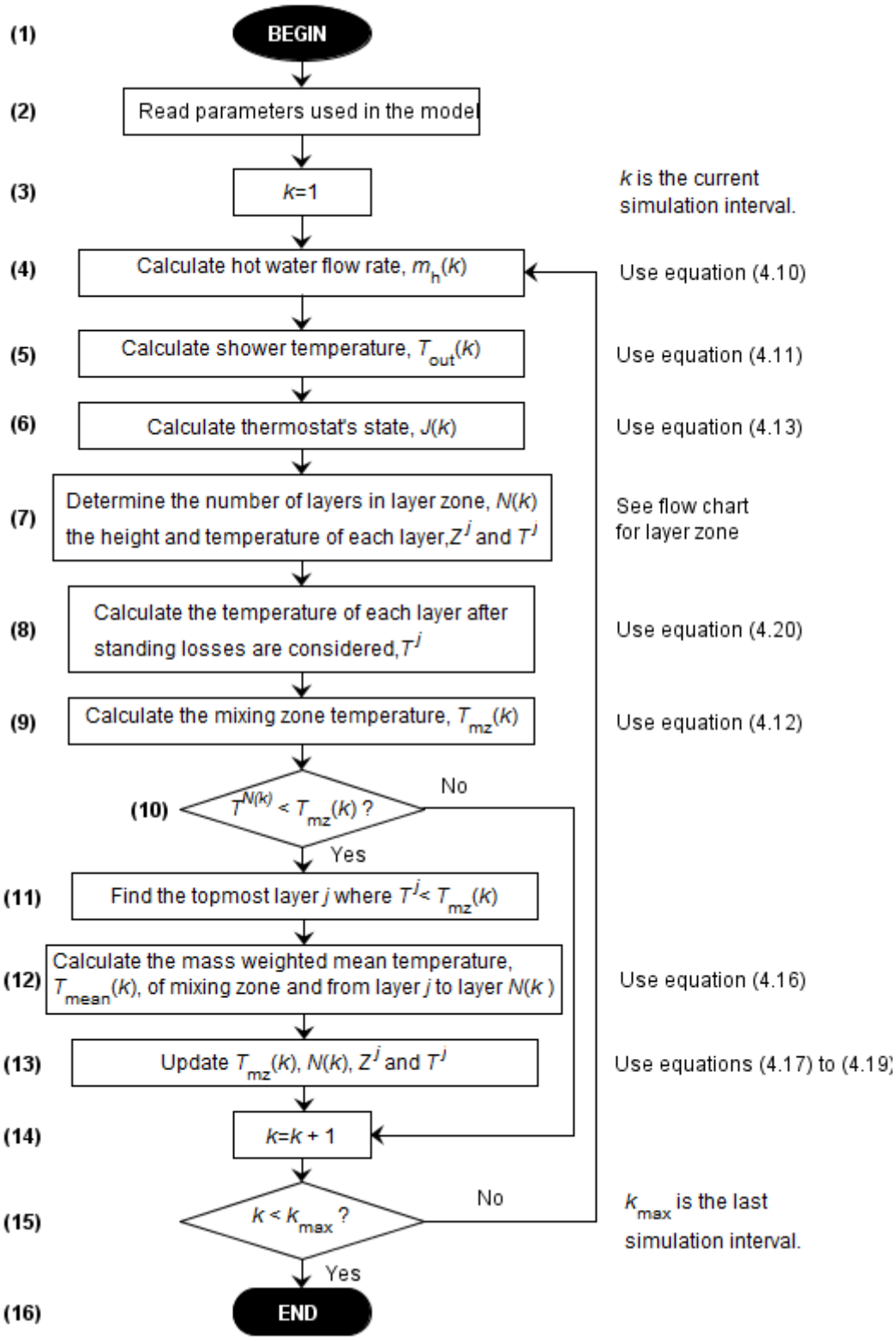

# Appendix 2 Flowchart for layer zone

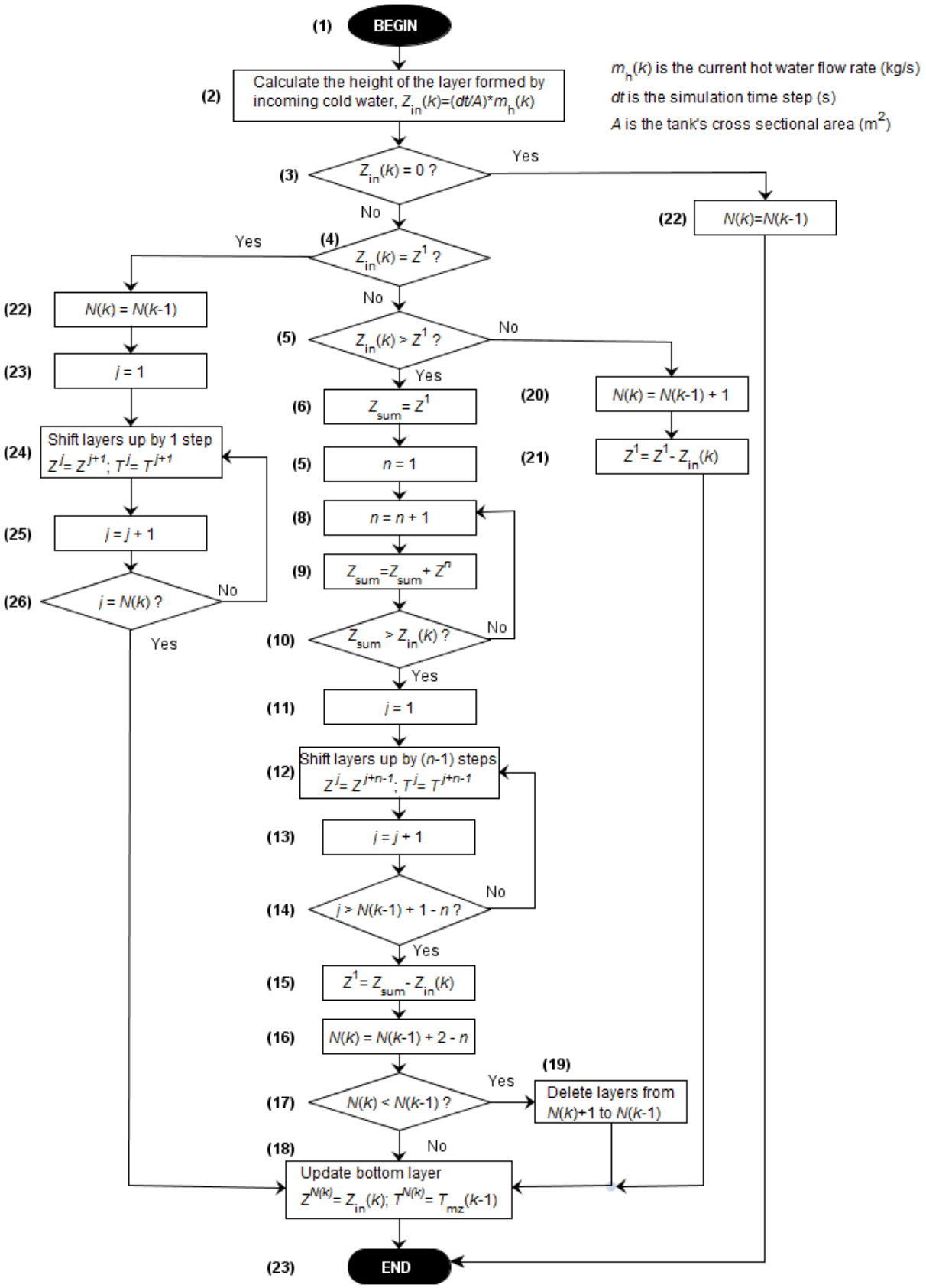

# Appendix 3 Flowcharts for hot water consumption generator

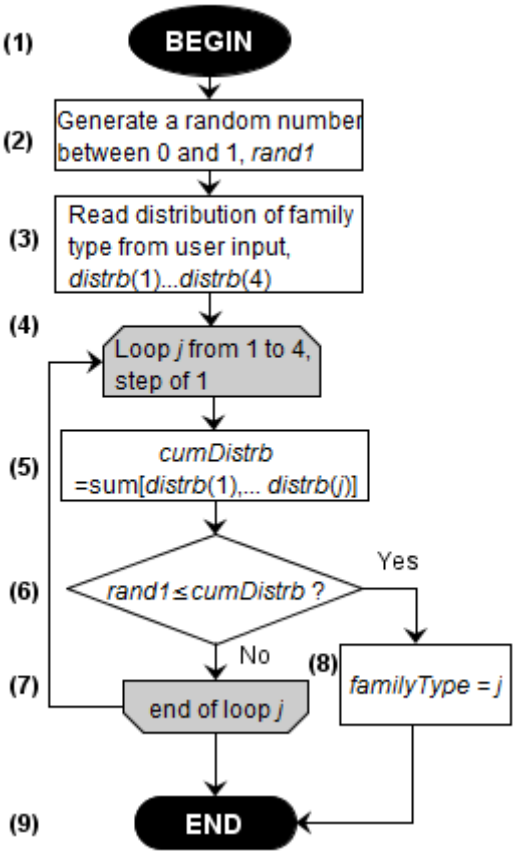


Flowchart to determine the family type of a household.

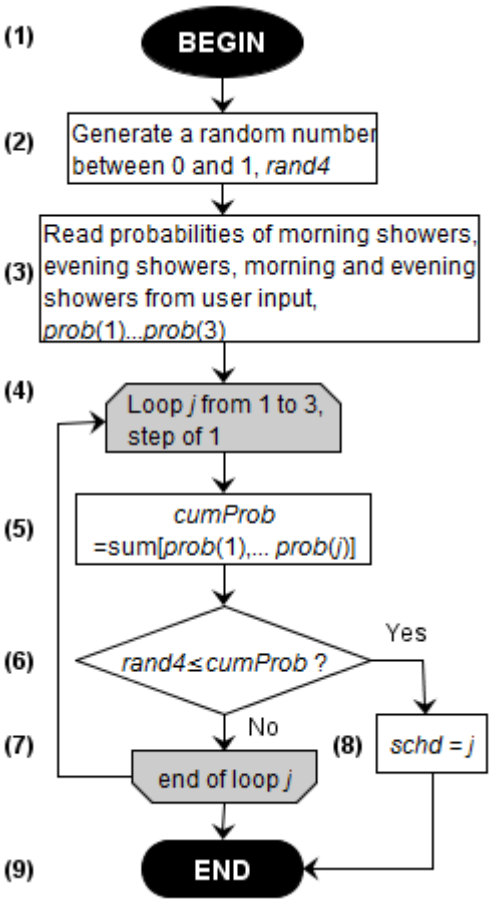


*Schd* equals 1, 2 or 3 correspond respectively to a household taking morning showers only, evening showers only, or morning and evening showers.

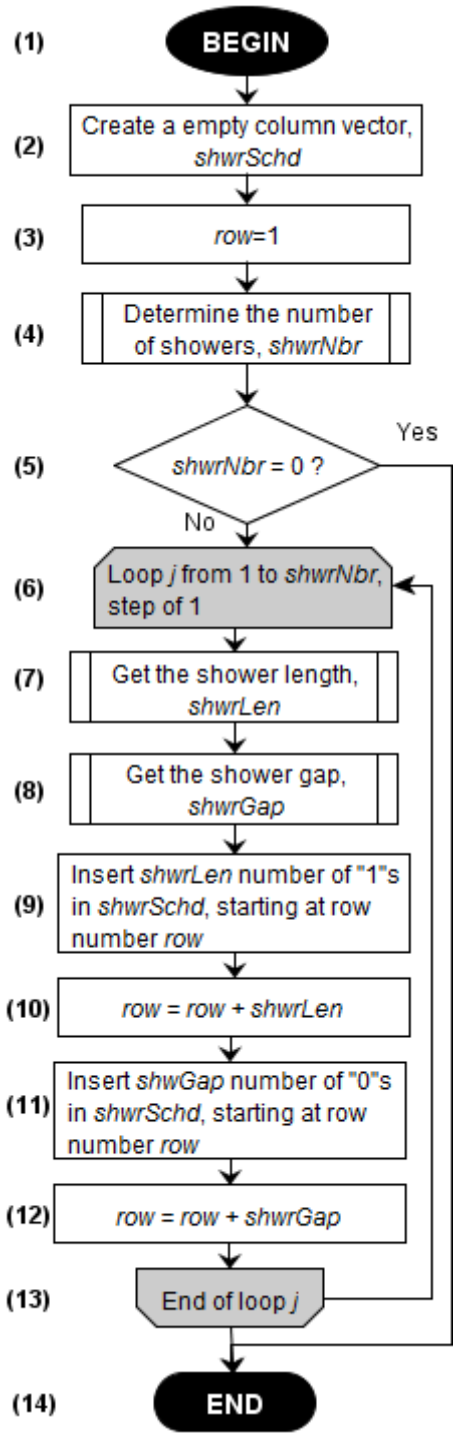


Flowchart to create a shower schedule.

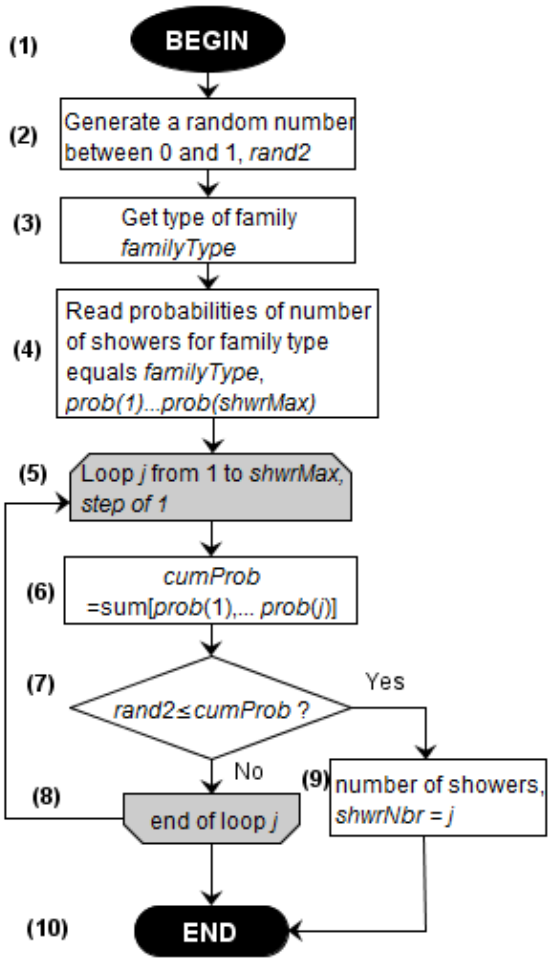


Flowchart to determine the number of showers. The tool specifies *shwrMax* as the maximum number of showers taken in a household.

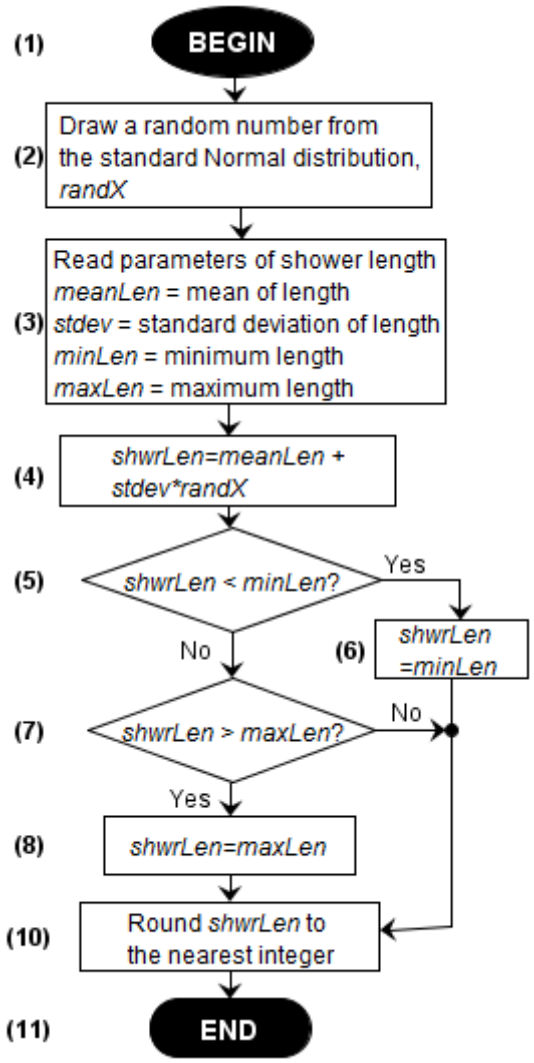


Flow chart to determine the length of a shower.

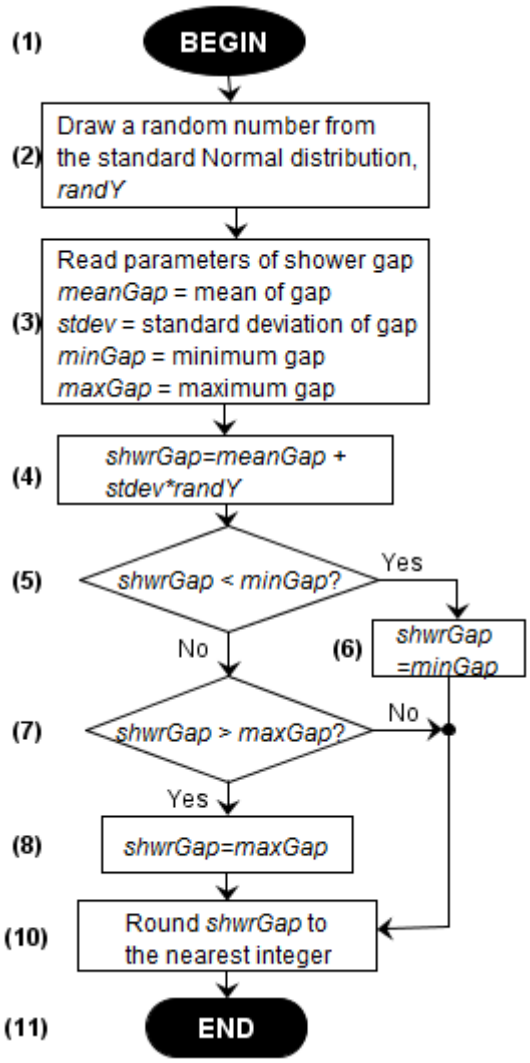


Flowchart to determine the gap between two successive showers.

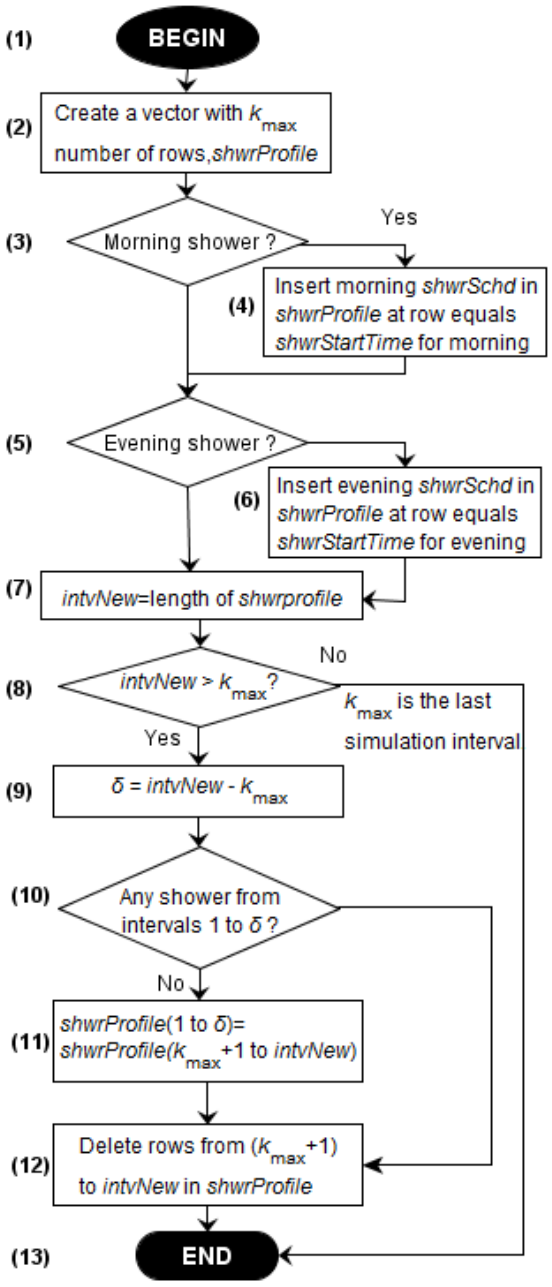


Flowchart to create a shower profile.

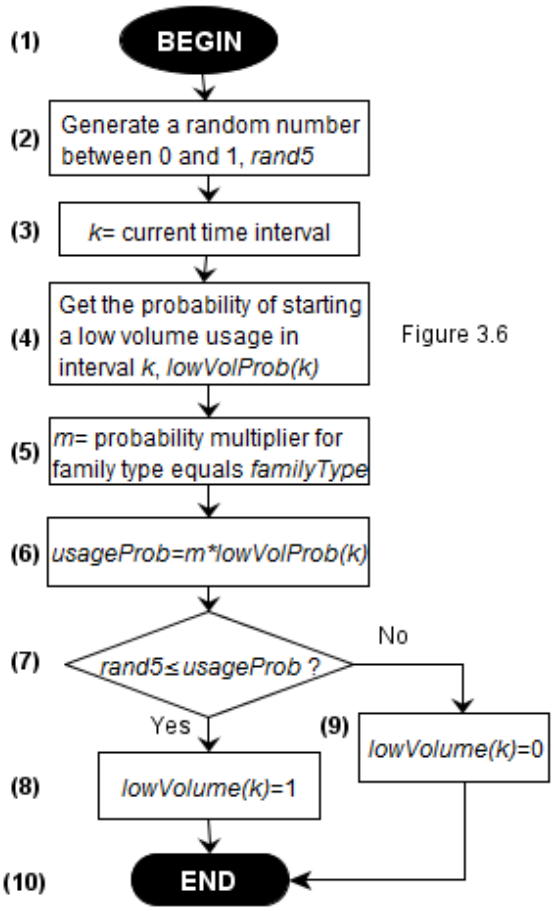


Figure 3.6

Flowchart to determine the low volume usage at a time interval.

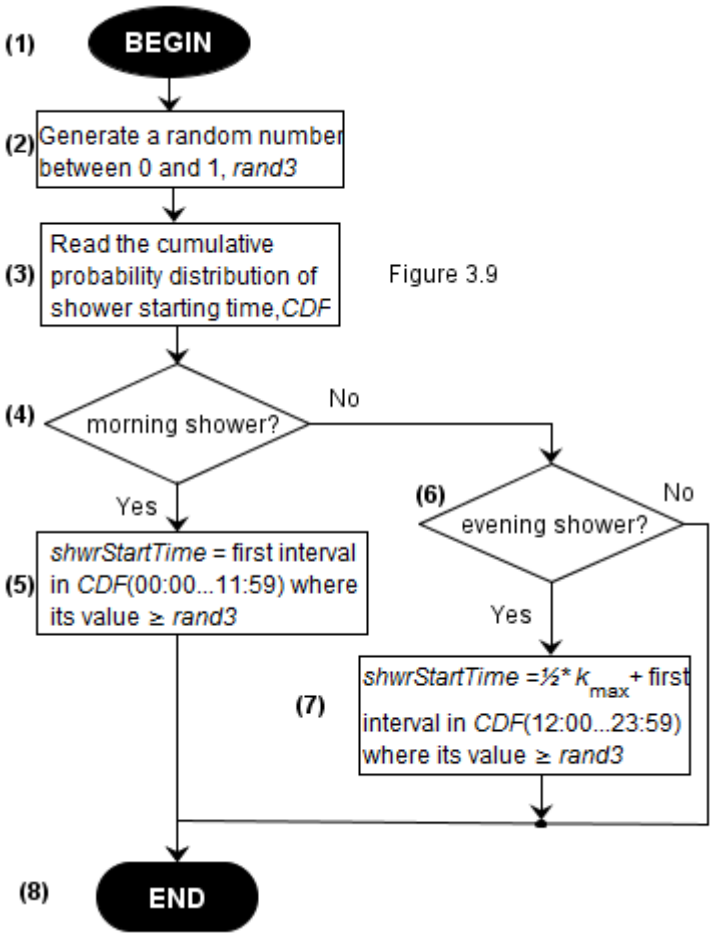


Figure 3.9

Flowchart to determine the starting time of a shower.

# Appendix 4 Questionnaire of hot water use survey

**Hot Water Use Questionnaire**

**Introduction**

*Aurora Energy is committed to providing customers with high quality service at the lowest possible cost. This survey is aimed at obtaining information regarding the use of hot water in your household. This information will be used to implement schemes that can potentially reduce your electricity bills.*

**Hot Water Use**

| | |
|---|---|
| **The next set of questions are on behalf of Aurora Energy and are aimed at obtaining information regarding the use of hot water in your household. This information will be used to implement schemes that can potentially reduce electricity bills.** | |
| **Q1. Firstly, how many residents are in your household?**<br><br>RECORD | |
| **Q2. How many showers do the residents in your household take during each of the following periods on a typical day?** | |
| **Q2.1. 6 AM – 10 AM**<br><br>RECORD | |
| **Q2.2. 5 PM – 8 PM**<br><br>RECORD | |
| **Q3. What is the average duration of each shower taken by the residents in your household on a typical day?**<br><br>RECORD | |
| **Q4. Do you have a dishwasher?** | 1. Yes<br>2. No – GO TO Q11 |
| **Q5. How many times do you typically use it between the following times each week?** | |
| **Q5.1. 6 AM – 10 AM**<br><br>RECORD | |
| **Q5.2. 5 PM – 8 PM**<br><br>RECORD | |

| | |
|---|---|
| **Q6. Do you use a warm or hot cycle in your washing machine?** | 1. Yes<br>2. No – GO TO Q13 |
| **Q7. How many times do you typically put on a warm or hot wash between the following times each week?** | |
| **Q7.1. 6 AM – 10 AM**<br><br>RECORD | |
| **Q7.2. 5 PM – 8 PM**<br><br>RECORD | |
| **Q8. What type of hot water system do you have?** | 1. Electric<br><br>2. Solar<br><br>3. Gas<br><br>4. Other (specify) |
| **Q9. If you have an electric hot water system, what is its size in litres? Is it…** | **1. Roughly 1 metre high**<br><br>**2. Roughly 1.5 metres high**<br><br>**3. Rough 2 metres high**<br><br>4. Don't know – DO NOT READ OUT |